CENTRAL REGION APPLIED RESEARCH PAPERS NO. 14

MARCH 1995

NATIONAL WEATHER SERVICE CENTRAL REGION SERIES OF CENTRAL REGION APPLIED RESEARCH PAPERS (CRARP)

The NWS Central Region Applied Research Paper (CRARP) series is an informal medium to compile and distribute a small part of the on-station research efforts being performed by the operational personnel of the Central Region. As the National Weather Service becomes more involved in using high technology to sample, describe, and forecast the weather, this medium has been made available to encourage the transfer of useful knowledge and skills to other NWS offices. Many times, on-station research efforts and case studies are only circulated locally due to the publication restrictions associated with Technical Attachments and Memorandum. The following ARP series is a vehical to distribute such scientific and operational information to other NWS offices.

The first three were published as Technical Memoranda: (1) CR 88 "Central Region Applied Research Papers 88-1 through 88-7," (2) CR 97 "Central Region Applied Research Papers 97-1 through 97-6," and (3) CR 99 "Central Region Applied Research Paper 99-1 through 99-7." Central Region Applied Research Papers Nos. 3 and 4 were a first attempt at starting a new series numbering system. However, due to an editorial error, CRARP No. 6 served as the beginning point for accurately reflecting the numbering for this series.

NWS CR 88	Central Region Applied Research Papers 88-01 through 88-07, May 1988.
NWS CR 97	Central Region Applied Research Papers 97-01 through 97-06, July 1989.
NWS CR 99	Central Region Applied Research Papers 99-01 through 99-07, Nov 1989.
CRARP No. 3	Central Region Applied Research Papers 03-01 through 03-07, July 1990.
CRARP No. 4	Central Region Applied Research Papers 04-01 through 04-05, December 1990.
CRARP No. 6	Central Region Applied Research Papers 06-01 through 06-07, May 1991.
CRARP No. 7	Central Region Applied Research Papers 07-01 through 07-04, November 1991.
CRARP No. 8	Central Region Applied Research Papers 08-01 through 08-06, September 1992.
CRARP No. 9	Central Region Applied Research Papers 09-01 through 09-10, April 1993.
CRARP No. 10	Central Region Applied Research Papers 10-01 through 10-12, September 1993.
CRARP No. 11	Central Region Applied Research Papers 11-01 through 11-10, January 1994.

Table of Contents

[1]Current affiliation, NWS Office Aberdeen, South Dakota.

14-04

14-05

14-06

14-10

ERRATA...

CENTRAL REGION APPLIED RESEARCH PAPERS NO. 13,
DECEMBER 1994,
PAPER 13-02

A VERIFICATION STUDY OF THE MRF-BASED STATISTICAL TEMPERATURE GUIDANCE FOR GRAND ISLAND, NEBRASKA by Daniel D. Nietfeld, NEXRAD Weather Service Forecast Office, Topeka, Kansas and David A. Skerritt, NEXRAD Weather Service Forecast Office, Omaha, Nebraska

CENTRAL REGION APPLIED RESEARCH PAPER 14-01

THE OPERATIONAL USE OF THE WSR-88D MID- AND HIGH-LEVEL LAYER COMPOSITE REFLECTIVITY PRODUCTS TO ASSESS THE SEVERE WEATHER POTENTIAL OF THUNDERSTORMS

Robin J. Turner
National Weather Service Office
Goodland, Kansas

1. Introduction

As part of the National Weather Service's ongoing modernization program, the installation of WSR-88D radars has significantly increased the amount of data usable for severe thunderstorm identification. The large quantity of products available from the WSR-88D has resulted in improved severe weather detection and increased accuracy of warnings.

In the past, conventional radar operators have successfully used the Lemon technique to identify potentially severe thunderstorms. While these techniques developed by Lemon (1980) pertain to conventional radars, they remain valid in the modernization era. Many WSR-88D products provide detailed information that (when analyzed using the criteria for severe weather set forth by Lemon) aids the radar operator in the warning decision process.

Utilizing the wealth of information generated by the WSR-88D can be overwhelming. Usually, the radar operator must discern which storms require further investigation before using other WSR-88D products to determine if a warning is warranted. Examples of these "first look" products include Composite Reflectivity graphics, Base Reflectivity products, and Vertically Integrated Liquid (VIL) displays. Another group of products that WSR-88D operators will find useful for this purpose includes the mid- and high-level Layer Composite Reflectivity Maximum (LRM) graphics.

2. The Layer Composite Reflectivity Maximum (LRM) Graphic

The LRM is an eight-data level product displaying a composite of the maximum reflectivity detected in a layer grid box (NEXRAD Joint System Program Office 1986). There are three defined layers for the LRM graphic, consisting of: the surface to 24,000 ft MSL, 24,000 ft - 33,000 ft MSL, and 33,000 ft -

60,000 ft MSL. Data is displayed in dBZ increments of 0-4, 5-17, 18-29, 30-40, 41-45, 46-49, 50-56, and ≥57. The products have a resolution of 4 x 4 km (2.2 x 2.2 nm).

3. The Operational Use of the Mid- and High-level LRM Products

In his paper, Lemon emphasized the relationships between storm updraft intensity and the characteristics of the radar echo associated with the updraft. Lemon states that a storm's " . . . peak reflectivity can be related to updraft strength . . .," and "in general, it is updraft strength that detects storm severity." Two of the guidelines that Lemon developed pertain to these relationships are as follows:

A. For a thunderstorm to be considered severe, at a minimum, the Video Integrator and Processor (VIP) 5 echo (≥55 dBZ) must extend to at least 27-30,000 ft AGL, with the height dependent upon location.

B. The first indication that a storm is becoming severe occurs when the mid-level echo increases rapidly in size and/or intensity as the Weak Echo Region (WER) develops.

The mid- and high-level LRM graphics can provide a quick assessment of these two characteristics, thereby allowing the radar operator to rapidly prioritize individually storms according to the strength of the reflectivities in the mid levels and above. This ability to determine which thunderstorms are more likely to be severe is especially important whenever there are many echoes detected by the radar.

To use the high-level LRM graphic operationally, one must remember the product parameters. Since the lowest boundary of the high-level LRM product is set at 33,000 ft MSL, WSR-88D sites with elevations between 2,000 and 5,000 ft MSL will have the resultant lowest elevation height located between 31,000 and 28,000 ft AGL. This range of heights corresponds well with Lemon's critical values in the first guideline above. Therefore, at those particular WSR-88D sites, when displaying the high-level LRM graphic, any thunderstorm producing reflectivities of ≥50 dBZ should be viewed as potentially severe, requiring further investigation using other WSR-88D products. There is one caveat: while the height of the VIP 5 echo has been used successfully in the past to differentiate between severe and non-severe thunderstorms, the enhanced performance capability of the WSR-88D radar necessitates local revisions of that particular guideline. Until such time that local experiences with these graphics produce a dBZ to height correlation that consistently identifies severe thunderstorms, one should use the LRM products only as a "first look" product or in conjunction with other WSR-88D graphics.

For WSR-88D sites with elevations below 2,000 ft MSL, radar operators may find the mid-level LRM product better suited to their location. Using the mid-level LRM graphic at these offices would place the top section between 31,000 and 33,000 ft AGL, and the lowest section between 22,000 and 24,000 ft AGL. Employing this graphic in a brief time lapse, the mid-level echo can be examined for rapid increases in size and/or intensity as noted in the second guideline above. A determination can then be made as to which cells require additional investigation. During cool season convective events, the mid-level LRM graphic may be a better choice than the high-level LRM for investigating the mid levels of a thunderstorm. Use this product with caution always, as the maximum reflectivity displayed may have only entered the lowest level of the layer.

The mid- and high-level LRM graphics have proven to be useful tools in detecting pulse severe thunderstorms. These storms, as described by Chisholm and Renick (1972) and named by Wilk et al. (1979), differ from non-severe pulse thunderstorms in that:

A. The first detectable echo develops higher aloft and displays a higher reflectivity.

B. The first detectable echo stays aloft longer than that of a non-severe pulse thunderstorm.

By employing the mid- and/or high-level LRM products, the WSR-88D operator can identify which first detectable echoes are producing higher reflectivities aloft and which echoes remain aloft longer.

4. Advantages of the Mid- and High-level LRM Products Versus Other WSR-88D Graphics

User functions set up to display and manipulate Base Reflectivity products are frequently used to investigate storm structure, as well as the intensity trend of the reflectivities aloft. A disadvantage of this method arises whenever thunderstorms are located at several different ranges from the radar site. Depending upon storm location, the Routine Product Set (RPS) list selected and the elevation slices displayed on screen by the user functions, the highest reflectivities of a thunderstorm may not be shown. The LRM graphics alleviate this problem, since all elevation slices performed by the Volume Coverage Pattern (VCP) are used in the generation of these products. Using a LRM graphic to examine the mid levels of a thunderstorm is therefore much faster and more convenient than having to manually select the elevation slices that intersect a particular storm within the advised levels.

There are several advantages to using the mid- and high-level LRM graphics over other "first look" products. When using the Composite Reflectivity

graphic, the height of the maximum reflectivity echo is unknown, and the maximum reflectivity displayed may be contaminated by anomalous propagation (Operational Support Facility 1993). No interpretation can be made of updraft strength. The mid- and high-level LRM products exhibit the maximum reflectivity in a known layer and display no ground clutter returns.

The VIL product, while widely used to interpret thunderstorm strength, has certain limitations due to how the product is generated. For each elevation angle, the VIL algorithm computes the liquid water contained in a grid box (4 x 4 km) and assigns the maximum value found within. Vertically integrated liquid values are derived by summing over all elevation angles within a volume scan for each grid box (NEXRAD Joint System Program Office 1986). This produces underestimated values for strongly tilted or fast-moving thunderstorms, and storms located close to the radar site. The VIL algorithm will also overestimate values for storms located near the limit of coverage (Operational Support Facility 1993). The mid- and high-level LRM graphics are not affected by storm tilt or movement and display only those maximum dBZ values detected within the layer in each grid.

The mid- and high-level LRM products often give an earlier indication of thunderstorm intensity trends than the VIL product. For example, consider a developing thunderstorm producing a 40 dBZ reflectivity echo maximum above 33,000 ft MSL (Figure 1). The high-level LRM graphic would display the maximum reflectivity detected (in this case, 40 dBZ). The VIL algorithm would compute the liquid water value found in each grid box for every elevation slice for that volume scan, and then sum these values over all elevation angles. Low and high angle elevation slices would report no values for liquid water as they would under- and overshoot the reflectivity echo. The resultant summation over all elevation angles within the volume scan would produce low VIL values.

As the reflectivity core descends (Figure 2), the VIL values would increase as more slices intersect the echo. Simultaneously, the high-level LRM often indicates a lowering of the reflectivity returns from above 33,000 ft MSL.

This phenomenon has been observed often from both the mid- and high-level LRM products generated by the WSR-88D in Goodland (GLD), Kansas. As the mid- or high-level LRM product reflectivity trend for a particular storm continues to increase, the VILs for a storm will often increase as well. Once the mid- or high-level reflectivity max decreases, indicating a lowering of the reflectivity core (therefore, weakening updraft), VIL values often display a marked increase in that same volume scan. Any storm that shows a rise in the maximum reflectivities in the LRM products will likely display an increase in VILs during the next volume scan. The use of the LRM products to forecast a storm's intensity trend has therefore frequently given the radar operator several additional minutes of lead time when completing the warning decision process. This

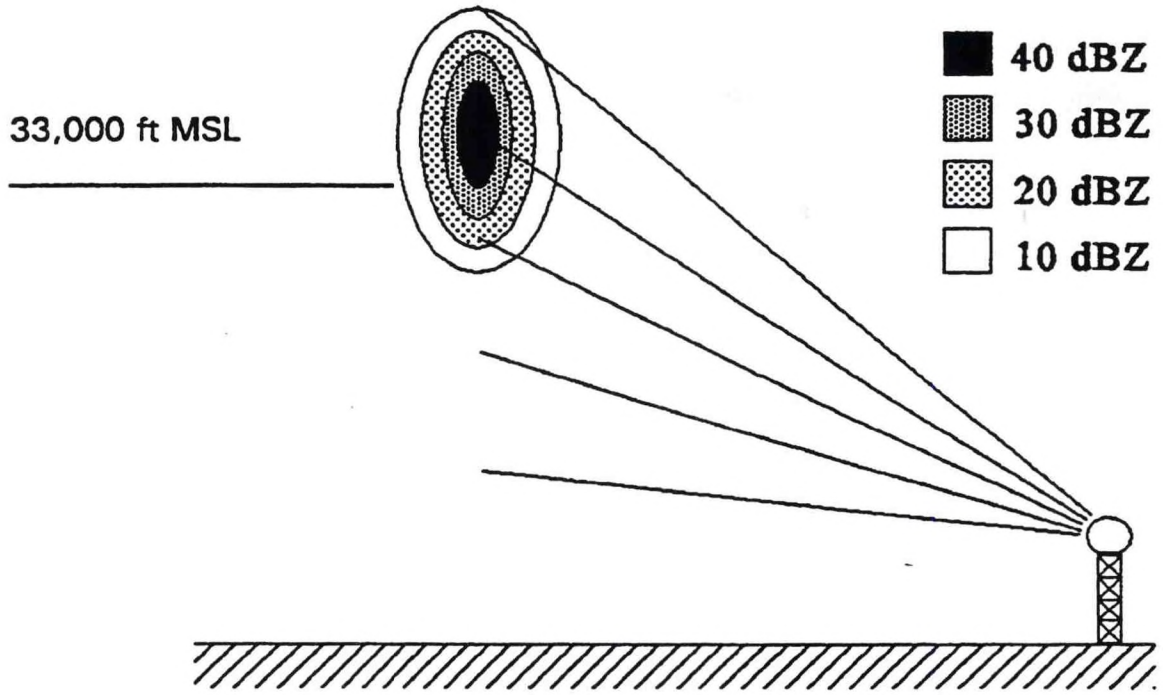

Figure 1. A 40 dBZ thunderstorm echo maximum developing aloft as detected by the five lowest elevation scans from the WSR-88D.

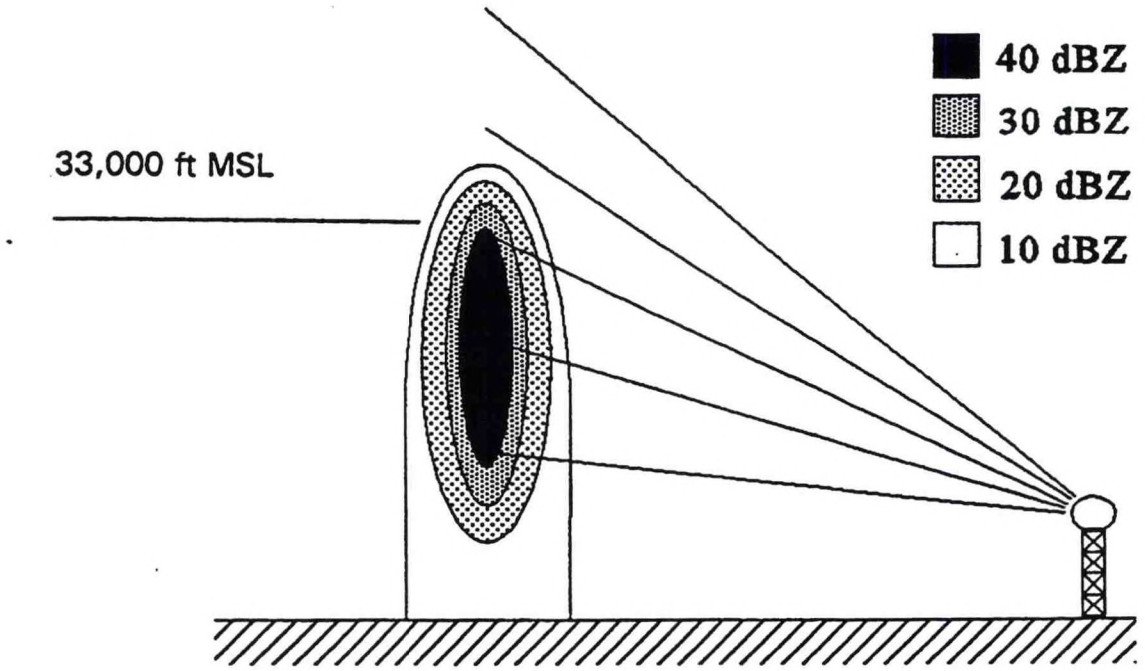

Figure 2. A descending 40 dBZ reflectivity core as detected by the five lowest elevations scans from the WSR-88D.

phenomenon does not occur exactly as depicted in the preceding example with every storm, as it is dependant upon when the VCP scan interrogates the thunderstorm updraft. It does, however, occur frequently enough that this technique should be incorporated into the routines used by all WSR-88D operators for investigating potentially severe thunderstorms.

5. Disadvantages of Using the Mid- and High-level LRM Graphics

Perhaps the biggest disadvantage affecting the LRM products is that the individual layers cannot be adjusted according to regional policies and radar elevation. The heights (measured in ft MSL) of the LRM graphics were set by the Program Management Committee (PMC) and cannot be altered locally. A lack of site-selectable heights for the LRM may limit the usefulness of these products at some offices.

A second disadvantage affecting LRM products is the length of time needed for the WSR-88D to generate these graphics after the end of a volume coverage scan. This disadvantage affects the VIL and Composite Reflectivity graphics as well, since they arrive at the Principal User's Processor (PUP) at approximately the same time (typically, seven minutes after the start of the volume coverage scan).

Additionally, the strength of the reflectivities in the high-level LRM product may be underestimated when the WSR-88D is operating in VCP 21. When thunderstorms are located at certain ranges from the radar, the beam may slice through the cell at an elevation several hundred meters above the bottom of the layer. Higher reflectivities could be located just below the radar beam, yet above the lowest level of the layer, and would therefore remain undetected.

6. An Example of the Use of the Mid-level LRM and VIL Products During a Marginal Severe Thunderstorm Event

During the mid-afternoon hours of April 20, 1994, thunderstorms began to develop over east central Colorado. While most of these storms remained below severe limits, one thunderstorm did become marginally severe, producing nickel-sized hail.

The April 20, 1200 UTC sounding from North Platte (LBF), Nebraska, was modified using the Skew-T Hodograph Analysis and Research Program (SHARP) (Hart and Korotky 1991) to reflect the expected conditions over the eastern Colorado portion of the GLD County Warning Area (CWA). The modified sounding produced a Lifted Index (LI) of -3 degrees, a Convective Available Potential Energy (CAPE) of 780 J/kg and a maximum vertical velocity of 39 m/s. The height of the wet-bulb zero was computed at 2,542 m (8,341 ft) AGL, with the Equilibrium Level (EL) calculated at approximately 10.76 km (35,300 ft) AGL. Little directional or speed shears were noted in the lowest 3 km.

The LI of -3 degrees, and the maximum vertical velocity of 39 m/s, was indicative of the potential for severe weather. In addition, the height of the wet-bulb zero level occurred within the most favorable layer, approximately 7,000 to 9,000 ft AGL, for large hail production (Miller 1972). These parameters led the forecaster/radar operator to determine that severe weather was possible over the eastern Colorado counties of Goodland's CWA.

The Goodland WSR-88D was operating in VCP 21, with the RPS list set to long range. The concentration of elevation scans provided by the long range RPS list was found to provide better coverage of these storms due to the distance from the radar (initially 83 to 148 km) and the low EL.

Between 2000 and 2022 UTC, one thunderstorm intensified as it moved east across Kit Carson County, Colorado, just south of Interstate 70. The mid-level LRM product from the 2022 UTC volume scan (Figure 3), which arrived at the Principal User's Processor (PUP) at 2029 UTC, indicated that the storm updraft (located to the south of Vona) had continued to increase in size and intensity (to 58 dBZ) from the previous volume scan. This increase alerted the radar operator to the intensity trend of the storm.

User functions that displayed and manipulated Base Reflectivity products in a four-panel format on the PUP were then employed. After analyzing the storm's structure, the decision to warn was made. The VIL for this thunderstorm increased as well during this volume scan, rising 6 kg/m2 from the previous scan, reaching 37 kg/m2 (Figure 4).

The 2028 UTC volume scan VIL graphic showed an increase to 47 kg/m2, indicating the reflectivity core had descended (Figure 5). The Base Reflectivity products from the 0.5 and 1.5 degree elevation scans (Figures 6 and 7) confirmed the lowering of the reflectivity core. The high VIL value also showed exactly where the largest hail fell from this storm (9 km southeast of Vona). The mid-level LRM displayed a slight decrease in reflectivities to 56 dBZ (Figure 8).

The 2034 UTC volume scan Base Reflectivity products recorded a return of 66 dBZ from the lowest level of the storm (Figure 9). This corresponded to a report of nickel-sized hail (2.25 cm) that occurred on a farm located 9 km southeast of Vona at 2035 UTC.

7. Conclusions from the April 20, 1994, Marginal Severe Weather Event

The mid-level LRM graphic, used in conjunction with Base Reflectivity products displayed and magnified through user functions, provided the necessary clues on storm structure and intensity trend for finalizing the warning decision process. The mid-level LRM graphic was very helpful in identifying which

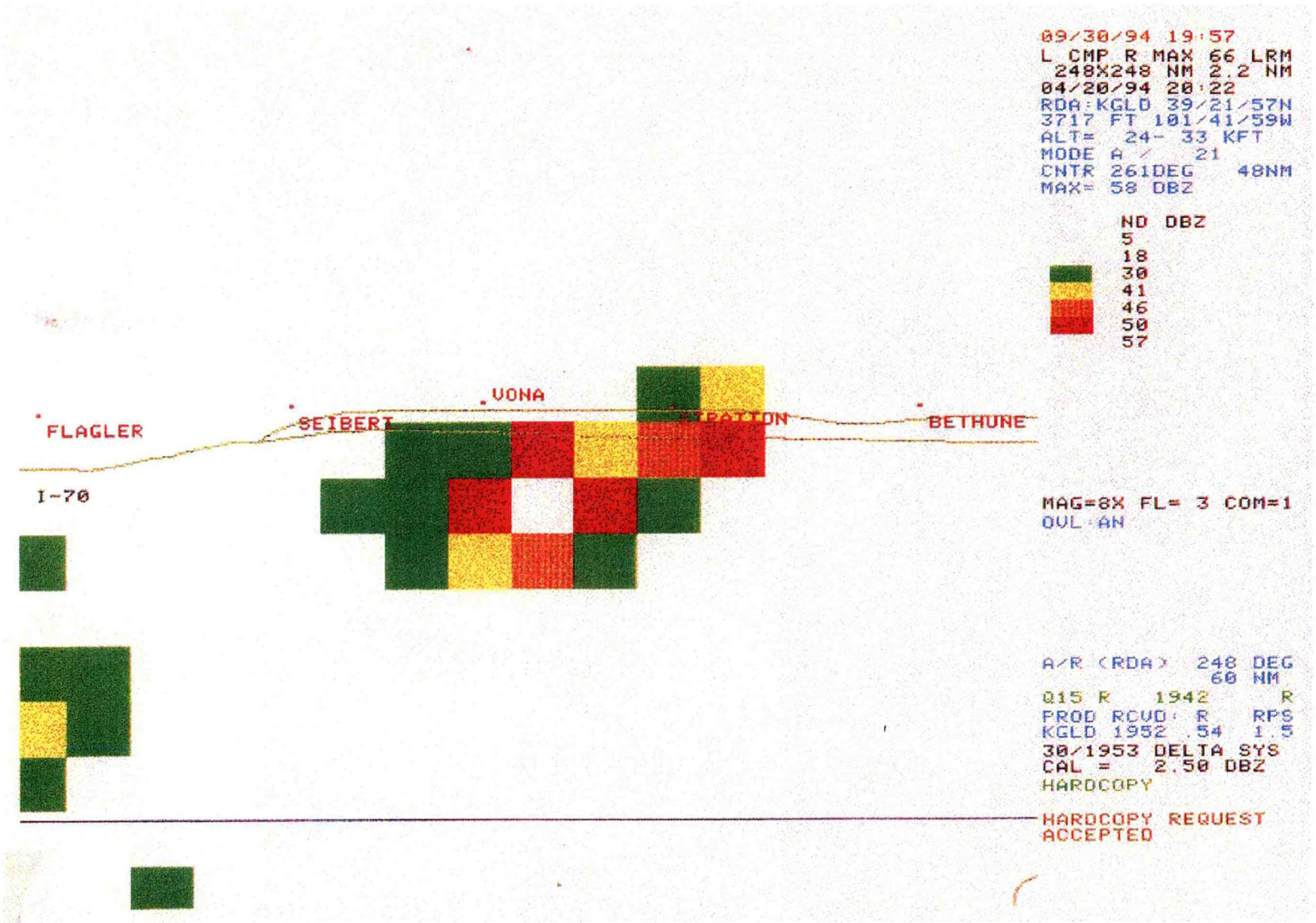

Figure 3. The mid-level LRM product from the 2022 UTC volume scan on 20 April 1994.

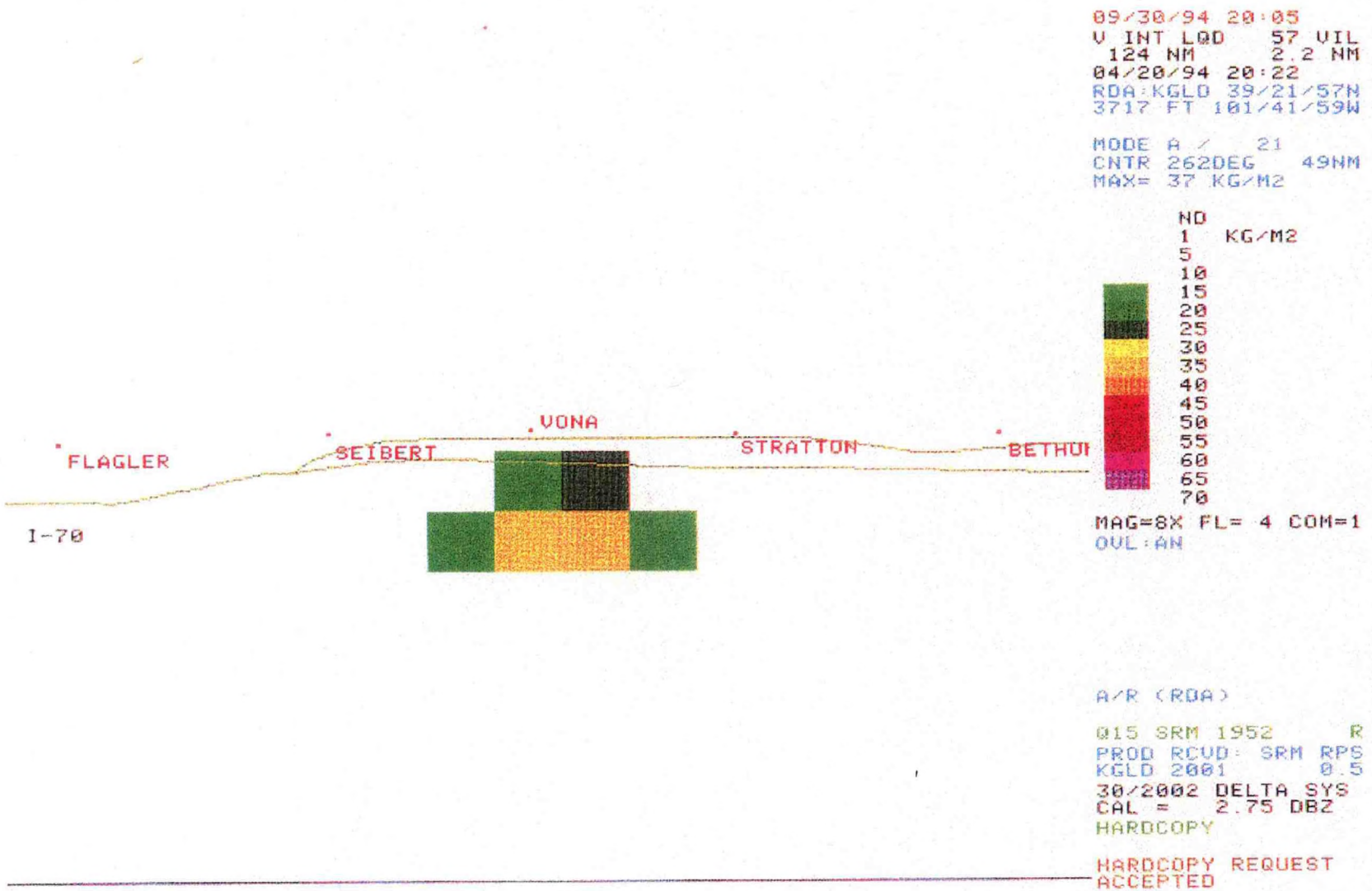

Figure 4. The VIL product from the 2022 UTC volume scan on 20 April 1994.

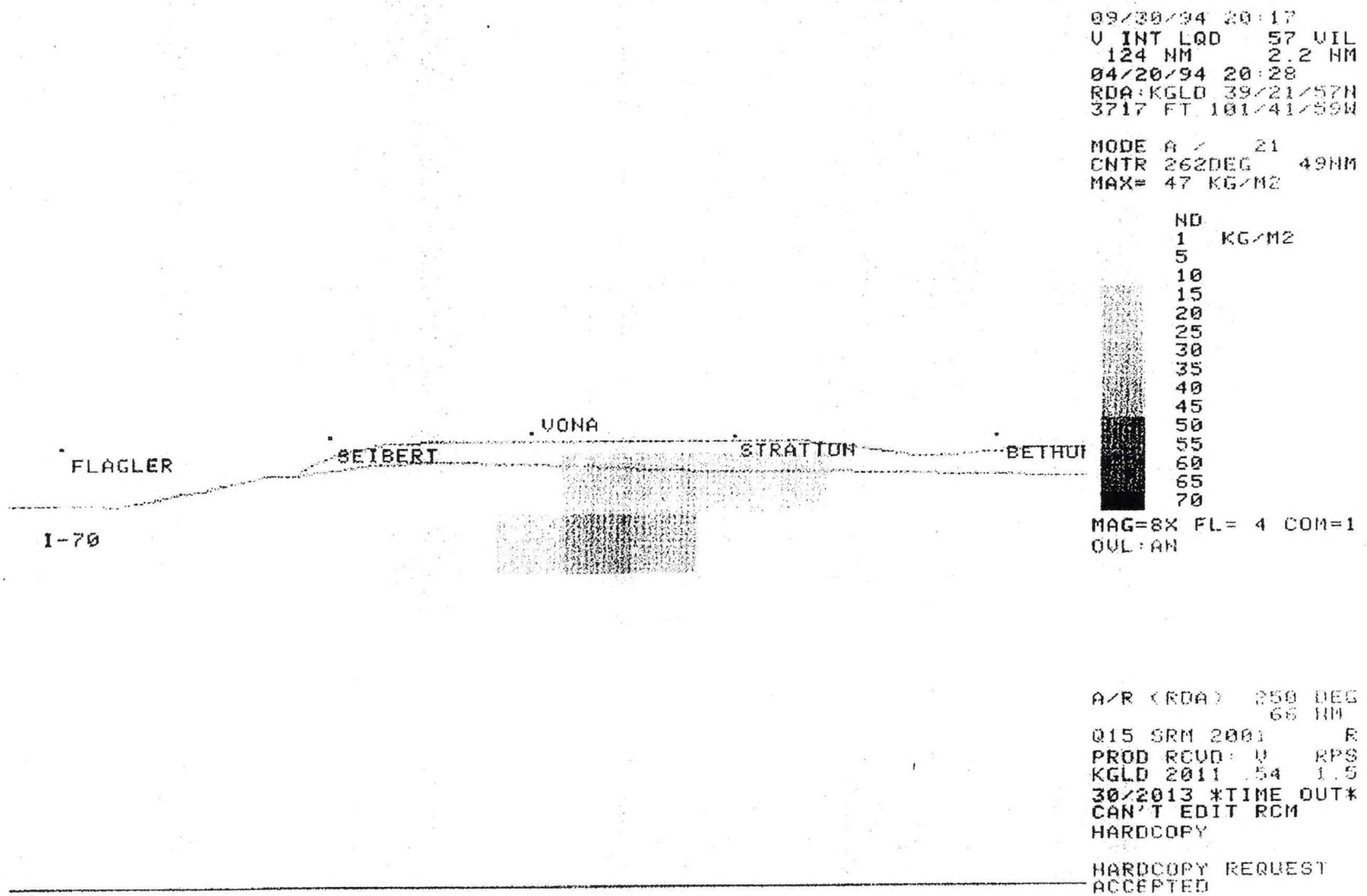

Figure 5. The VIL graphic from the 2028 UTC volume scan on 20 April 1994.

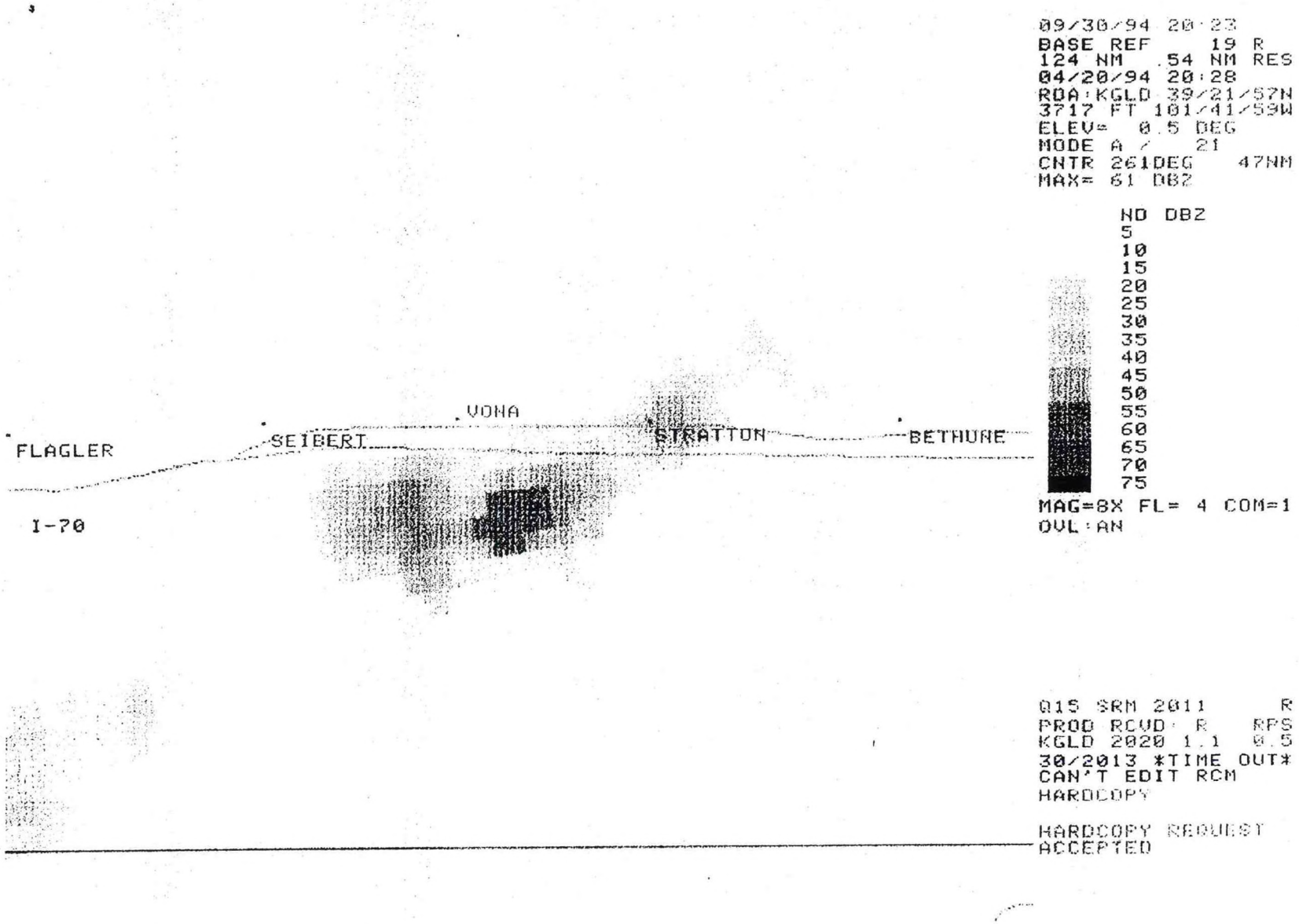

Figure 6. The 0.5 degree elevation angle Base Reflectivity graphic from the 2028 UTC volume scan from 20 April 1994.

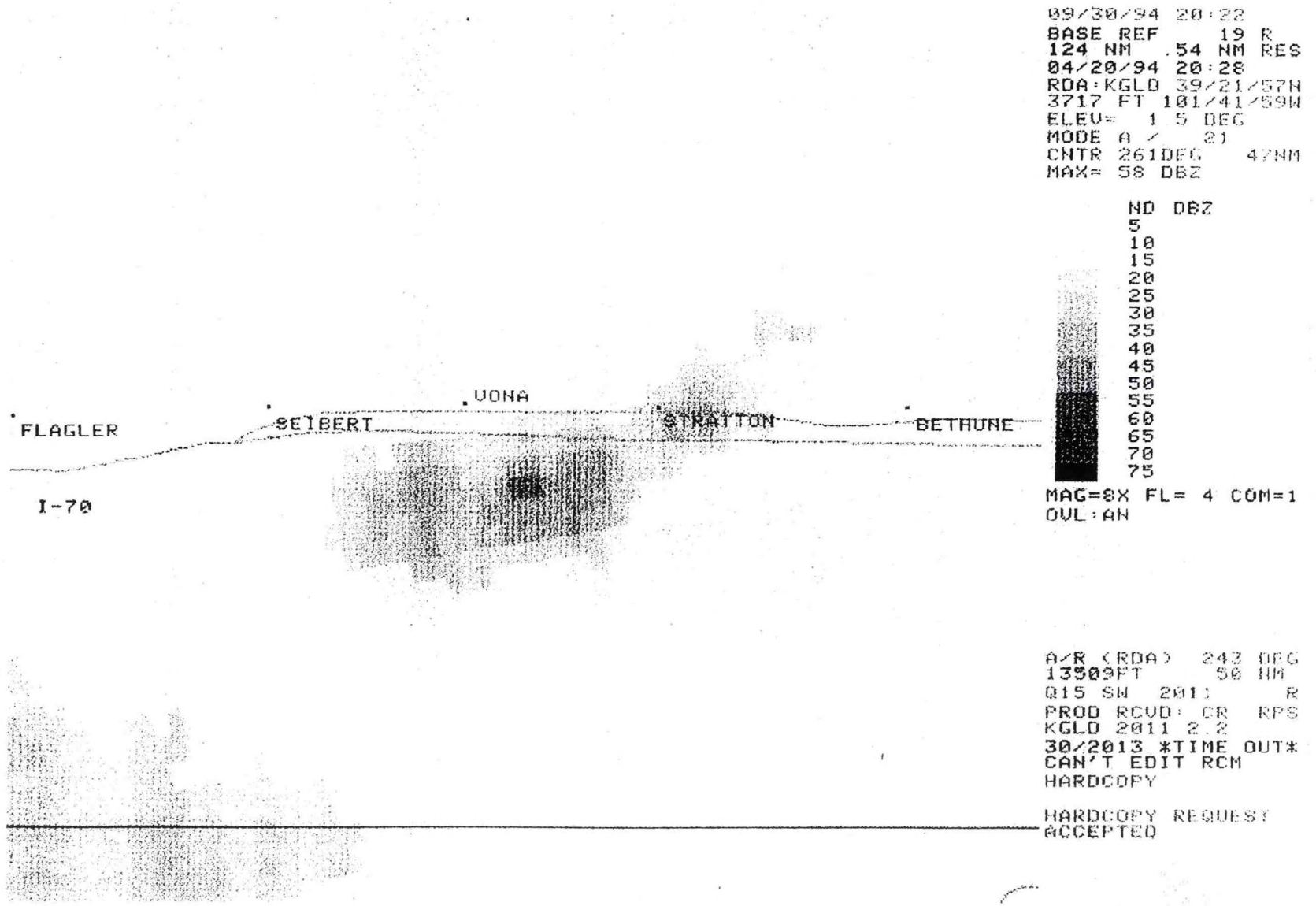

Figure 7. The 1.5 degree elevation angle Base Reflectivity graphic from the 2028 UTC volume scan from 20 April 1994.

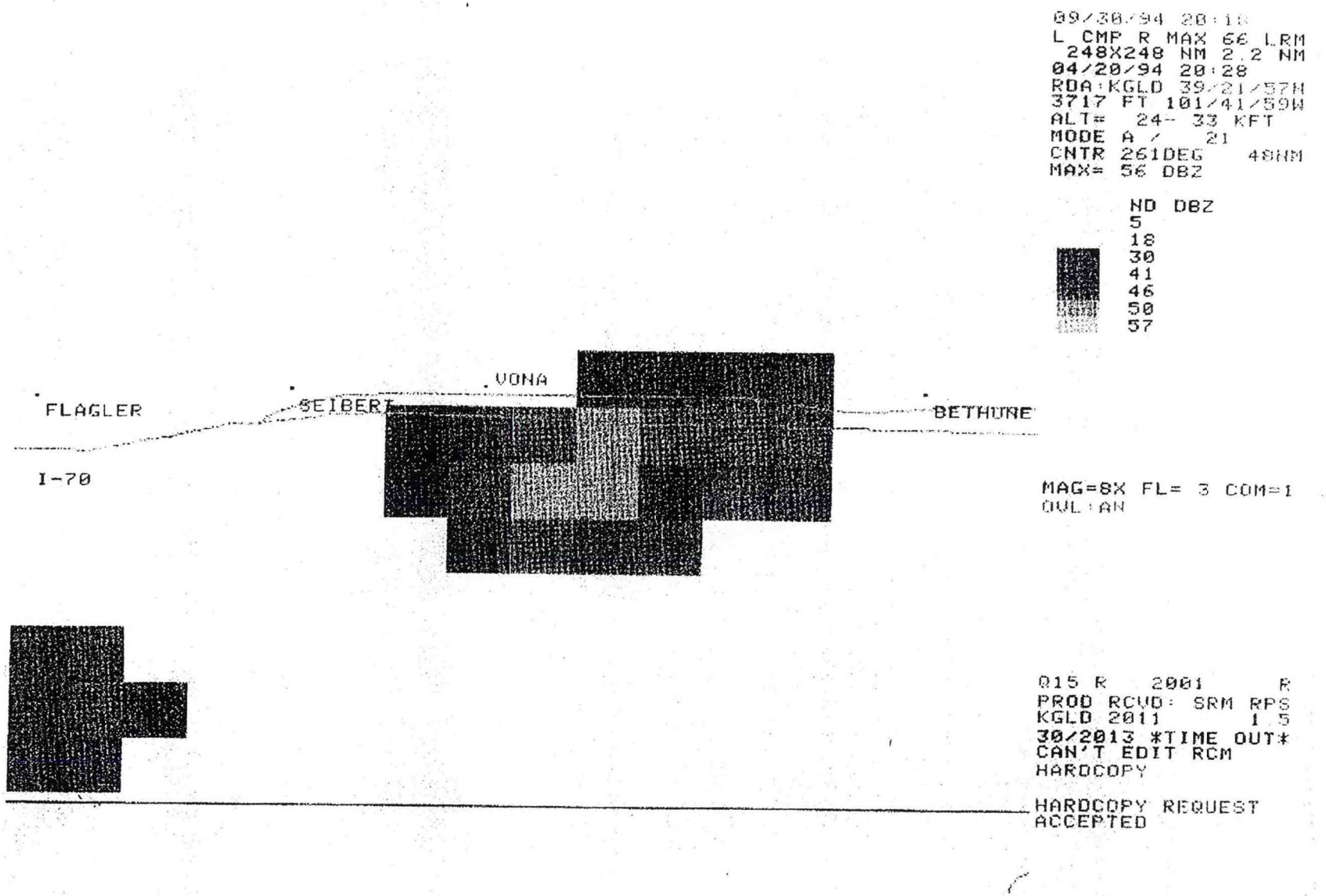

Figure 8. The mid-level LRM from the 2028 UTC volume scan from 20 April 1994.

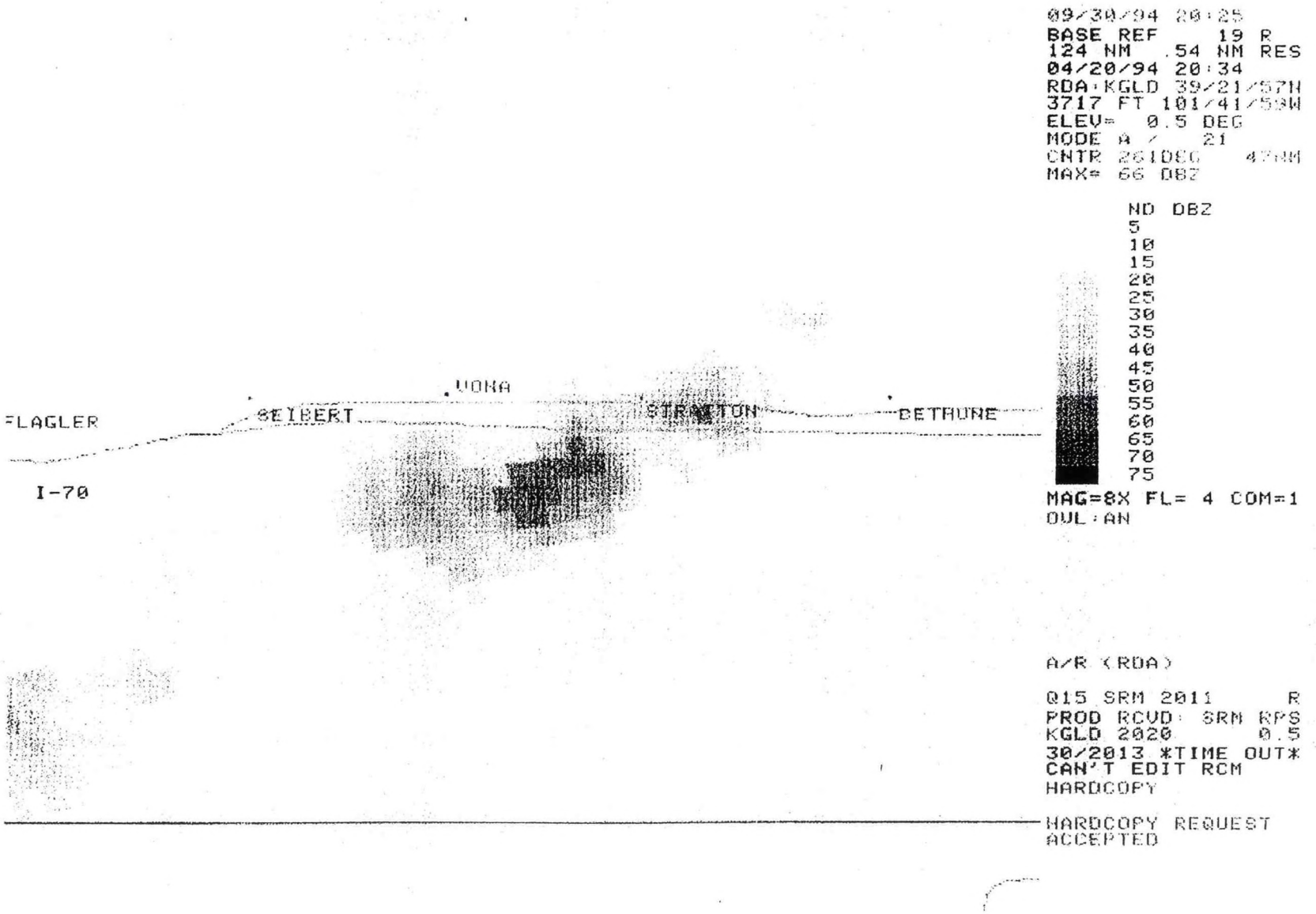

Figure 9. The 0.5 Base Reflectivity from 2034 UTC volume scan from 20 April 1994.

storms over eastern Colorado had the highest potential to produce severe weather. Used as a "first look" product, the mid-level LRM allowed the radar operator to concentrate on those storms that displayed the strongest returns in the mid levels.

The VIL product, on its own, was useful in finding where the largest hail had fallen from this storm, but failed as a predictor of severe weather. The VIL increase indicated in the 2022 UTC volume scan was not enough to alert the radar operator to the potential of severe weather. Waiting to issue the warning until the 2028 UTC volume scan VIL graphic was received (2035 UTC) would have resulted in a missed severe weather event.

8. Summary

The mid- and high-level Layer Composite Reflectivity Maximum products should help WSR-88D operators quickly and efficiently identify those thunderstorms that have the greater potential to produce severe weather. The LRM products are easily interpreted, and when combined with other WSR-88D graphics, can provide clues to a storm's updraft strength and intensity trend. The LRM products also have distinct advantages over other "first look" WSR-88D generated graphics.

9. Acknowledgements

The author wishes to express his appreciation to John Kwiatkowski, Science Operational Officer (SOO), and Dennis Hull, Warning Coordinator Meteorologist (WCM), for the extensive technical input on this paper. Special thanks to Greg Jackson, Meteorologist, for the excellent graphics he produced, and Llyle Barker, Meteorologist, for the many helpful suggestions. In addition, I want to thank Lynn DiPlacito, Secretary, for the grammatical review of this paper.

10. References

Chisholm, A.J., and J.H. Renick, 1972: The kinematics of multicell and supercell Alberta hailstorms. Alberta Hail Studies, Research Council of Alberta Hail Studies, Report No. 72-2, Edmonton, Canada.

Hart, J.A., and J. Korotky, 1991: The SHARP workstation v1.50 user's manual. DOC, NOAA, National Severe Storms Forecast Center, Kansas City, MO, 30pp.

Lemon, L.R., 1980: Severe thunderstorm radar identification techniques and warning criteria. NOAA Technical Memorandum NWS NSSFC-3, DOC, NOAA, National Severe Storms Forecast Center, Kansas City, MO, 60pp.

Miller, R.C., 1972: Notes on the analysis and severe-storm forecasting procedures of the Air Force Global Weather Central. Tech. Report 200 (rev.), U.S. Air Force, 181 pp.

NEXRAD Joint System Program Office, 1986: Next generation weather radar product description documents. DOC, NOAA, NWS, 121 pp.

Operational Support Facility, 1993: WSR-88D Operations Training Manual, Topic 8. Operations Training Branch, DOC, NOAA, NWS, Norman, OK.

Wilk, K., L.R. Lemon, and D.W. Burgess, 1979: Interpretation of radar echoes from severe thunderstorms: A series of illustrations with extended captions. Prepared for training of FAA ARTCC Coordinators, National Severe Storms Laboratory, Norman, OK, 55 pp.

CENTRAL REGION APPLIED RESEARCH PAPER 14-02

A 10-YEAR CLIMATOLOGICAL STUDY OF DENSE FOG OCCURRENCES IN ROCHESTER, MINNESOTA

Robin L. Teske
and
Jonathan C. Fox
National Weather Service Office
Rochester, Minnesota

1. Introduction

Fog, particularly when it is dense, is one of the most common and persistent weather hazards encountered in aviation. The rapidity at which fog sometimes forms makes it even more hazardous, especially during a plane's takeoff or landing. The accurate forecasting of dense fog is not only vital for pilots' safety, but also for the smooth operation of the airports. The formation of dense fog can limit visibilities below the minimum values established by airports, thus restricting landings and departures. These aeronautic delays can lead to an increase in airline fuel consumption, additional financial costs and many other problems. By studying the records of dense fog and its characteristics, forecasters may be able to produce more accurate fog predictions for both the airports and pilots.

2. Fog Definitions

Fog is defined as a hydrometer consisting of a visible aggregate of minute water droplets suspended in the atmosphere, near the earth's surface, which can reduce horizontal visibility to several hundred feet (Huschke 1986). Simply put, fog is a cloud whose base rests on the ground. Dense fog is defined as a reduction of the horizontal visibility by fog to less than 5/16 of a mile (NWS 1988).

The formation of fog occurs when air near the earth's surface becomes saturated in a stable environment. Cooling the air temperature, coupled with the evaporation of water vapor into the air, is one method that leads to the development of fog. Turbulence and mixing of the air can prevent a shallow layer of cool, moist air from forming near the surface; therefore, light winds are typically favored for fog development (Wallace & Hobbs 1977).

There are many distinct fog producing processes that will be touched upon in this study, in which most are interwoven processes. Radiation fog is the most common, where on a clear, calm night, radiational cooling decreases the air temperature to its dew point. Advection fog occurs when warm, moist air is cooled to saturation as it flows over a colder surface; this can happen over land or water. Upslope fog forms when moist, stable air is cooled adiabatically to saturation as it is lifted orographically (Petterssen 1956).

3. Methodology

In the past ten years, dense fog has been reported at the National Weather Service in Rochester an average of 28 days each year. During this period, the greatest number of days with dense fog occurred in 1992, when a total of 46 days had reports of visibilities with less than 5/16 of a mile. Since 1984, the fewest number of days with dense fog occurred during the drought year of 1988 with only 16 days. Nonetheless, dense fog is a weather phenomenon that periodically affects the Rochester area and most of the time, develops rapidly. Naturally, this has a dramatic and costly impact on the aviation industry at the Rochester Municipal Airport.

The National Weather Service is housed at the Rochester Municipal Airport, which is perched upon a ridge approximately 300 feet higher in elevation than the city of Rochester. The highest point on airport grounds is 1320 feet; the airport is eight miles south of the city. The terrain surrounding the airport is characterized as rolling, ranging from level farm fields to abrupt bluffs and ravines carved out by small streams. This is considered typical topography for southeast Minnesota. There are no large water bodies, lakes, or bog areas within the immediate vicinity of the airport (Figure 1). This leads to the mystery on how and why dense fog periodically develops and persists in the Rochester Airport area.

This 10-year investigation into the occurrences of dense fog at the Rochester Municipal Airport was broken down regarding the time of year, time of day, and wind direction and speed. Each hourly and special observation since 1984, when fog reduced the visibility of less than 5/16 of a mile, was recorded, along with the reported wind speed and direction. This exhaustive amount of data was then entered into a spreadsheet, where calculations and statistics could be completed. The findings from this fog investigation were, for the most part, explainable; however, some unique and local characteristics also emerged.

4. Dense Fog vs. Time of Year

Just over 42 percent of the total dense fog observations occurred during the months of December through February. During the spring months of March through May, 28 percent of the dense fog observations were recorded. Twenty

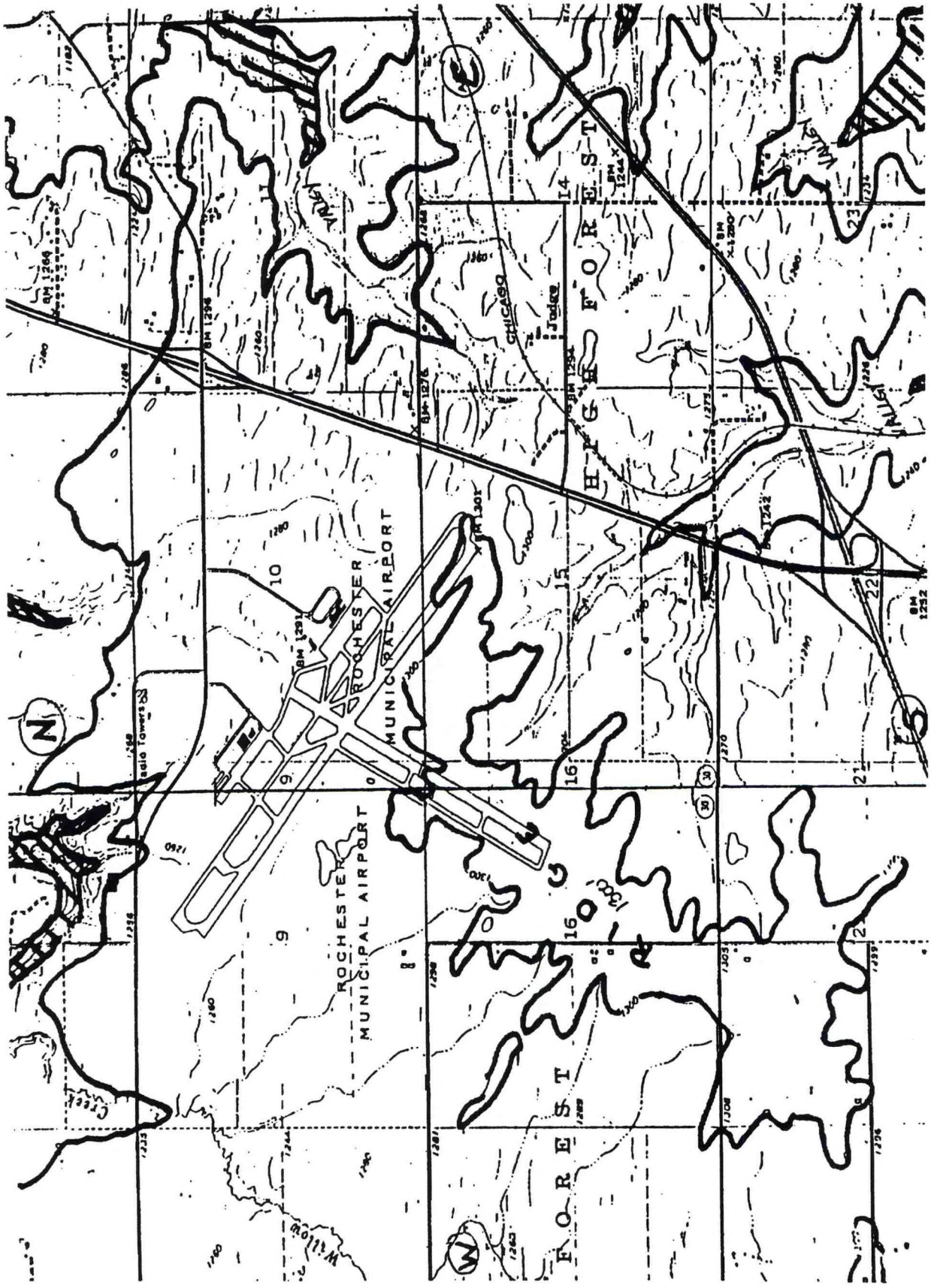

Figure 1. Topographical map of the area surrounding the Rochester Municipal Airport.

percent of the observations occurred during the autumn months of September through November. The fewest occurrences of dense fog at the Rochester Municipal Airport were during the summer. Only 9 percent of the total dense fog observations were during the months of June through August (Graph A). One reason for this annual distribution can be attributed to the long nights of the winter, early spring, and late autumn, which are conducive to increased radiational cooling. This extensive period of cooling obviously will lead to a longer diurnal temperature decline, which in turn will more readily produce saturation; fog.

1984-1993 dense fog occurrences
(by season)

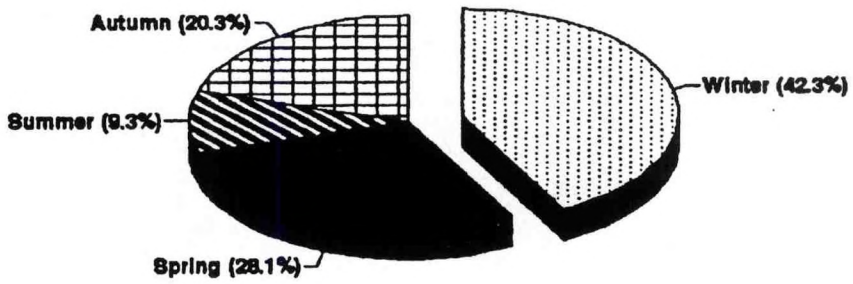

Graph A: Distribution of dense fog observations by *meteorological season.* Includes all hourly and special observations with visibilities < 5/16 mile due to fog. (Winter: December, January, February; Spring: March, April, May; Summer: June, July, August; Autumn: September, October, November.)

Besides long nighttime hours, a snow cover may also be an important factor to the development of dense fog. In Rochester, the snow season can typically last from November to March. Comparing the number of dense fog observations when snow covered the ground versus when the ground was free of snow, the results were simply astounding. More than 70 percent of the dense fog observations occurred when the ground was snow covered (Graph B). Snow is an excellent absorber of long wave radiation from the ground below, and thus amplifies nocturnal cooling, compared to that of bare ground. Also, a blanket of snow creates a cold surface that can cool moist air to condensation, promoting the development of advection fog. Snow cover is a readily available source of water vapor that can lead to saturation of the air immediately above it. Examples include addition of moisture due to melting and sublimation. This moisture can then remain trapped in a shallow layer near the earth's surface when an inversion exists to promote fog formation.

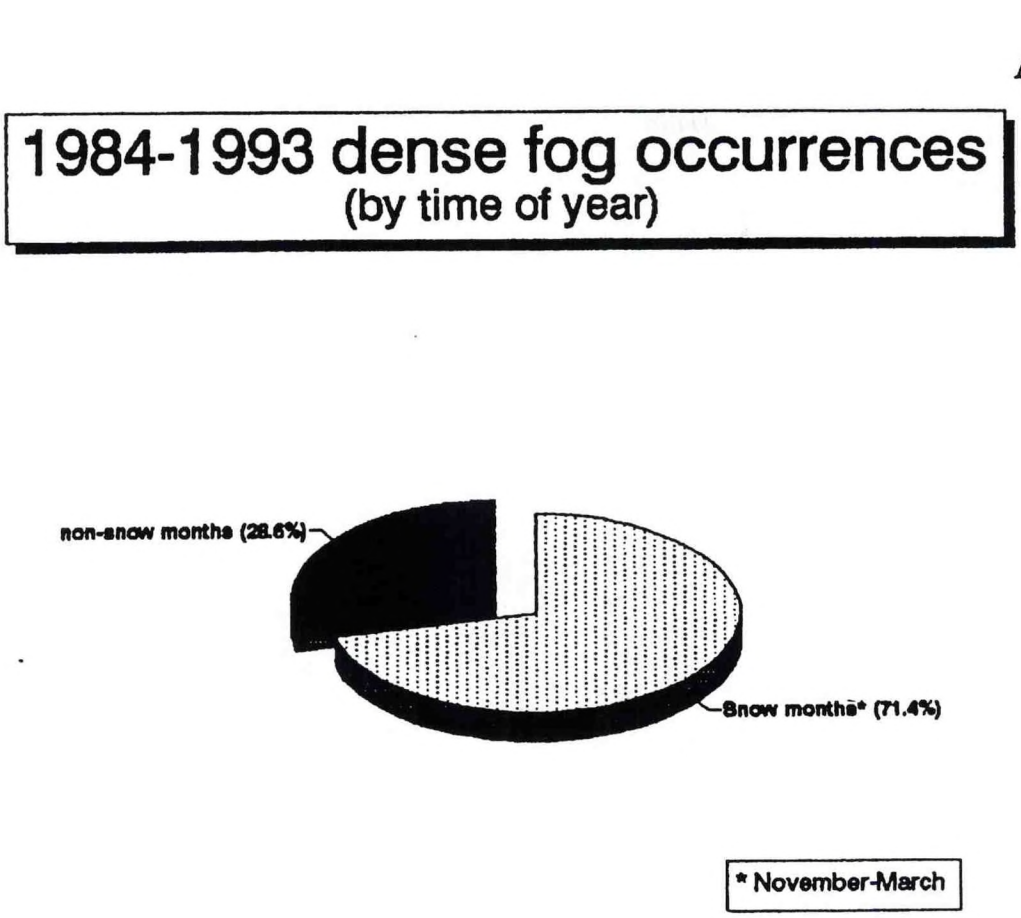

Graph B: Distribution of dense fog observations comparing the influence of *snow cover vs. without snow cover.* Includes all hourly and special observations with visibilities < 5/16 mile due to fog. Snow season typically spans from November through March.

5. Dense Fog vs. Time of Day

Half the dense fog observations were reported between the hours of 1:00 a.m. to 8:00 a.m.. The fewest number of dense fog observations, 14 percent, occurred during the hours between noon and 7:00 p.m. (Graph C). This diurnal variation in dense fog occurrences is due simply to the diurnal temperature variations; fog normally forms during the cool nighttime hours. Once the sun rises, solar heating will increase the air temperature. As the air temperature increases, so will the air's capacity to hold water vapor, and then there is no longer enough water vapor to saturate the air. The best time for dense fog to occur was right near sunrise between the hours of 5:00 a.m. and 7:00 a.m. (Graph D). Typically right before dawn, the air temperature reached their lowest level.

6. Dense Fog vs. Wind

When investigating the prevailing direction of the wind when dense fog occurred, the results were conclusive. Winds out of the south to southeast were reported in 40 percent of the dense fog observations at the Rochester Municipal

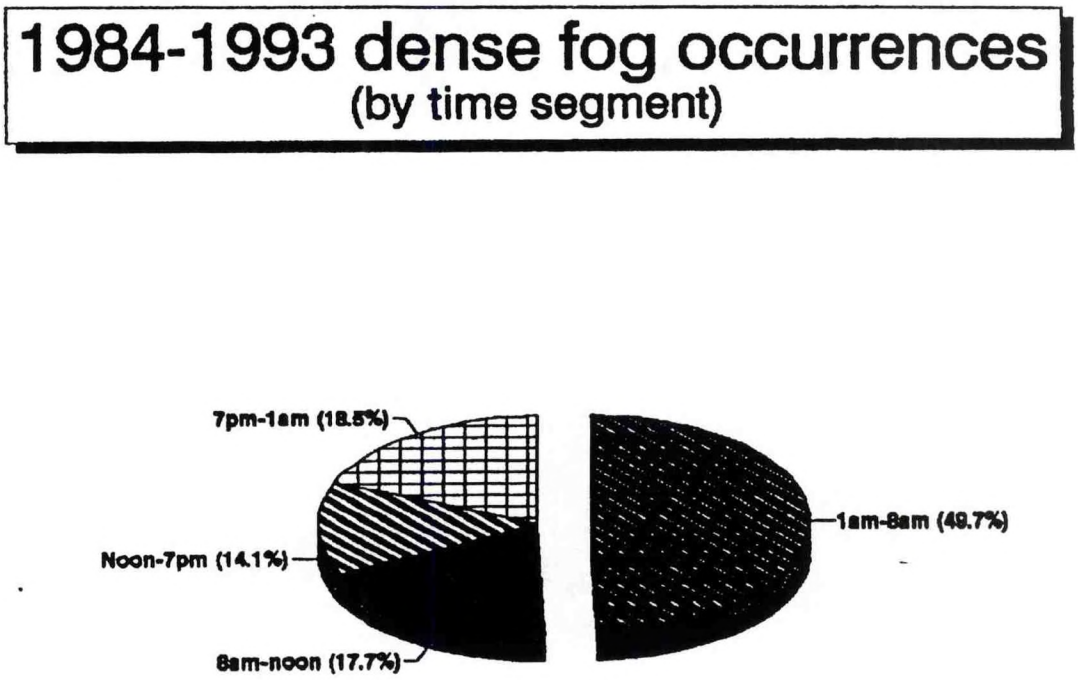

Graph C: Distribution of dense fog observations by *time segment* in a 24-hour day. Includes all hourly and special observations with visibilities < 5/16 mile due to fog.

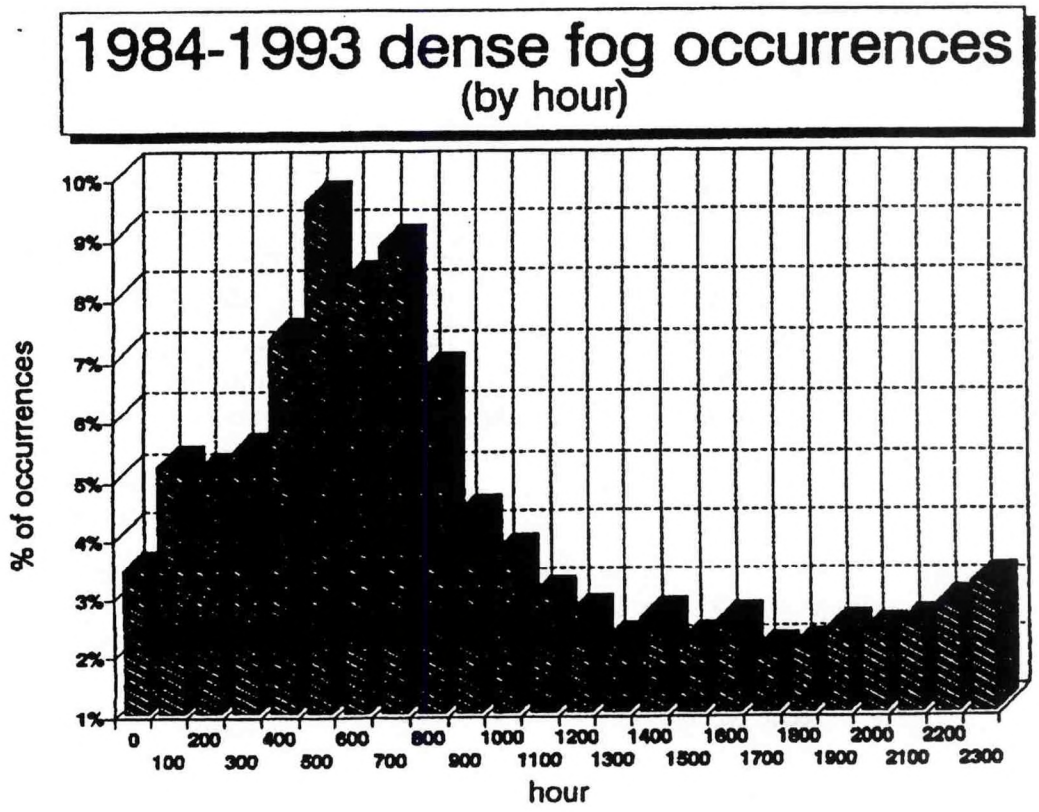

Graph D: Distribution of dense fog observations by *individual hour.* Includes all hourly and special observations with visibilities < 5/16 mile due to fog.

Airport. This suggested a trajectory flow of warm, moist air from the south over the cooler climes of southern Minnesota, which lead to greater occurrences of advection-type fog. The least likely wind direction to accompany a dense fog observation would be a dry flow from the southwest with only 7 percent of the occurrences (Graph E).

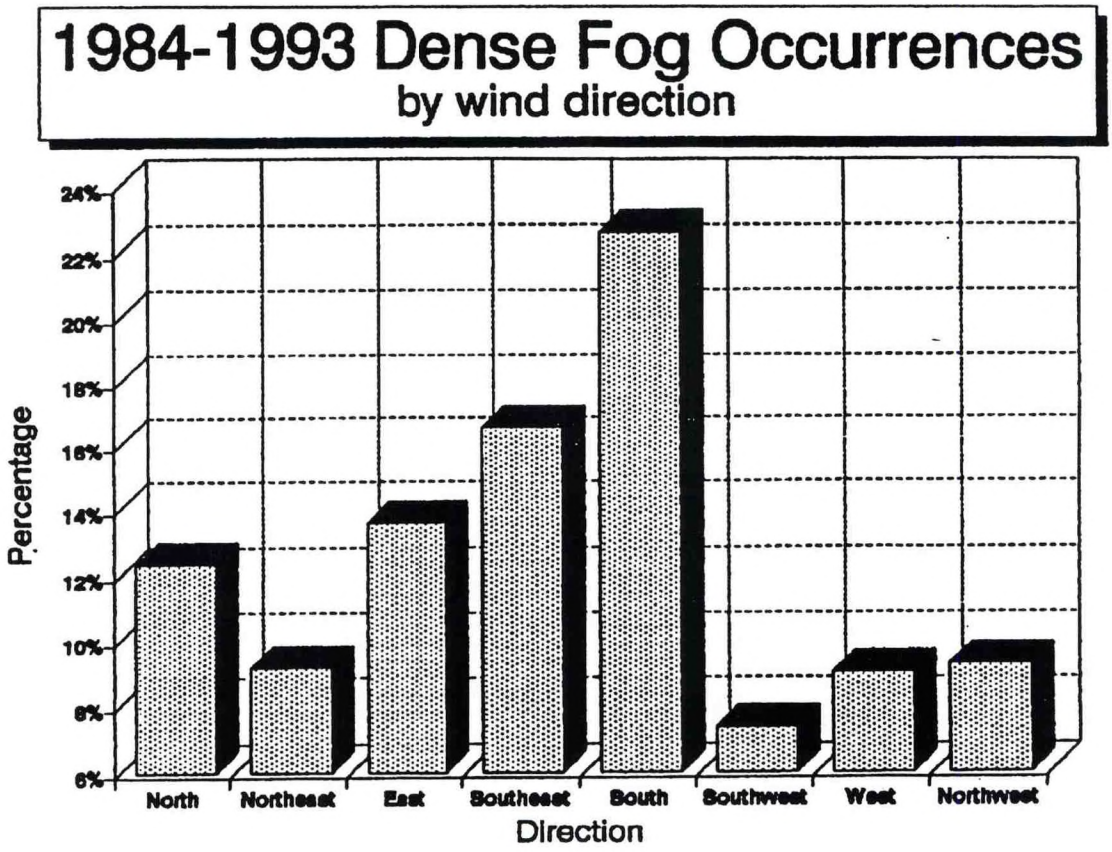

Graph E: Distribution of dense fog observations by *wind direction.* Includes all hourly and special observations with visibilities < 5/16 mile due to fog.

The most interesting aspect of this study was revealed when investigating dense fog occurrences as compared to the prevailing wind speed. Rochester Airport has always had a history of having gusty winds. The wind speed that accompanied the most occurrences of dense fog was eight knots (9 mph) (Graph F). When comparing wind speed groupings, wind speeds of 8 to 14 knots (9 to 16 mph) was found in 57 percent of the dense fog observations at the Rochester Municipal Airport (Graph G). Radiation fog is highly sensitive to wind speeds, usually leading to the development of fog when wind speeds range from 3 to 7 knots. With these new found facts, it appears that the development of radiational fog is not the main source of dense fog at the Rochester Airport. This leads to the belief that most of the fog occurrences are mainly advection fog or possibility a combination of advection/upslope fog, due to the favored high wind speeds at the Rochester Airport.

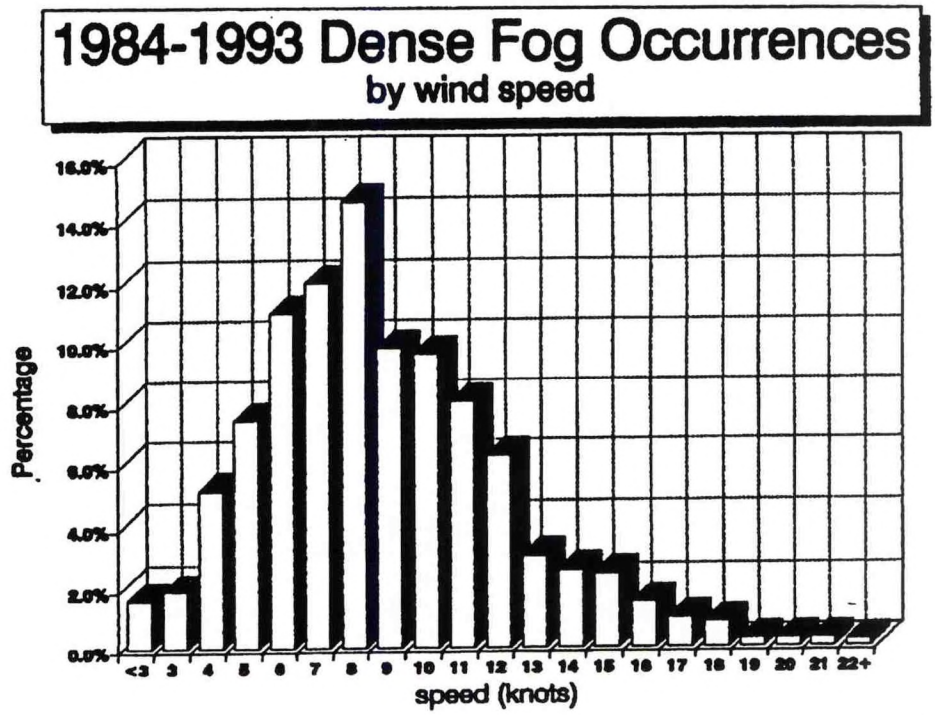

Graph F: Distribution of dense fog observations by *wind speed.* Includes all hourly and special observations with visibilities < 5/16 mile due to fog.

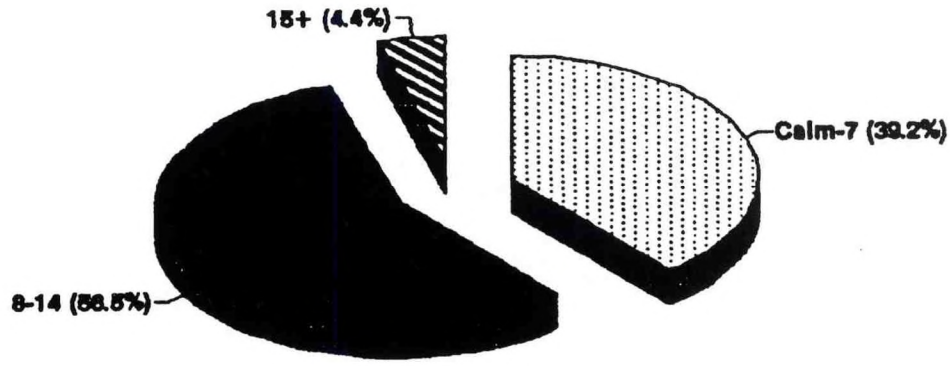

Graph G: Distribution of dense fog observations by *wind speed groupings.* Includes all hourly and special observations with visibilities < 5/16 mile due to fog.

There also was some topographical influence on the fog formation as well. The Rochester Airport sits upon the highest elevation in the local vicinity. For the most part, the topographical slope is small; however, to the south and southeast, the land dips approximately 100 feet in less than a mile (Figure 1). With the predominant wind flow emanating from the south to southeast, dense fog may have also formed when relatively warm, moist air was forced orographically up the ridge to the Airport. It is local knowledge that of times when dense fog persists at the Airport, a deck of low stratus with unrestricted surface visibilities will frequently be seen in the city of Rochester, eight miles to the north and almost 300 feet lower in elevation.

7. Summary and Conclusion

We conclude from this study that advection plays an important role in the creation of dense fog at the Rochester Airport. With the peak time of the day for dense fog ranging from 5:00 a.m. to 7:00 a.m., this would lend some credence that radiation fog often acts in tandem with advection to create the dense fog. There is also a hint of an orographic influence with the dense fog occurrences, simply due to the varying topography surrounding the Rochester Municipal Airport.

As guidance to produce better forecasts for dense fog at the Rochester Municipal Airport, here are a few clues to look for:

A. During the winter and early spring, snow cover leads to an increased frequency of dense fog formation.

B. Dense fog is most likely to form between the hours of 1:00 a.m. to 8:00 a.m. with the peak time right near sunrise.

C. A wind out of the south to southeast is the favorable trajectory for dense fog formation.

D. Wind speeds of 8 to 14 knots accompanied more than half of all dense fog occurrences.

Hopefully this fog distribution study will lead to a greater accuracy for forecasting this unique site in southeast Minnesota.

8. References

Huschke, R.E., 1986: *Glossary of Meteorology.* American Meteorological Society, Boston, MA, 638pp.

Federal Aviation Administration/ National Weather Service, 1975: *Aviation Weather.* FAA/NWS, Silver Spring, MD, 257pp.

National Weather Service,, 1988: *Federal Meteorological Handbook No. 1. Handbook of Surface Observations.* Government Printing Office (GSA), Silver Spring, MD, pp. A7-6-A7-7.

Petterssen, S., 1956: *Weather Analysis and Forecasting.* McGraw-Hill, New York, NY, 428pp.

Wallace, J.M., Hobbs, P.V., 1977: *Atmospheric Sciences, An Introductory Survey.* Academic Press, Inc., New York, NY, 467pp.

CENTRAL REGION APPLIED RESEARCH PAPER 14-03

A COMPARISON BETWEEN MANUAL OBSERVATIONS AND ASOS OBSERVATIONS FOR WSO HURON, SOUTH DAKOTA

Daniel P. Mohr[1]
National Weather Service Office
Huron, South Dakota

1. Introduction

Before commissioning the Automated Surface Observing System (ASOS) at Huron, South Dakota, a comparison was necessary between manual observations and the ASOS observations. The comparison was achieved by using 100 standard hourly observations for the following dates (Table 1):

Table 1
Observations compared (TA and TS=ASOS, SA and RS=Manual).
Most remarks were left out when transcribing observations.
Time is in CST.

AUGUST 26, 1993
TA 1456 14 SCT 10+ 147/74/67/MM/999
SA 1450 16 SCT 75 SCT E250 BKN 15 149/73/67/3312/999
TA 1556 M14 OVC 10+ 149/70/65/MM/999/ OVC V BKN
SA 1552 16 SCT E250 BKN 15 151/72/66/3312/000
TA 1656 M14 OVC 10+ 156/68/64/MM/001
RS 1651 M13 OVC 12 161/69/64/3513/002
TA 1756 M14 OVC 10+ 161/67/62/MM/002
SA 1752 M15 BKN 75 OVC 12 167/68/63/3412/004
TS 1856 14 SCT M70 OVC 10+ 165/65/63/MM/003
RS 1851 16 SCT M75 OVC 10 170/65/63/3212/004
TA 1956 M80 OVC 5RF 154/63/62/MM/000
SA 1950 19 SCT M80 OVC 7RW- 159/64/63/0209/001
TA 2056 M110 OVC 10+ 160/63/62/MM/002
SA 2052 20 SCT M110 OVC 10 164/64/63/3209/003
TA 2156 CLR BLO 120 10+ 167/63/61/MM/004
SA 2150 21 SCT E120 OVC 10 169/64/62/3407/005

[1]Current affiliation, NWS Office Aberdeen, South Dakota.

SEPTEMBER 07, 1993
TS 0556 1 SCT 6 SCT M100 BKN 1/4F 218/45/45/MM/017
SA 0550 100 SCT 1F 223/46/45/0203/019/VSBY S-SW 6

SEPTEMBER 12, 1993
TA 0056 M15 BKN 23 OVC 10+R- 064/57/53/MM/973
SA 0050 M15 OVC 7RW- 071/57/53/3009/975
TA 0156 38 SCT M45 BKN 100 OVC 5RF 057/54/52/MM/971
RS 0150 M20 BKN 40 OVC 7R 062/54/52/0213/973
TA 0256 M41 BKN 55 OVC 10+ 019/52/50/MM/960
RS 0251 20 SCT M40 OVC 7 026/53/51/3617G33/962
TS 0856 11 SCT M17 OVC 7R- 111/43/41/MM/986
SA 0851 11 SCT M15 OVC 4R- 115/43/41/3217/987
TS 0956 10 SCT M15 OVC 5RF 103/43/41/MM/983
SA 0951 11 SCT M15 OVC 4R- 103/43/41/3221/983

SEPTEMBER 19, 1993
TA 0656 M9V BKN 19 OVC 3RF 121/53/53/MM/989/ CIG 6V12
RS 0650 M8 BKN 21 OVC 2R-F 128/54/53/1114/990
TA 0756 9 SCT M17 OVC 21/2RF 118/54/53/MM/987/ OVC V BKN
SA 0750 M9 BKN 19 OVC 2RWF 123/54/53/0914/989
TA 1156 9 SCT M17 BKN 30 OVC 13/4RF 102/54/54/MM/983
RS 1151 8 SCT M13 OVC 3RWF 109/55/54/0814/984
TA 1756 M5V BKN 9 OVC 1R+F 070/57/57/MM/974/ CIG 2V7
RS 1753 M3 BKN 25 OVC 1RW+F 076/57/57/1108/975

SEPTEMBER 20, 1993
TA 0056 3 SCT M7 OVC 31/2R-F 088/53/52/MM/979
RS 0052 M7 OVC 2L- 092/53/53/3312/979
TS 0756 M6 OVC 7 135/51/50/MM/992
SA 0750 M5 OVC 10 138/52/50/3212/993

SEPTEMBER 21, 1993
TA 0156 CLR BLO 120 5F 178/47/46/MM/004
SA 0151 CLR 6F 184/46/46/1506/006
TA 0556 4 SCT 4F 159/48/47/MM/999
RS 0551 1 SCT 250 -SCT 3F 163/48/48/1410/000
TA 0656 M4 OVC 31/2F 157/49/48/MM/998
SA 0650 -X M4 BKN 250 BKN 3F 161/49/48/1411/000/F1
TA 0756 M4 BKN 4F 145/51/50/MM/995
RS 0751 M5 BKN 250 OVC 4F 152/51/50/1416/997
TA 0856 8 SCT 7 133/54/52/MM/992
RS 0852 8 SCT E100 BKN 250 BKN 7 138/55/52/1418/993

SEPTEMBER 22, 1993
TS 0056 2 SCT 5F 145/56/55/MM/996
RS 0050 CLR 4F 151/57/56/3311/998/FEW ST 2 HND

SEPTEMBER 25, 1993
TS 0656 CLR BLO 120 3/4F 114/39/39/MM/985
SA 0651 CLR 6F 119/39/39/1104/987/ FEW AC E-SE

OCTOBER 15, 1993
TS 0656 M5 BKN 40 OVC 5F 107/49/47/MM/983
RS 0651 M5 OVC 7 111/49/47/1003/985
TA 0756 M3 OVC 31/2F 107/50/50/MM/984
RS 0751 M3 BKN 13 OVC 3F 109/51/50/1305/984
TA 1256 M3 OVC 5F 104/53/52/MM/982
SA 1251 M5 OVC 6F 108/54/52/3005/983
TA 2256 M1 BKN 9 OVC 1/4F 126/41/41/MM/989
RS 2250 -X M1 BKN 9 BKN 1F 131/40/40/2805/990/F6
TA 2356 W2X <1/4F 124/41/41/MM/988
SA 2352 W2 X 1/8F 131/40/40/2403/990

OCTOBER 16, 1993
TS 0056 W1X 1/4F M/M/M/MM/989
SA 0050 W2 X 1/4F 132/43/43/2804/990
TA 0356 W1X 1/4F M/M/M/MM/991
SA 0350 W1 X 1/8L-F 135/45/45/2203/992
TA 0656 W1X 1/4F 140/44/44/MM/993
SA 0650 W4 X 1/4F 144/45/45/3505/994
TA 0856 M1 OVC 1/4F 145/44/44/MM/996/ BKN V OVC
SA 0852 M1 OVC 1/4L-F 150/45/45/3109/995
TS 1356 11 SCT 21 SCT M32 OVC 4F M/52/48/MM/995
SA 1354 9 SCT M15 BKN 30 OVC 5F 155/53/49/3606/997
TA 1456 M38 BKN 4F M/51/47/MM/994
SA 1451 15 SCT 30 SCT M40 OVC 4F 151/52/48/3609/996

OCTOBER 17, 1993
TS 0456 6 SCT M16 OVC 5F 135/45/44/MM/991
SA 0450 8 SCT M15 OVC 6F 139/46/44/2204/993
TA 0856 5 SCT M22 BKN 38 OVC 3F 136/48/45/MM/991
RS 0850 7 SCT M23 BKN 37 OVC 3F 142/48/46/2004/993
TS 2056 CLR BLO 120 3/4F 138/40/40/MM/992
RS 2050 -X 11/2F 144/43/43/0000/993/F1
TS 2256 1 SCT M33 OVC 1/2F 139/39/39/MM/992
SA 2251 W1 X 1/4F 146/39/39/1103/994
TA 2356 W1X 1/4F 141/37/37/MM/993
RS 2352 -X 1/4F 146/37/37/0000/994/F7

OCTOBER 18, 1993
TA 0056 1 SCT M36 BKN 1/2F 145/36/36/MM/994
RS 0052 -X 1 SCT 1F 150/37/37/0000/996/F1
TA 0156 M1 BKN 6 OVC 1/4F 146/36/36/MM/994
SA 0150 -X 1/4F 151/36/36/0103/996/F8
TA 0356 M39 OVC 1/4F 147/37/37/MM/995
SA 0353 -X M40 BKN 1/8F 154/37/37/0000/997/F7
TS 0456 M1 BKN 43 OVC 1/2F 150/37/37/MM/996
SA 0451 -X M44 BKN 1/2F 156/38/38/0000/997/F4
TA 0856 W1X <1/4F 166/41/41/MM/999
SA 0850 W1 X 1/8F 171/42/42/1705/001
TA 1056 M1 OVC 4F 165/49/49/MM/000
SA 1050 M3 BKN 5F 171/49/48/1405/001
TA 1156 CLR BLO 120 10+ 161/57/50/MM/999
SA 1150 9 SCT 120 SCT 250 -BKN 10 166/58/50/1507/000

NOVEMBER 12, 1993
TA 1256 M32 BKN 42 OVC 3RF 070/34/30/0812/969
SA 1251 20 SCT M33 OVC 7R- 077/34/30/0811/971
TA 1356 M24 OVC 2RF 046/33/31/0414/962
RS 1353 3 SCT M24 OVC 21/2R-F 054/33/32/0511/964
TS 1556 M12 OVC 13/4R+F 022/34/32/0710/955
RS 1550 3 SCT M11 OVC 11/2RF 025/34/34/0713/956
TS 1656 M10V OVC 3RF 018/34/32/0710/954
RS 1653 M9 OVC 2R-F 026/35/34/0712/956
TS 1856 M12 OVC 21/2S-F 011/33/32/0510/952
RS 1852 M9 OVC 2R-IPS-F 017/33/33/0410/954
TS 1956 5 SCT M14 OVC 21/2S-F 000/32/32/0210/949
RS 1952 M4 BKN 15 OVC 21/2S-F 006/33/33/0209/951
TS 2056 M11 OVC 31/2R-F 996/33/32/0108/948
RS 2051 M11 OVC 21/2L-F 003/33/33/0209/950
TA 2156 M11 OVC 5R-F 988/33/29/0109/946
RS 2153 M9 OVC 4L-F 993/33/33/0111/947
TA 2256 4 SCT M9 OVC 7R- 983/32/31/3611/945
SA 2251 M9 OVC 5L-F 985/33/32/3611/945
TS 2356 5 SCT M11 OVC 7R- 983/32/31/3613/945
RS 2353 4 SCT M15 OVC 4S-F 987/33/32/3514/946

NOVEMBER 30, 1993
TA 0056 CLR BLO 120 5F 193/23/19/1523/004
SA 0050 110 SCT 6F 199/24/21/1519G26/005
TA 0256 CLR BLO 120 5F 181/24/22/1523/001
SA 0253 110 SCT 7 189/25/22/1519G26/003
TA 0456 CLR BLO 120 4F 165/26/24/1623G29/996
SA 0450 110 SCT 7 175/27/24/1620G28/999
TA 0656 CLR BLO 120 5F 162/27/24/1620/996
SA 0651 110 SCT 7 170 27/25/1619/997
TA 0856 CLR BLO 120 5F 155/29/25/1524/994
SA 0850 220 -BKN 7 164/29/25/1522/996

DECEMBER 05, 1993
TA 1356 M13 OVC 10+ 037/34/30/3223G31/960
SA 1350 M12 OVC 9 040/34/30/3225G32/961
TS 1456 M9V BKN 15 BKN 20 OVC 2S-F 056/32/30/3332/966/ CIG 8V12
SA 1450 M13 OVC 5S- 056/33/30/3227G36/966
TS 1556 3 SCT M9 BKN 15 OVC 1/2S-F 082/31/30/3331G39/973 BKN V SCT
RS 1550 -X M9 OVC 1/2S-BS 082/32/31/3227G38/973
TS 1656 7 SCT M13 BKN 18 OVC 1/4SF 107/30/30/3230G39/980/ OVC V BKN
RS 1652 W5 X 1/4S-FBS 108/31/30/3230G39/981
TA 1756 10 SCT M16 BKN 27 OVC 1/2S-F 123/29/28/3333G39/985
RS 1752 W2 X 1/4S-FBS 125/29/28/3229G39/986
TA 1856 12 SCT M29 BKN 45 OVC 3/4R+F 134/28/27/3330G40/988
RS 1851 W6X 5/8S-FBS 138/29/27/3230G41/989

DECEMBER 21, 1993
TS 0056 W6X 3/4S-F 103/16/14/1709/976
RS 0050 W8 X 1S-F 112/16/14/1809/979
TA 0156 W3X 3/4S-F 104/18/16/1704/977
RS 0150 W2 X 3/8SF 110/18/16/1906/978
TS 0256 M8V BKN 14 OVC 31/2S-F 105/19/17/1904/977/ CIG 7V13
RS 0250 -X M11 OVC 13/4S-F 110/19/17/1706/979
TS 0356 W11X 1S-F 104/22/21/3103/977
RS 0351 -X M14 OVC 11/2S-F 110/23/21/3004/979
TS 1056 22 SCT M28 BKN 43 OVC 13/4S-F 113/29/26/2925G31/981/ OVC V BKN
RS 1053 -X M43 OVC 1S-BS 115/30/26/2924G30/981/BS7
TS 1156 M17 BKN 27 BKN 47 OVC 3/4S-F 120/25/22/3124/982 BKN V SCT
RS 1150 -X M12 BKN 41 BKN 65 OVC 3/4S-BS 123/25/22/3222G32/983/BS5
TS 1256 16 SCT 20 SCT M45 BKN 2S-F 126/21/17/3223G27/984
SA 1250 12 SCT 50 SCT 130 SCT 2BS 131/21/17/3223/985
TS 1356 M15 BKN 23 OVC 1/2S-F 138/17/14/3228G35/987
RS 1350 -X 21 SCT 3/4VS-BS 140/18/11/3227G34/988/VSBY 1/2V1

DECEMBER 31, 1993
TA 2056 M17 BKN 26 BKN 37 OVC 11/4S-F 082/28/26/3616/973
RS 2051 27 SCT E35 OVC 11/2S- 086/28/26/3620/974
TS 2156 6 SCT M11 OVC 1/2SF 094/25/23/3624G28/976
RS 2151 8 SCT M25 OVC 5/8S- 096/36/24/3521G32/977
TS 2256 M10 BKN 24 BKN 35 OVC 2S-F 108/23/21/3518G24/980/ OVC V BKN
SA 2250 9 SCT M50 OVC 1S- 110/24/21/3519G29/981
TA 2356 M10 OVC 5R-F 130/20/17/3521G27/987
SA 2350 M12 BKN 40 OVC 13/4S- 134/21/18/0123G28/988

JANUEARY 05, 1994
TA 0856 M15 OVC 11/4S-F 097/09/05/1213/973
RS 0850 -X M16 OVC 1S-F 104/9/5/1214/975/S4
TS 0956 M15 OVC 1S-F 090/11/07/1215/972
SA 0951 -X M16 OVC 1S-F 098/11/7/1213/974/S3
TS 1156 M17 OVC 11/4S-F 069/13/09/1214/965
RS 1152 -X M17 OVC 11/2S-F 078/13/9/1114G21/968/S2
TA 1756 M18 OVC 7 077/14/10/0906/968
SA 1752 M18 OVC 7S- 081/14/11/0807/969

JANUARY 06, 1994
TA 1056 CLR BLO 120 31/2H 227/-7/-14/3218/010
SA 1052 CLR 4BS 230/-7/-13/3219G28/011
TS 1156 9 SCT 3H 234/-7/-14/3221/012
SA 1151 -X 23/4BS 238/-7/-13/3220G28/013/BS1
TS 1356 M13 OVC 1H 246/-9/-16/3226/015
SA 1354 -X 13 -SCT 1BS 252/-9/-15/3222G28/017/ BS2
TS 1456 9 SCT M15 BKN 33 OVC 4H 256/-9/-16/3221/018/ BKN V OVC
RS 1450 20 SCT 3BS 258/-8/-16/3219G25/018
TS 1556 M10 BKN 15 OVC 3H 266/-10/-16/3217/021
RS 1550 12 -SCT 3BS 271/-9/-16/3218G25/022
TS 1656 M10 OVC 4H 275/-11/-18/3215/023
SA 1653 12 -SCT 4BS 279/-11/-17/3114/024
TA 1856 M12 OVC 10+ 286/-12/-20/3014/025
SA 1852 13 -BKN 7 293/-12/-19/3013/027
TA 2056 M10 OVC 10+ 292/-13/-19/3115/027
SA 2050 12 -BKN 10 298/-12/-19/3114/028

FEBRUARY 07, 1994
TS 1156 M21 BKN 28 OVC 3S- 354/-12/-20/0106/045/ BKN V OVC
RS 1150 -X M41 BKN 50 OVC 2S- 363/-9/-19/3607/047/S6
TA 1256 M20 BKN 34 OVC 2S- 348/-12/-20/0503/043
RS 1250 -X M29 BKN 43 OVC 21/2S- 355/-8/-19/0406/045/S4
TA 1356 M47 BKN 60 OVC 5S- 334/-11/-19/0506/039/ OVC V BKN
SA 1350 M70 OVC 5S- 344/-9/-19/0306/042

FEBRUARY 09, 1994
TS 0856 M13 OVC 1/2H 330/-34/-40/1903/033
SA 0850 -X 1/4IF 337/-34/-39/2003/035/F2
TS 0956 M13 OVC 1H 328/-28/-33/1607/033
SA 0950 -X 1/4IF 334/-27/-33/1407/035/F2

All of the compared observations had at least a restriction to visibility of six miles or less and/or cloud heights less than or equal to 3000 feet. The observations were chosen because of their significance to aviation interests, while also providing a good comparison for other interests such as forecasters and researchers. The following elements of the observations were compared: cloud heights, visibility, temperature, dew point, altimeter, wind direction, wind speed, and monthly precipitation (Table 2).

Table 2
Monthly Precipitation

Month	MANUAL Precip.	ASOS Precip.
August, 1993	2.39	1.67(E)
September	1.74	1.62
October	.63	.62
November	1.78	1.46
December	.72	.42(E)
January, 1994	.93	.22
February	.70	.28
March	.27	.00(E)
April	2.75	.18(E)
May	1.67	.59(E)
June	5.12	4.70
As of July 21	2.93	.91(E)

2. Cloud Heights and Visibility

Ceiling and visibility are the most critical elements of the surface observation to aviation users. The aviation categories of LIFR, IFR, MVFR and VFR are defined by the ceiling height and/or visibility restriction (Table 3). The first comparison examined ASOS calculated aviation categories with manual observations. The comparison was considered a success if ASOS categories were either lower or equal to manual observation categories. For example, if the manual observation had an LIFR ceiling and visibility, the corresponding ASOS observation had to have at least an LIFR ceiling and/or visibility to be considered a success. Based on this criterion, ASOS failed eight times out of all the observations checked. Five of the eight failures occurred during one day.

TABLE 3

Category		Ceiling	and/or	Visibility
LIFR	(1)	< 500'		< 1 mi
IFR	(2)	500' < CIG < 1,000'		1 mi < VSBY < 3 mi
MVFR	(3)	1,000' < CIG < 3,000'		3 mi. < VSBY < 5 mi.
VFR	(4)	> 3,000' or none		> 5 mi.

(1) Low Instrument Flight Rules
(2) Instrument Flight Rules
(3) Marginal Visual Flight Rules
(4) Visual Flight Rules

The ceiling heights and/or visibilities for the eight ASOS and manual observations were on the borderline between aviation categories. For example, one manual observation was IFR with a ceiling of 900 feet and visibility of two miles. The corresponding ASOS observation was MVFR with a ceiling of 1000 feet and visibility of three miles. One should consider that individual observers may determine a slightly different cloud height and visibility for the same prevailing conditions. Also, ASOS and manual observations are taken at different times. Even given their discrepancies, ASOS was very successful in this comparison with a 92 percent success rate.

The second comparison found the actual differences in visibility and cloud heights from ASOS to the manual observation. In 83 percent of the observations the ASOS cloud height was within 200 feet of the manual cloud height (Figure 1). The average difference of the ASOS cloud height from the manual was approximately 150 feet.

In 78 percent of the observations the ASOS visibility was within two miles of the manually observed visibility. When the manually observed visibility was greater than or equal to three miles the ASOS visibility differed by an average of 1½ miles. When the manually observed visibility was less than three miles, ASOS differed by an average of ½ mile. Finally, when the manually observed visibility was less than or equal to one mile the ASOS visibility differed by an average of 3/16 of a mile. Keep in mind, ASOS does not report visibilities for less than ¼ mile. Figure 2 is a scatter plot showing how the ASOS visibility compared with the manual visibility.

3. Temperatures and Dew Points

In 92 percent of the observations, ASOS temperatures were the same or lower one degree than the manual temperature (Figure 3). In 90 percent of the observations the ASOS dew point temperature was the same or one degree lower than the manually observed dew point temperature (Figure 4).

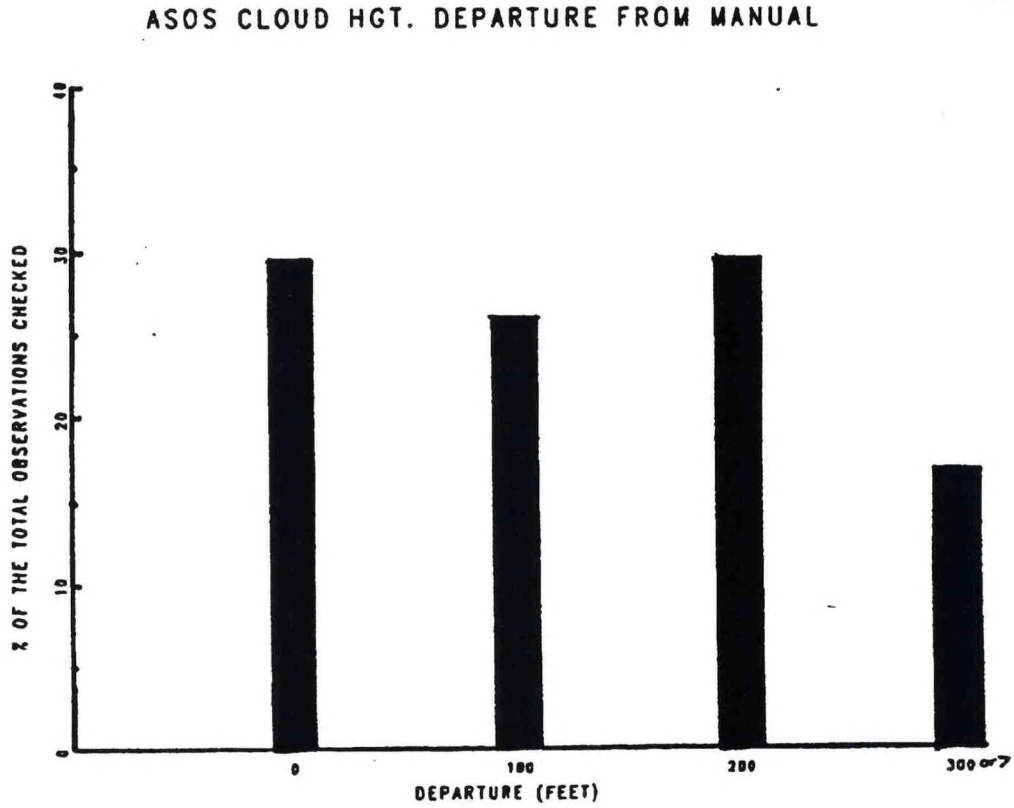

Figure 1. ASOS cloud height departure from manual.

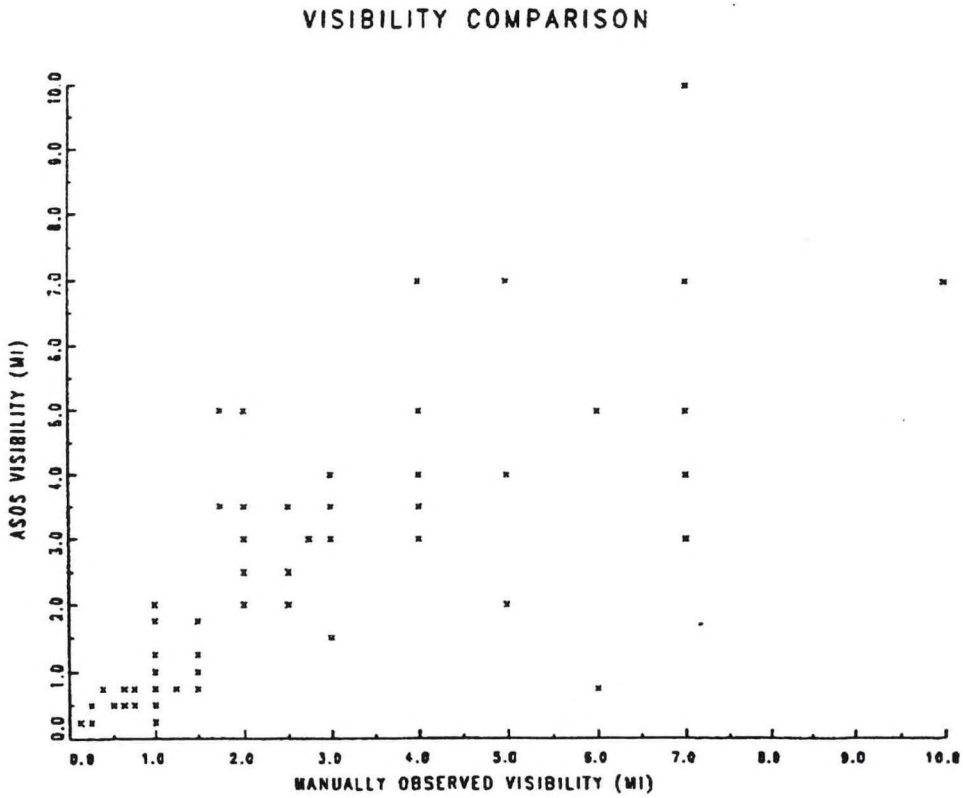

Figure 2. Scatter plot of ASOS vs. manually observed visibilities.

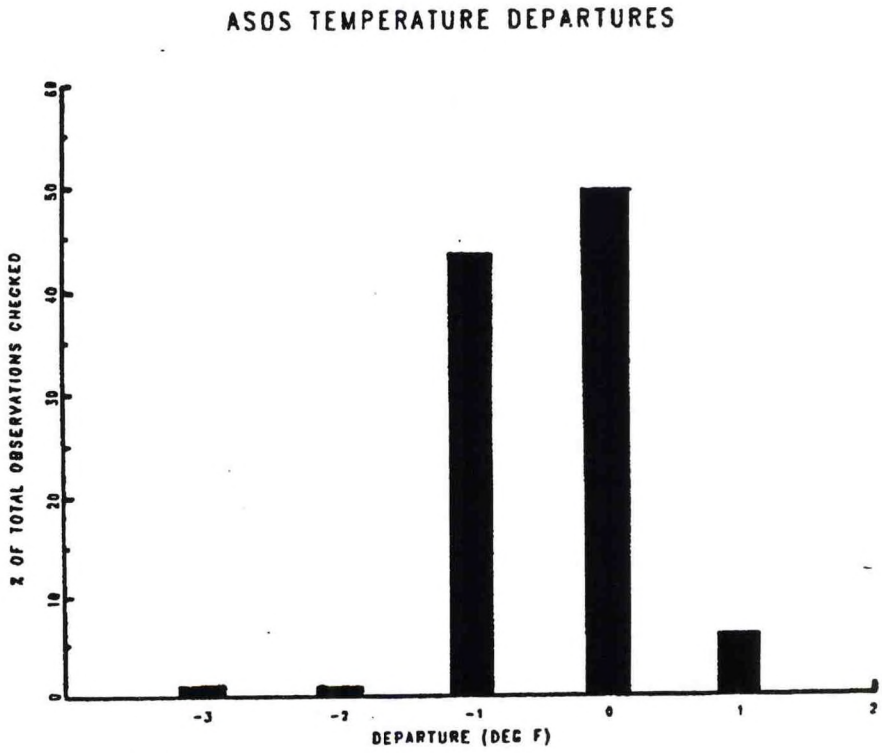

Figure 3. ASOS Temperature departures.

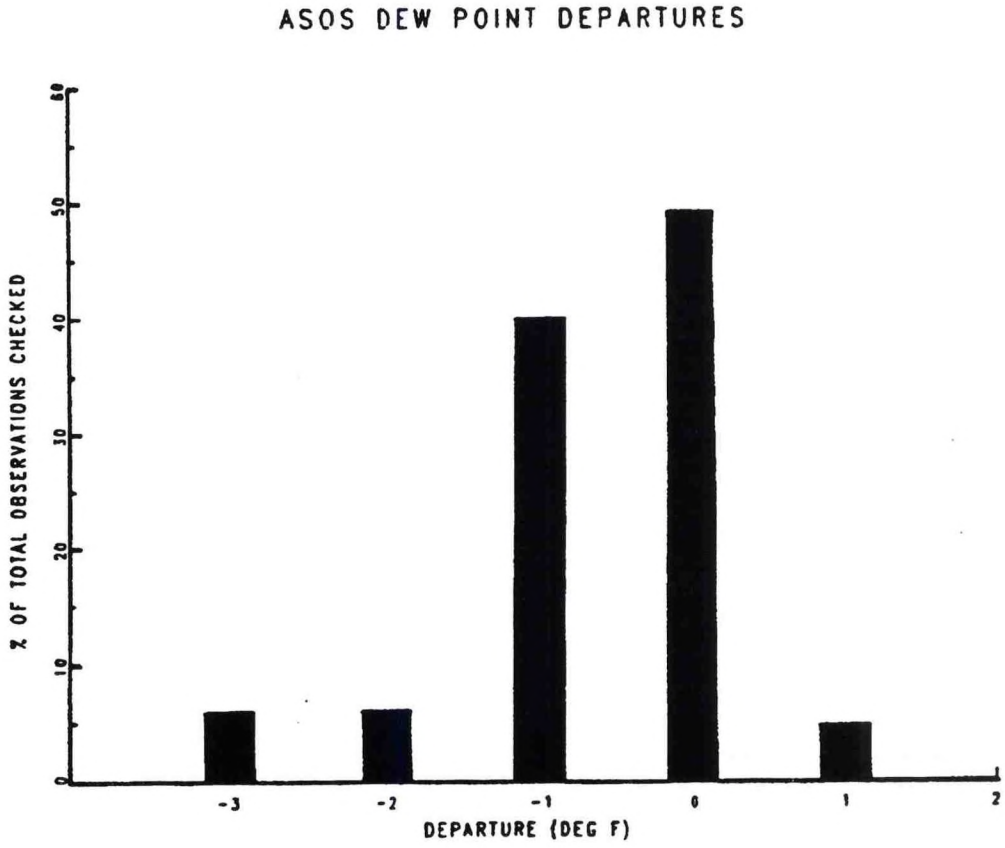

Figure 4. ASOS dew point departures.

4. Wind Direction and Speed

In 92 percent of the observations, the ASOS wind direction was within 10 degrees of the manually observed wind direction (Figure 5). In 90 percent of the observations the ASOS wind speed was within two knots of the manual (Figure 6).

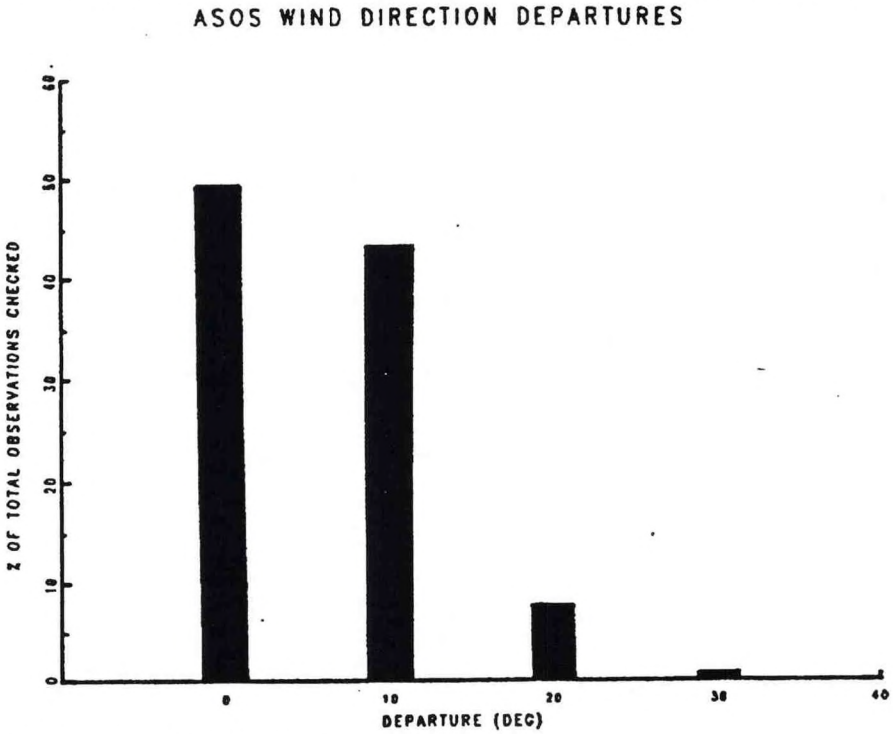

Figure 5. ASOS wind direction departures.

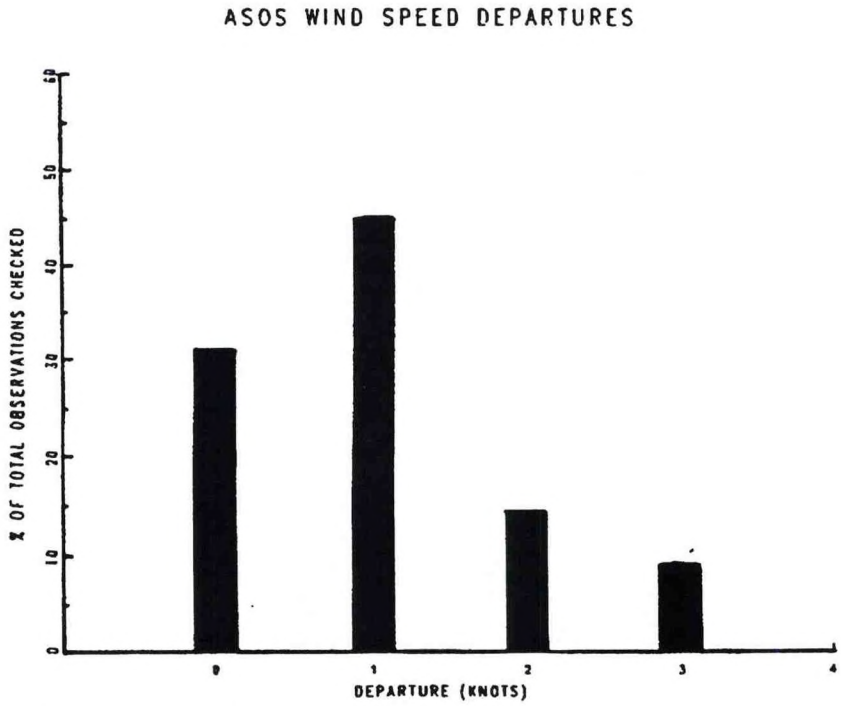

Figure 6. ASOS wind speed departures.

5. Altimeter

In 98 percent of the observations, ASOS was one to two hundredths lower than the manual altimeter reading. From further stratification, 59 percent of the ASOS observations were one hundredth lower and 39 percent of the ASOS observations were two hundredths below the manually observed altimeter reading.

6. Monthly Precipitation

Figure 7 shows ASOS's precipitation as a percentage of the manual weighing rain gage precipitation. In the months where ASOS's precipitation was not in error, this automated system averaged 72 percent of the manual precipitation. With the error months included (denoted by E, meaning Estimated; the amount was estimated by ASOS because of the error involved with counting the "tips" from the tipping bucket rain guage; defied as the "error" in this study), ASOS averaged 53 percent of the manual precipitation.

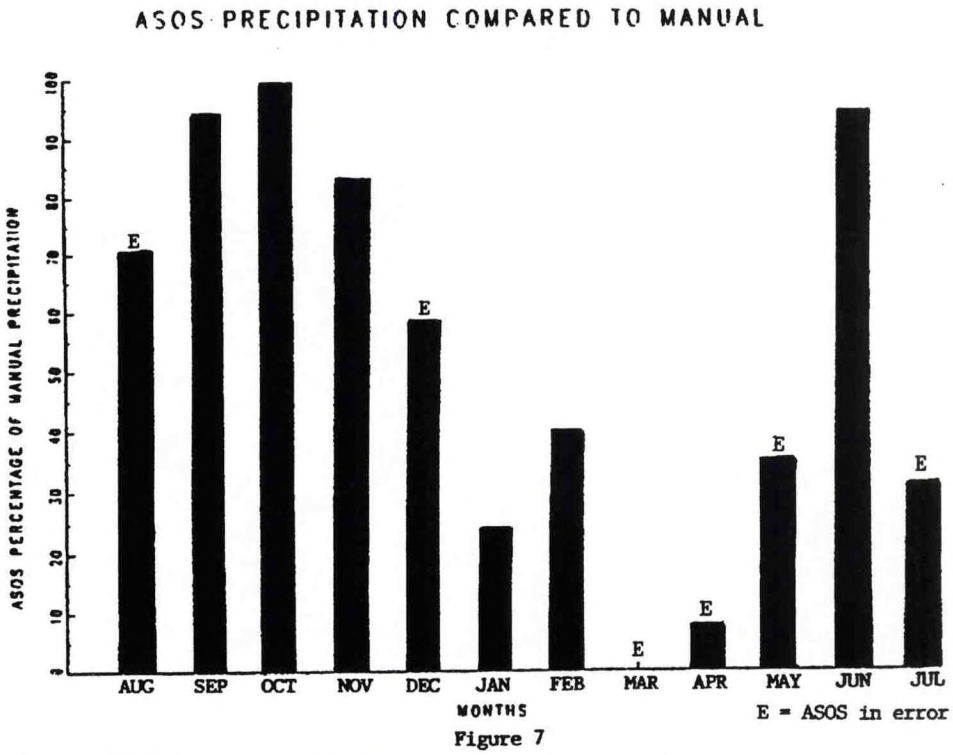

Figure 7. ASOS precipitation compared to manual.

7. Other Differences

ASOS reported more fog and haze than the manual observer. "Patchy" fog was also missed by ASOS. During cold weather with a strong inversion, often ASOS would report a ceiling when in fact there was no ceiling in the manual observation. ASOS also missed several snow flurry events. Lastly, ASOS missed several scattered layers.

8. Conclusion

This comparison study between the ASOS observations and the manual observations was done to show the station manager how these two observations differed before ASOS's proposed commissioning in the fall of 1994. ASOS was successful with all elements of the surface observation as compared to the manual observation except precipitation. ASOS also differed from the manual observation in several fog and flurry events.

The benefits from ASOS should be substantial with the increase in the number of observations available from future locations where there are no observations now. These benefits should produce better aviation and public forecasts, more data for case studies, and increase confidence for aviation planning purposes.

9. Acknowledgements

I would like to thank several people at WSFO Sioux Falls for critiquing this paper. Especially helpful were Greg Harmon, AMIC, and Scott Mentzer, SOO (currently the MIC at WFO Goodland, Kansas).

CENTRAL REGION APPLIED RESEARCH PAPER 14-04

OUTFLOW MERGERS AND RESULTANT THUNDERSTORMS

Allan H. Fisher
Central Weather Service Unit
Aurora, Illinois

1. Introduction

On Monday afternoon 1 August 1994, an unstable air mass was located over northern Illinois and southern Wisconsin. Weak troughs in the sea-level pressure field (MSLP) and "aloft" helped to initiate scattered thunderstorms. During the afternoon, numerous convective outflow boundaries merged which all resulted in new 50-59 dBZ thunderstorms at or near their intersections. The end result was a major disruption to air traffic, with an eventual 2½ hour national ground stop for the Chicago area. The purpose of this study is to diagnosis this episode using the base reflectivity product from the WSR-88D. This product was superior in detecting and displaying the outflow boundaries compared to either base velocity or base spectrum width.

2. Discussion

Northern Illinois and southern Wisconsin were covered by an unstable air mass (temps mid 80s, dew points upper 60s, CAPE greater 2000 Joules/Kg). A weak northeast to southwest oriented trough in the MSLP field was moving very slowly south through southern Wisconsin. This trough set off a band of thunderstorms along Madison (MSN)-Milwaukee (MKE) line between 1800 UTC - 1900 UTC. Meanwhile, a very weak 500-mb trough in the geopotential height field was located over northern Illinois and helped to initiate thunderstorms from northern Illinois-southern Lake Michigan between 1900 UTC - 2000 UTC. All thunderstorms were moving 15 kts or less as all "upper level" winds were between 10-20 kts.

The very slow motion of the thunderstorms allowed the outflow boundaries to spread out from the storms in an organized fashion. The first outflow interaction began at approximately 2125 UTC.

Figure 1 shows thunderstorms over extreme southeast Wisconsin, which were developing south along the lake Michigan shoreline. Milwaukee (KMKX) WSR-88D (not shown) indicated an associated outflow/lake breeze boundary inland from the lake shore. A satellite picture depicted a cumulus band (C) over extreme northern Illinois that the Chicago (KLOT) WSR-88D depicted as a weak line of returns with a 45 dBZ cell on the east end. WSR-88D time lapse showed an outflow boundary (A) from thunderstorms south of the Chicago area moving north northwest around 20 kts toward a cumulus line at (B). This line (B) was a southward extension from the lake Michigan cells. Small showers were along this band just southwest of Midway (MDW) Airport (Figure 2).

Figure 3 (2125 UTC) revealed that the earlier features (A) and (B), shown in Figure 2 (a magnification of Figure 1 to better see the small scale features), had merged resulting in the rapid formation of a new line of thunderstorms (D). Chicago center officials were advised that this line of thunderstorms would continue to rapidly develop and cut off all aircraft operation to the south-southeast of the metro area. This area is very critical to moving air traffic in and out of Chicago. At (E), an outflow boundary was now evident from the Wisconsin storms. This outflow was about to intersect the cumulus band (C) which already contained a 45 dBZ cell.

By 2154 UTC (Figure 4), a broken line of 50-59 dBZ cells existed from southwest of the radar (KLOT) to southern Lake Michigan. The old outflow boundary (A) became better defined and was renamed (F). It was moving north northwest at 25 kts, to the north of the new thunderstorm line. To the north, the southward moving outflow boundary (E) has collided with the weak cumulus line (C) (Figure 3) which resulted in a cluster of rapidly growing thunderstorms.

As shown in Figure 5 (2241 UTC), outflow (F) continued to move north northwest while outflow (E) was headed south and accelerating. Time lapse suggested that these two old outflow boundaries would merge in about 15-20 minutes near O'Hare field (ORD) and that outflow (E) will pass through ORD. The passage of the outflow at ORD shifted the surface winds from southwest to northeast, which resulted in a total change in runway usage at the field (that is because landing aircraft need to land into the wind). This runway change and the resultant change in aircraft approach positions only compounded already heavily impacted aircraft operations in the Chicago area. Outflow (E) went on to merge with new outflow (G) the latter which emanated from a cell over Kane County, to the west of ORD.

Figure 6 (2316 UTC) indicates the results of several outflow boundary mergers. Around 2300 UTC old outflows (E) and (F) merged; the result was new 50 dBZ cells developing just southeast of ORD. Where (E) and (G) merged (Figure 5), a 50 dBZ cell resulted (G). New outflow (H) exists from the storms over Lake Michigan. Outflows (E), (F), and (H) are now merging. Outflows (I) and (J) are merging along with (J) and (E).

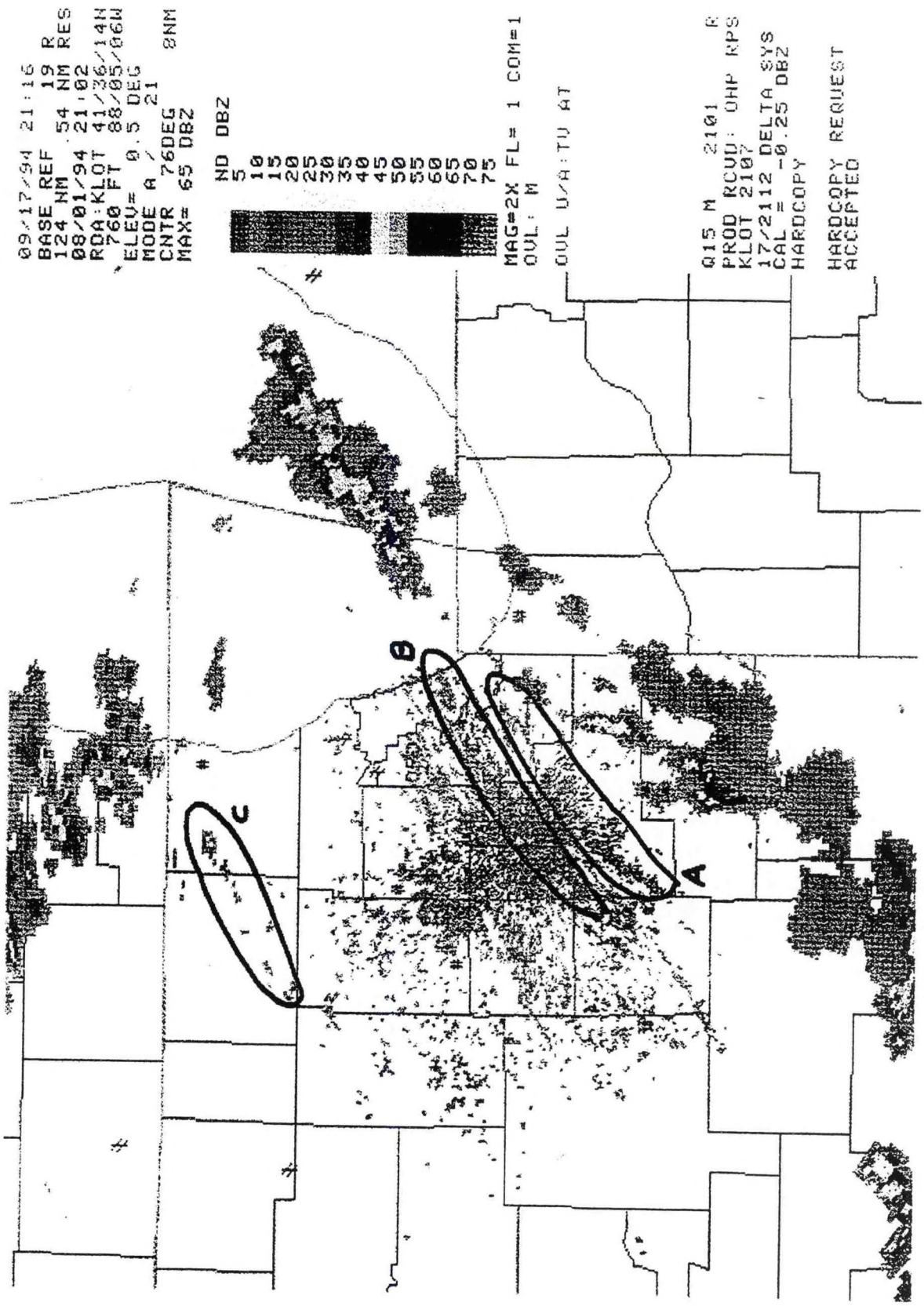

Figure 1. Base reflectivity product WSR-88D KLOT valid 2102 UTC 1 August 1994. Elevation angle 0.5 degrees, mode A, VCP 21. Outflow/cumulus lines A,B,C.

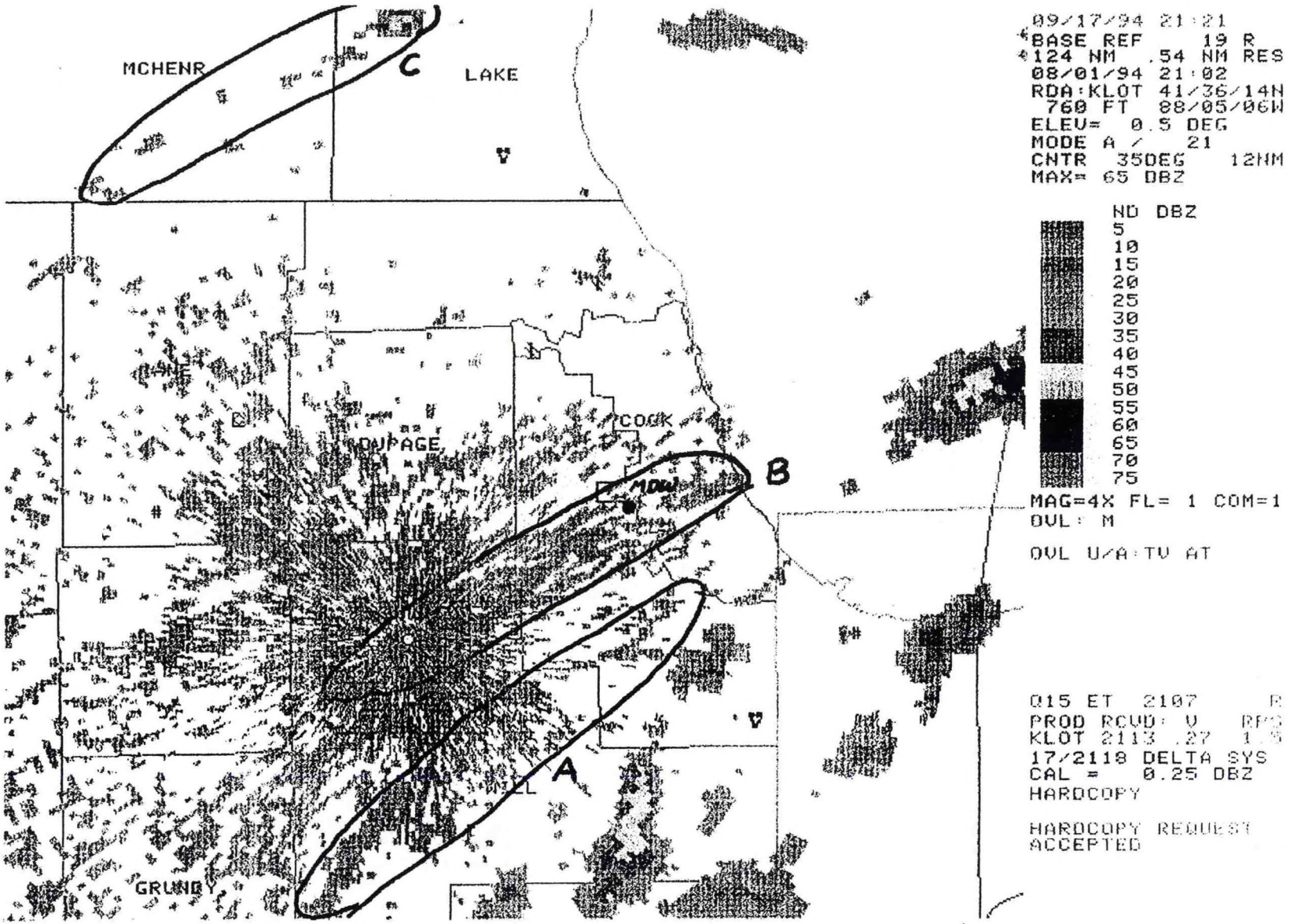

Figure 2. Same as Figure 1. Outflows/cumulus lines A,B.

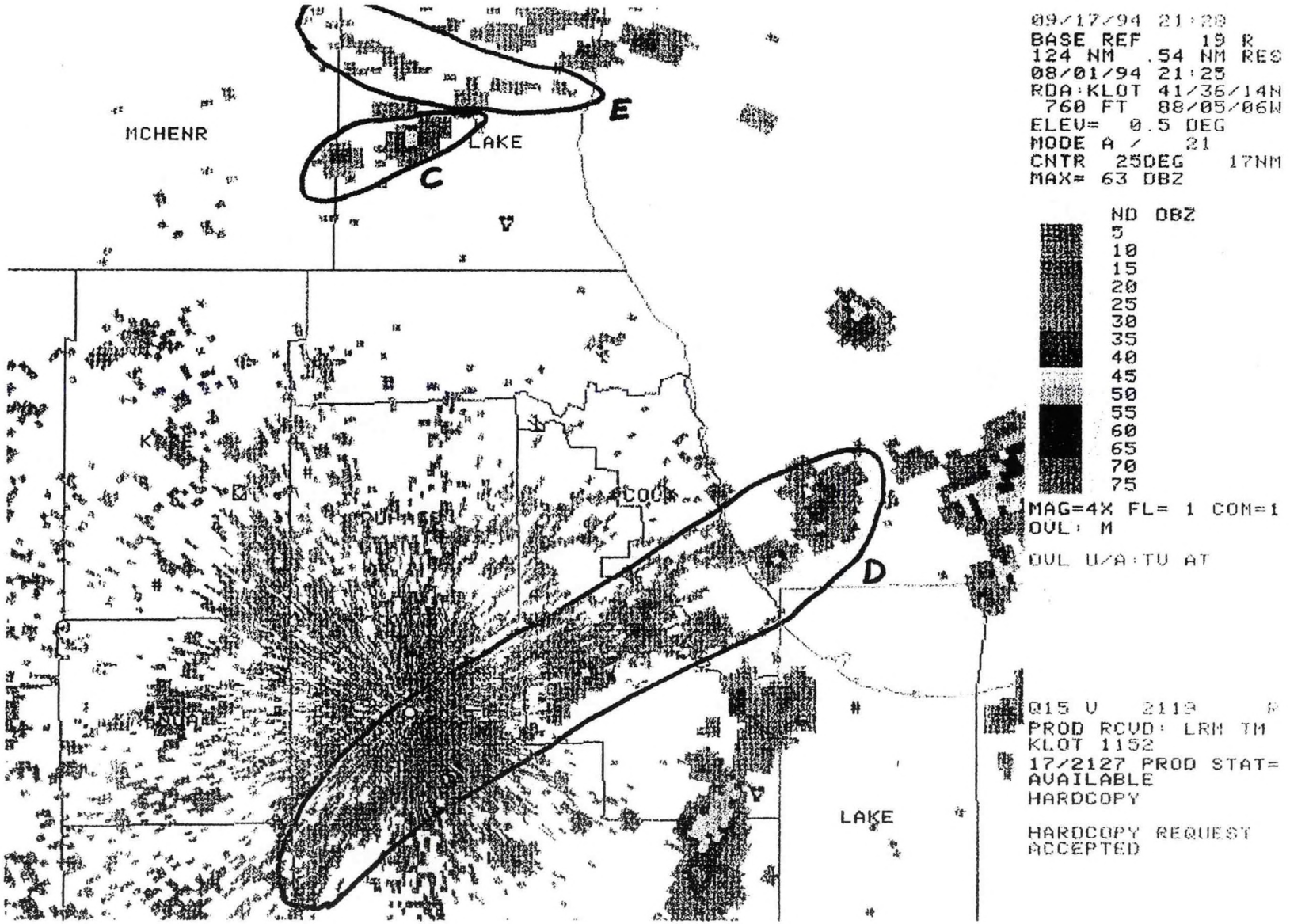

Figure 3. Same as Figure 1, valid 2125 UTC. Outflows/cumulus line/tstm lines C,D,E.

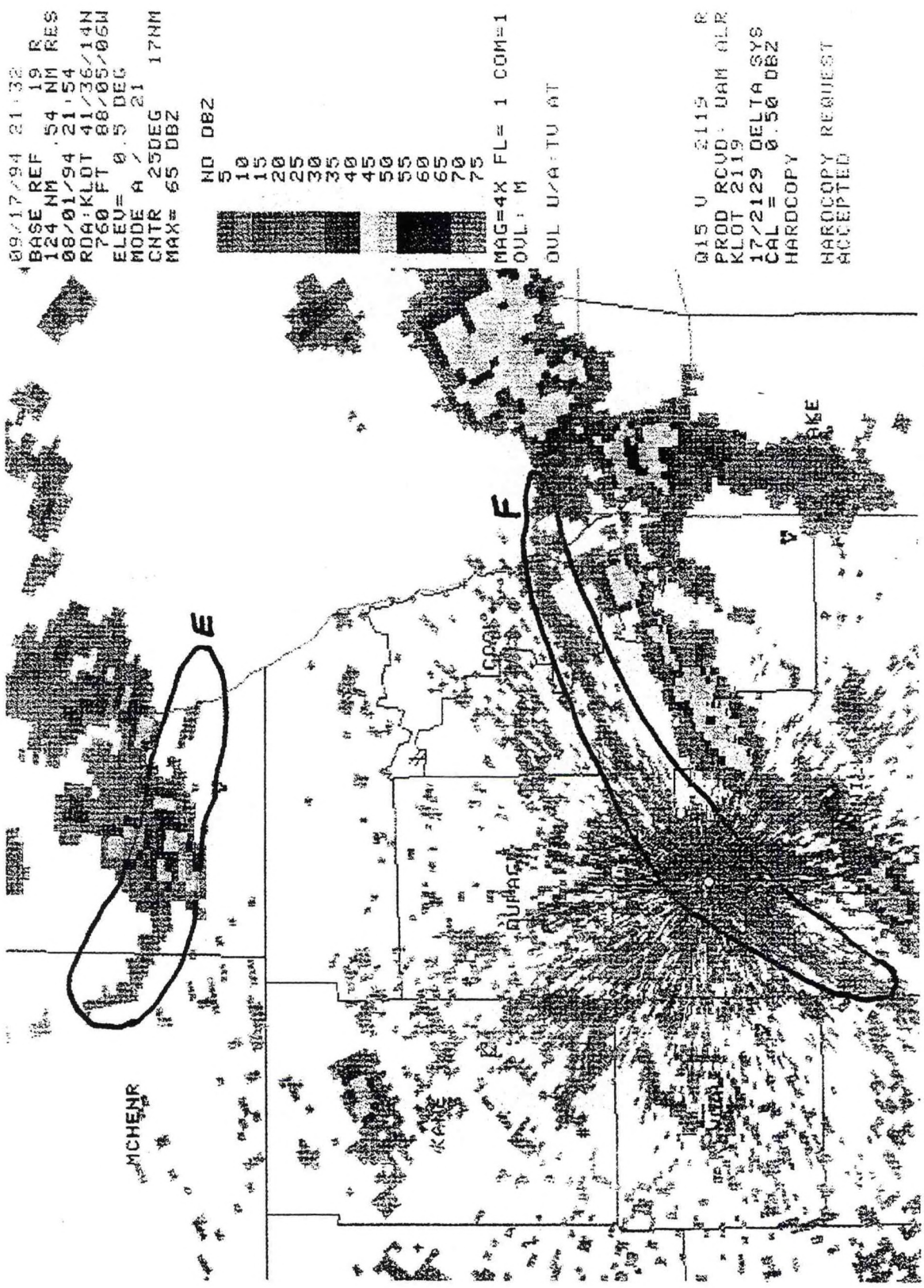

Figure 4. Same as Figure 1, valid 2154 UTC. Outflows E,F.

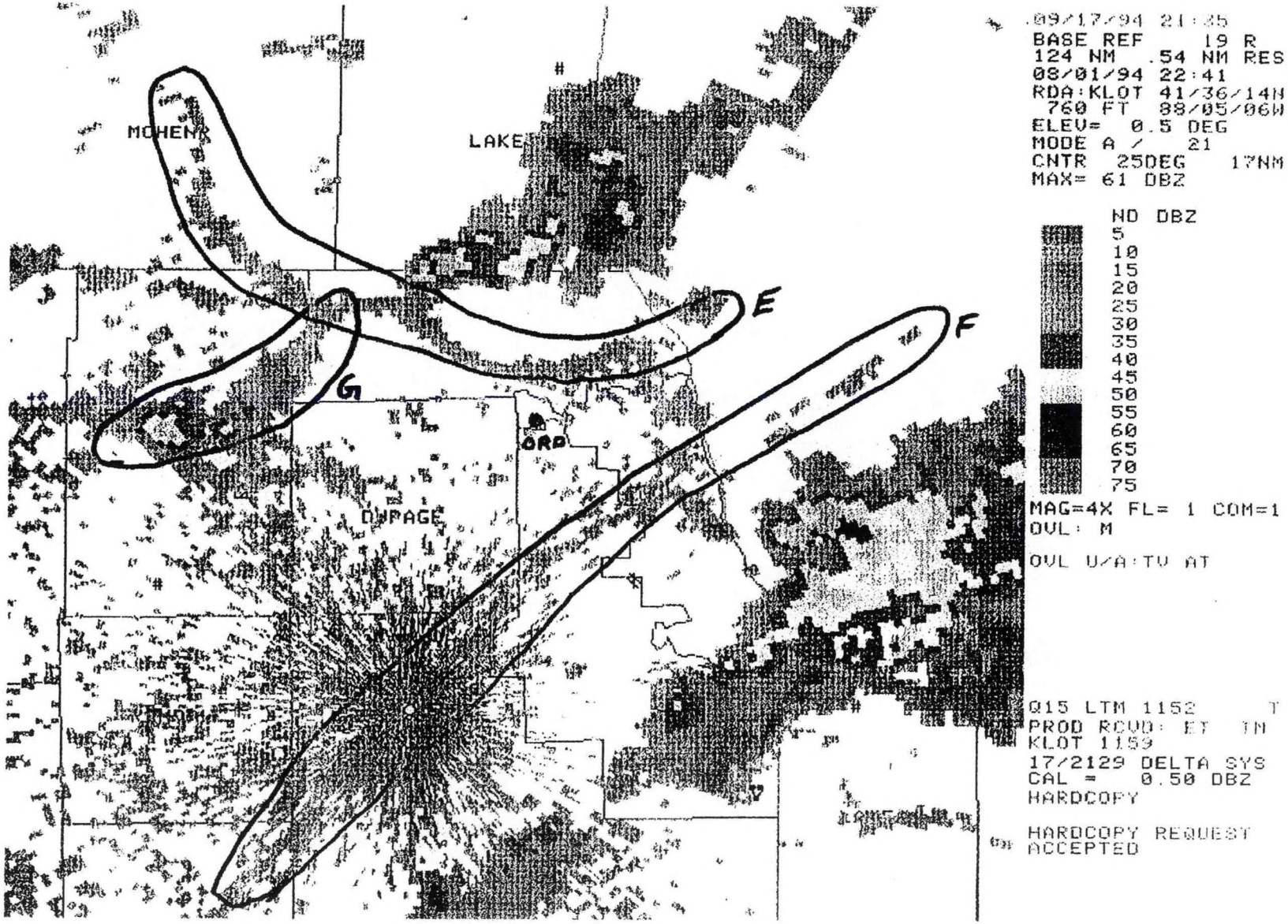

Figure 5. Same as Figure 1, valid 2241 UTC. Outflows E,F,G.

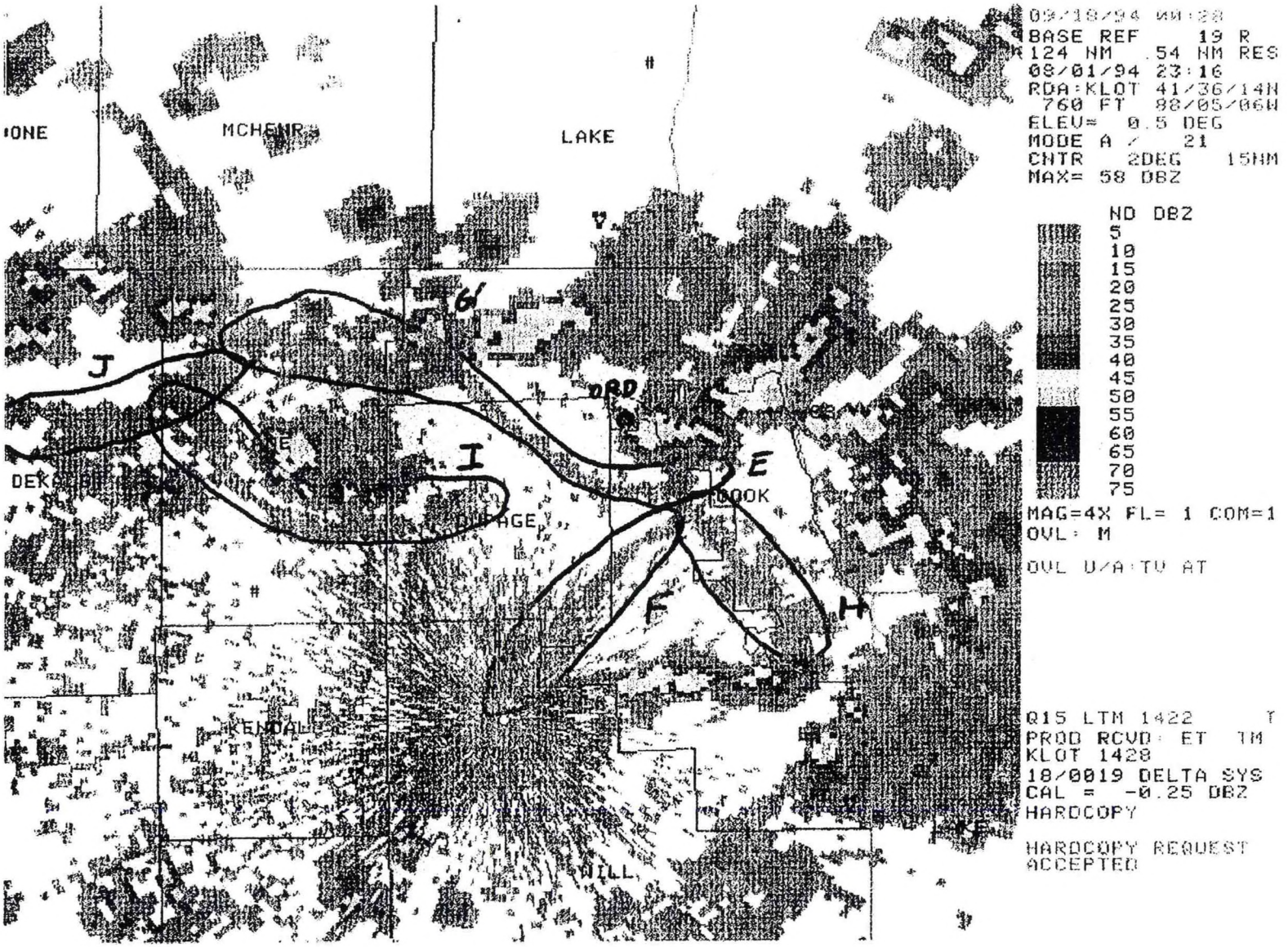

Figure 6. Same as Figure 1, valid 2316 UTC. Outflows E,F,H,I,J.

Figure 7 (2351 UTC) depicts the results of all these mergers. A small band of 50-59 dBZ cells (K) was south of ORD. This was the result of the (E)-(F)-(H) merger. At (L) 50-59 dBZ cells formed from the merger of outflows (J) and (E). New 50 dBZ cells (M) developed where outflows (I) and (F) (Figure 6) intersected. By this time, Chicago metro air traffic came to a halt. During this entire time both the Chicago Center traffic officials and the meteorologists at the FAA Central Flow Control Facility (CF^2) were constantly advised to location and probable development of thunderstorms over a very busy airspace.

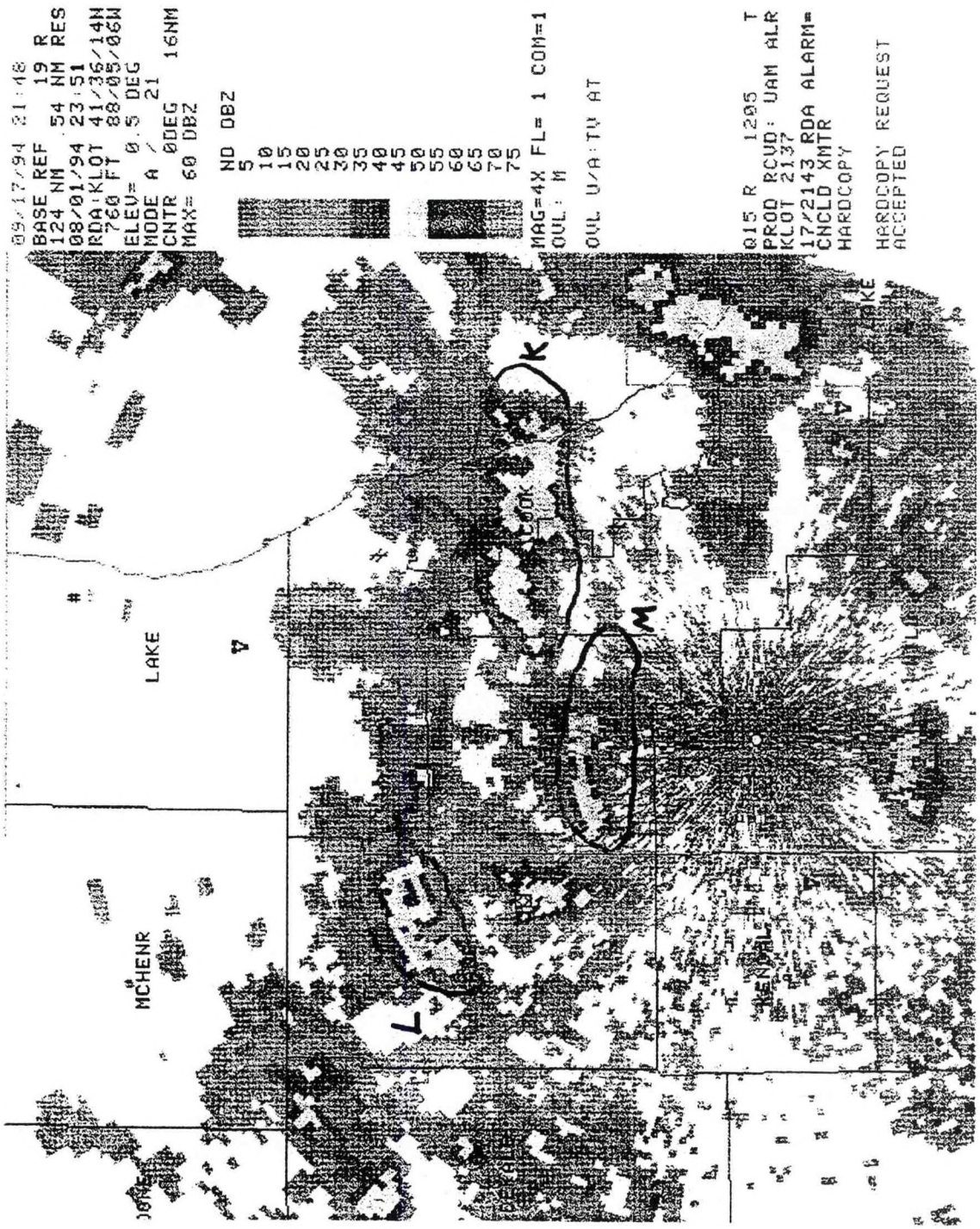

Figure 7. Same as Figure 1, valid 2351 UTC. Tstms K,L,M.

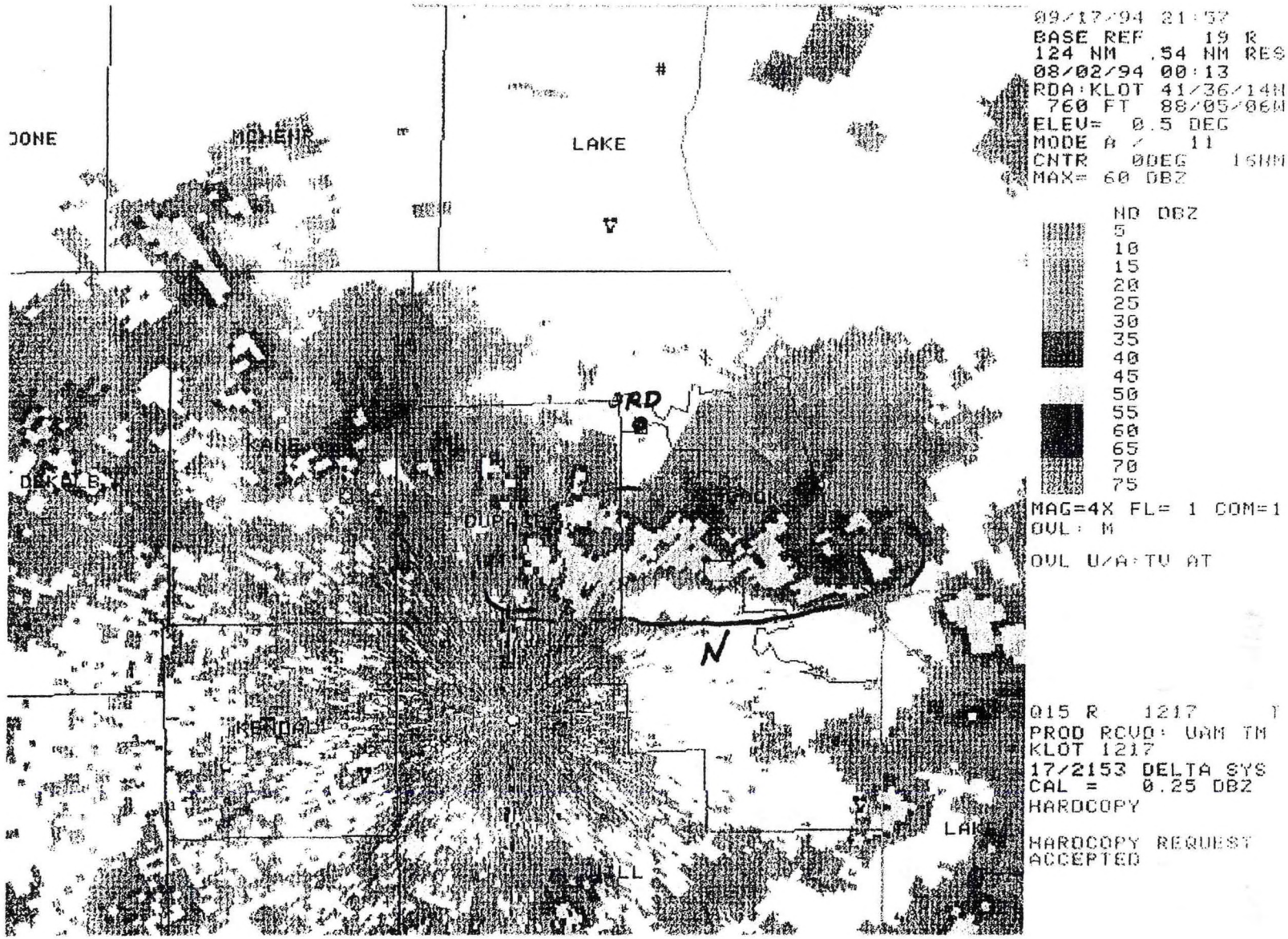

Figure 8. Same as Figure 1, valid 0013 UTC 2 August 1994. Tstms N.

The final depiction of the spatial distribution of the thunderstorms, from KLOT, is shown in Figure 8. The E-W thunderstorm band (N) is the result of the mergers of storm bands (K) and (M) (Figure 7).

3. Conclusion

Thunderstorms formed over the Chicago metro area during the late afternoon of 1 August 1994. The storms initially started as two separate areas, one over southeast Wisconsin and the other to the southeast of the Chicago area. Initial storm motion was ESE at only 15 kts. This slow speed may have allowed the thunderstorm outflow boundaries to control the future direction and development of additional deep moist convection. (Keeping in mind, of course, that the response of outflow boundaries and resultant deep moist convection is a direct function of the environmental vertical wind shear profile, in addition to other considerations.) The main factor was the northward and southward movements of the outflows from the initial thunderstorm areas. As these outflows merged with either existing cumulus lines or each other, new cells formed. These cells then formed their own outflows that produced further outflow interactions. With the CWSU meteorologist closely watching a one hour time lapse loop on the NEXRAD PUP, FAA officials were constantly being advised on what to expect in the way of thunderstorm development and timing.

4. Acknowledgements

I would like to thank Edward Green and Patricia Wontroba of Chicago CWSU for their initial reviews. Ken Labas, SOO from WSFO Chicago, is acknowledged for his helpful comments.

CENTRAL REGION APPLIED RESEARCH PAPER 14-05

THE APPLICATION OF GRIDDED MODEL OUTPUT TO DETERMINE THE IMPORTANCE OF DIABATIC PROCESSES WITH RESPECT TO A RAIN VS. SNOW FORECAST

Christopher T. Noles
National Weather Service Forecast Office
Topeka, Kansas

1. Introduction

On March 25, 1994, statistical guidance and the Zone Forecast (not shown) for north central Kansas predicted rain with high temperatures from 45 to 50°F. What happened in reality was that there was snow. Snow began at the Concordia, Kansas, Automated Surface Observing System (ASOS) around 1850 UTC. Between 1850 and 1920 UTC, the visibility dropped from 7 miles to 3/4 of a mile. By 2005 UTC, ASOS reported moderate snow and fog with a visibility of 1/2 of a mile. The snowfall finally ended at 2058 UTC.

While only a trace of snowfall was recorded due to warm ground conditions, it was still an unforecast event. The purpose of this paper is to demonstrate how the PCGRIDDS software package, utilizing gridded model output from the Eta, may have been useful in forecasting snow as the precipitation type.

2. Model Forecasts

The Eta model run from 0000 UTC 25 March 1994 initial conditions predicted a 700-mb shortwave trough to move from northeast Colorado at 1200 UTC March 25 to central Nebraska by 0000 UTC March 26 (Figures 1 and 2). During this period, 850-700-mb layer Q-vector forecasts indicated significant Q-vector convergence (implying quasi-geostrophic "forcing" for upward vertical motion) moving from eastern Colorado through northern Kansas (Figures 3 and 4).

Figure 5 shows an overlay of forecast thickness values considered useful in determining the rain/snow line, along with forecast 850-mb and boundary layer temperatures near 0°C valid at 1800 UTC. Arguments could be made for predicting either rain or snow, according to these air column temperature assessment measures. For instance, the forecast 850-mb temperature was less than -2°C at Concordia, Kansas, indicating the possibility of snow, while the 0°C

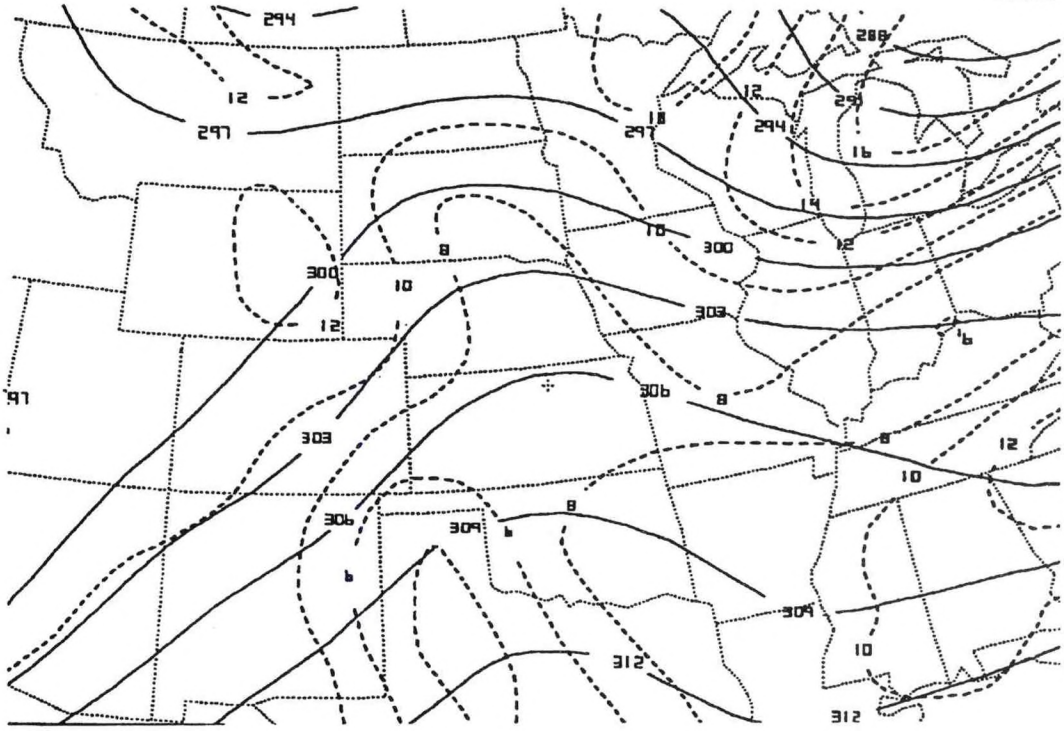

Figure 1. Eta model 12-hour forecast of 700-mb heights (solid contours every three decameters) and absolute vorticity (dashed contours every 2 x 10^{-5} s^{-1}) for 1200 UTC 25 March 1994. Plus (+) symbol over north central Kansas indicates location of Concordia.

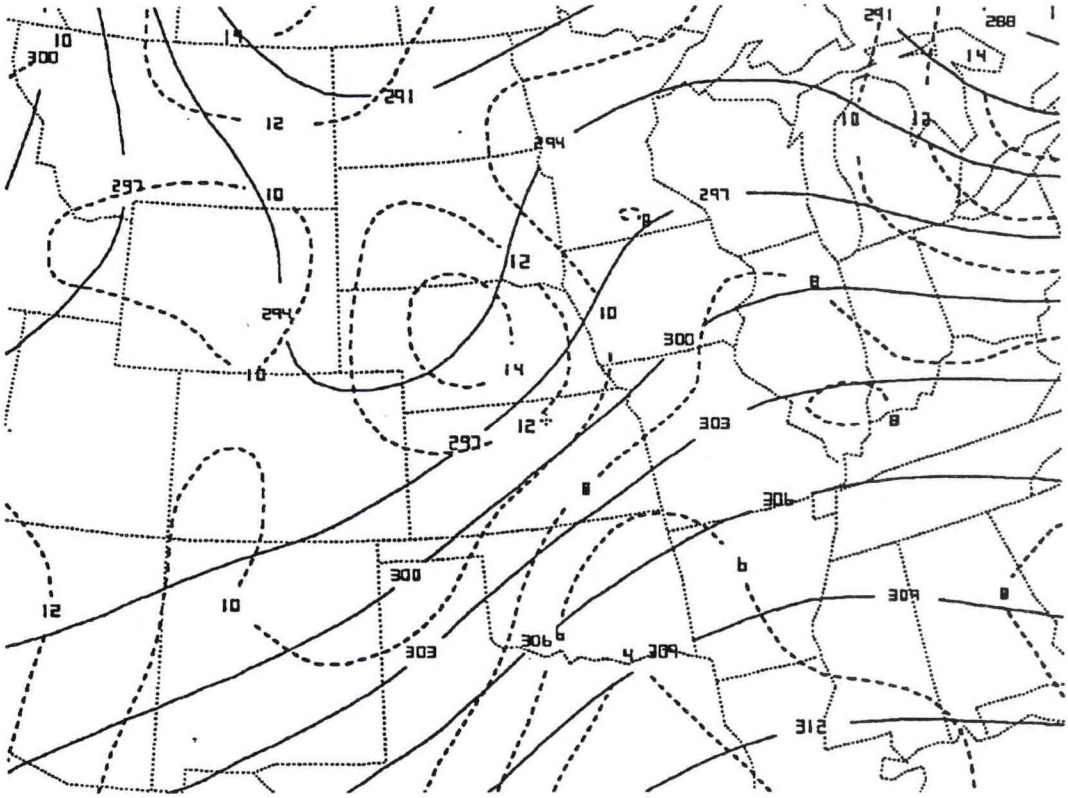

Figure 2. Same as Figure 1 except for 24-hour forecast valid 0000 UTC 26 March 1994.

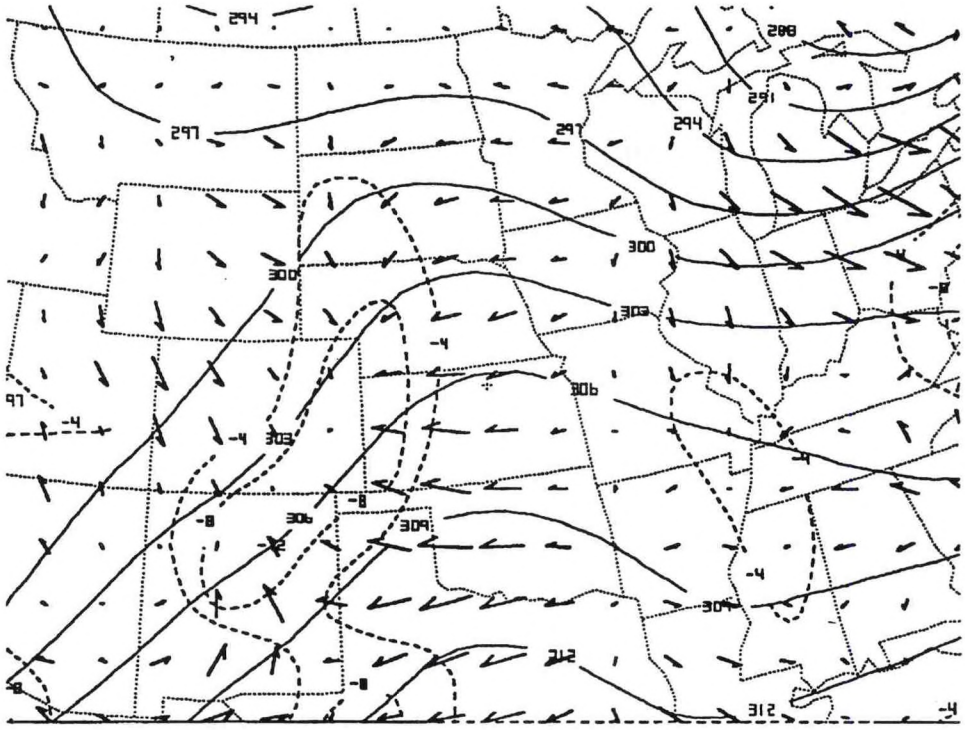

Figure 3. Eta model 12-hour forecast of 700-mb heights (solid contours every three decameters), 850-700-mb layer Q-vectors, and associated Q-vector divergence (only dashed contours indicating Q-vector convergence are shown) for 1200 UTC 25 March 1994.

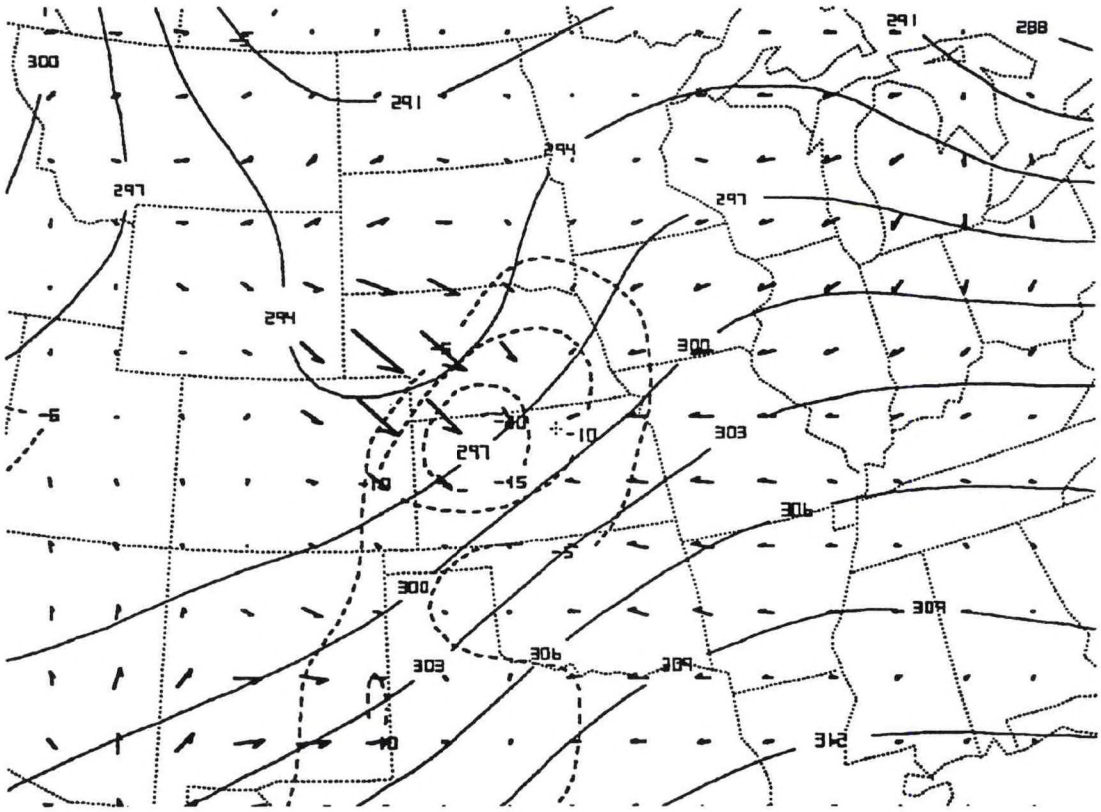

Figure 4. Same as Figure 3 except for 24-hour forecast valid 0000 UTC 26 March 1994.

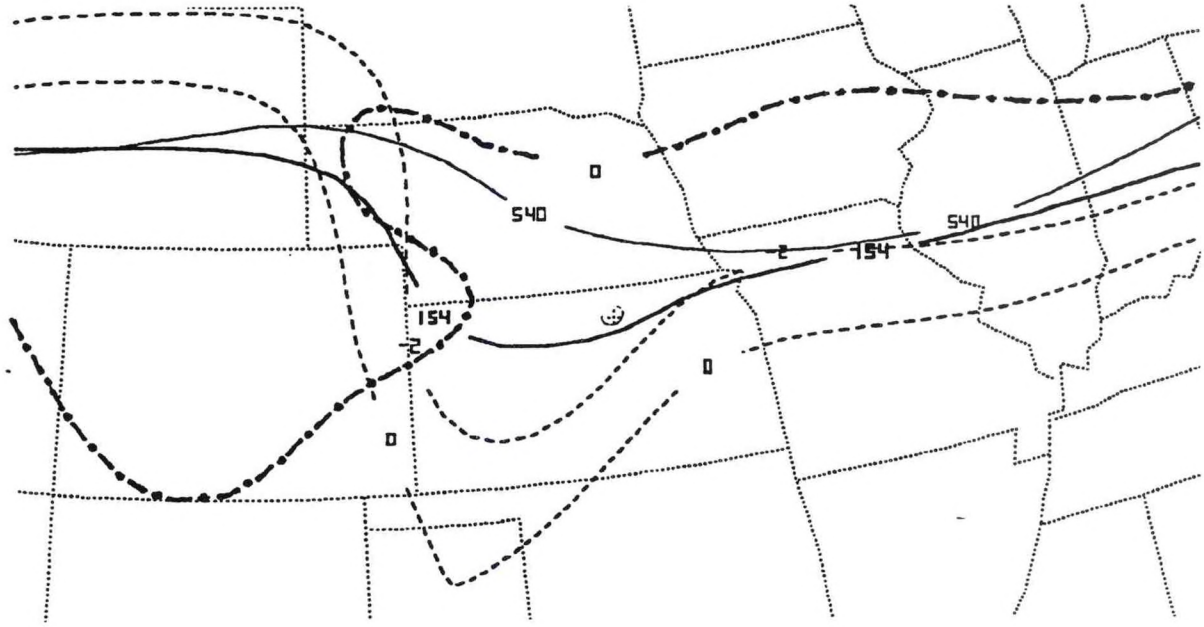

Figure 5. Eta model 18-hour forecast of 540 decameter 1000-500-mb thickness (thin solid contour), 0°C and -2°C temperature from 850-mb (dashed contours), 154 decameter 850-700-mb thickness (thick solid contour), and the 0°C boundary layer temperature (dash-dotted contour) valid 1800 UTC 25 March 1994.

isotherm in the boundary layer extended from northern Nebraska into east central Iowa indicating rain would be likely. The 540 decameter contour of the 1000-500-mb layer thickness, which is often correlated with the rain/snow line, extended from northwest Nebraska into northwest Missouri with higher thickness over northern Kansas. However, the 154 decameter line from the 850 to 700-mb layer thickness extended through northwest and north central Kansas into northwest Missouri, indicating that Concordia could be on the rain/snow line.

Statistical guidance from the 1200 UTC 25 March NGM run (FWC) forecasted a temperature at Concordia of 47°F at 1800 UTC. Additionally, the air temperature was predicted to rise to 53°F by 2100 UTC. In association with these surface air temperatures, the FWC forecasted the precipitation type to be rain (Figure 6).

Figure 7 is a time series cross section of relative humidity derived from gridded model output from the 0000 UTC 25 March Eta model run. A layer of relatively dry air was forecast from the surface to 750-mb (relative humidity < 60%) with the driest air around 850-mb. Relative humidity was forecast to increase only slightly at the surface by 1800 UTC, and remain quite low around 850-mb. This is close to the time when precipitation first began at Concordia, Kansas.

```
FOUS14 KWBC 251544
CNK  SC   NGM MOS GUIDANCE    E/25/94  1200 UTC
DAY /MAR  25 /MAR  26                  /MAR  27                  /
HOUR   18 21 00 03 06 09 12 15 18 21 00 03 06 09 12 15 18 21 00
MN/MX                    41             47             29       48
TEMP   47 53 50 44 43 43 43 44 43 43 42 38 36 33 30 36 43 45 44
DEWPT  23 24 26 29 34 36 38 39 36 33 30 25 23 22 21 22 22 21 21
CLDS   OV BK BK OV OV OV OV OV OV OV OV OV BK SC SC SC SC SC SC
WDIR   14 15 14 14 15 10 06 36 35 35 35 35 33 31 31 31 31 30 30
WSPD   09 13 14 13 14 13 12 13 15 20 21 21 19 16 12 18 20 20 12
POP06        6     13     83     83     47     19      8      4       0
POP12                    67             77             23              3
QPF        0/     0/    3/3    3/    1/3    0/    0/0    0/     0/0
TSV06    7/ 4 19/ 7 42/10 41/ 9 46/ 0 36/ 0 11/ 0  1/ 0  0/19
TSV12       18/ 8        58/16        58/ 0        12/ 0
PTYPE  R  R  R  R  R  R  R  R  R  R  R  R     R      S      S      S
POZP   2  5  2  4  2  5  1  3  3  0  1     0      0      0      0
POSN  24 10  2  0  1  1  4  5  4  5 24    52     81     91     67
SNOW       0/     0/    0/0    0/    0/0    0/    0/1    0/     0/0
CIG     7  6  6  6  6  5  2  2  3  3  4     7      6
VIS     5  5  5  5  5  5  3  3  3  4  5     5      5
OBVIS   N  N  N  N  N  N  F  F  F  F  N     N      N
```

Figure 6. FWC guidance for Concordia, Kansas from the 1200 UTC 25 March 1994 NGM model run. Temperature (TEMP) and precipitation type (PTYPE) forecasts for the period of snowfall are shaded.

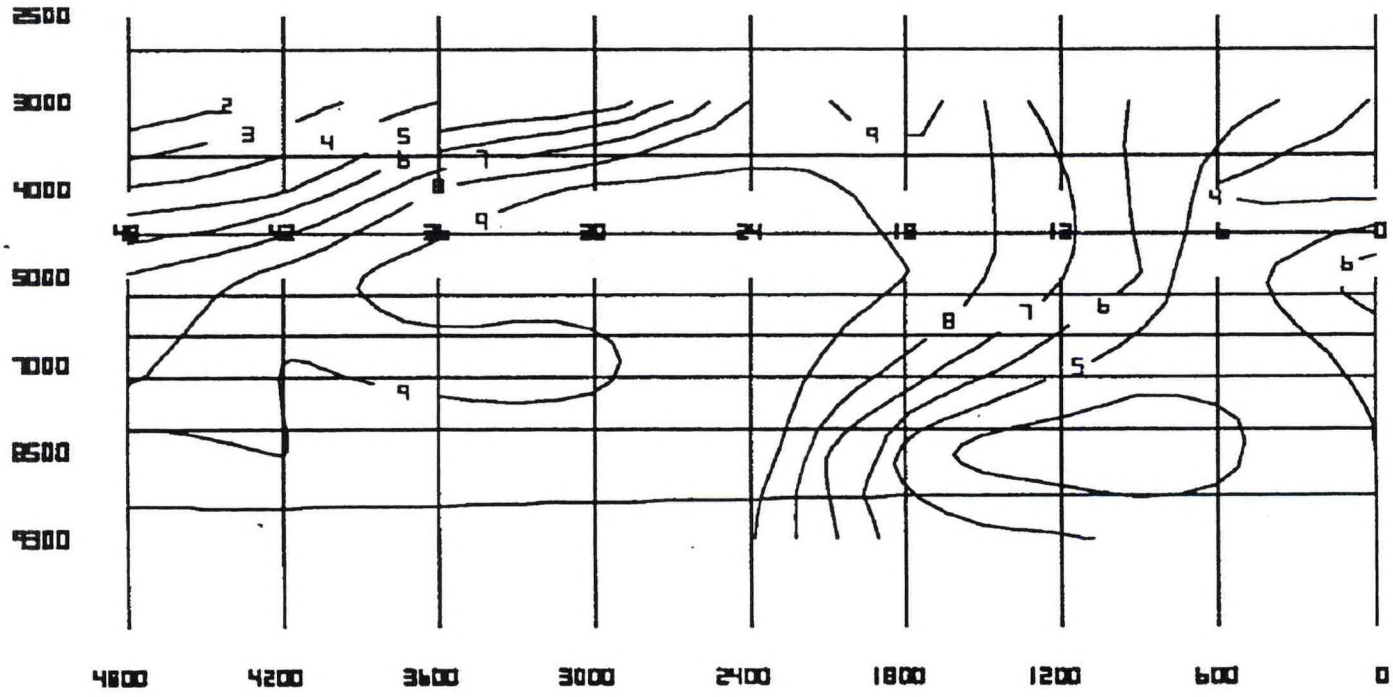

Figure 7. Forecast time series cross section of relative humidity (solid contours every 10%) from the 0000 UTC 25 March Eta model run.

3. Analysis of Rawinsonde Data

Rawinsonde data from 1200 UTC 25 March 1994 indicated that the 850-mb observed temperature at Topeka, Kansas, was 0°C with a wet-bulb temperature of about 23°F (well below 0°C). This sounding (Figure 8) indicates relatively dry air up to 700-mb, (the dew point depression at 850-mb was 22°C). Moisture is indicated above 700-mb with a dew point depression of 5°C at 500-mb.

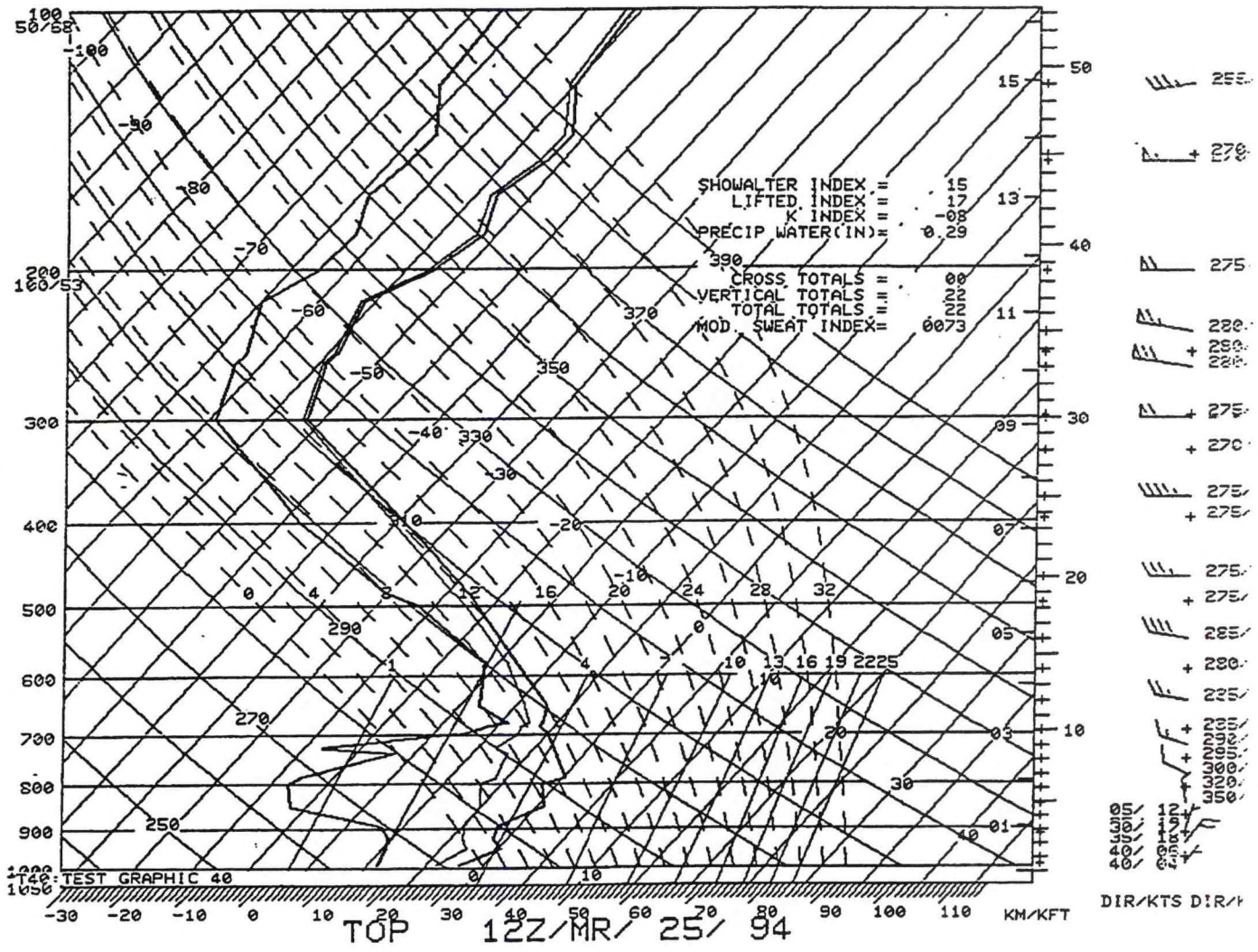

Figure 8. Topeka, Kansas sounding valid 1200 UTC 25 March 1994.

4. The Evolution of Precipitation Across Northern Kansas.

Light rain showers developed across southwest Kansas around 1530 UTC. By 1800 UTC, a large area of snow, sleet and rain had expanded north and east, covering much of northern and central Kansas (Figure 9). The precipitation across northern Kansas fell as snow.

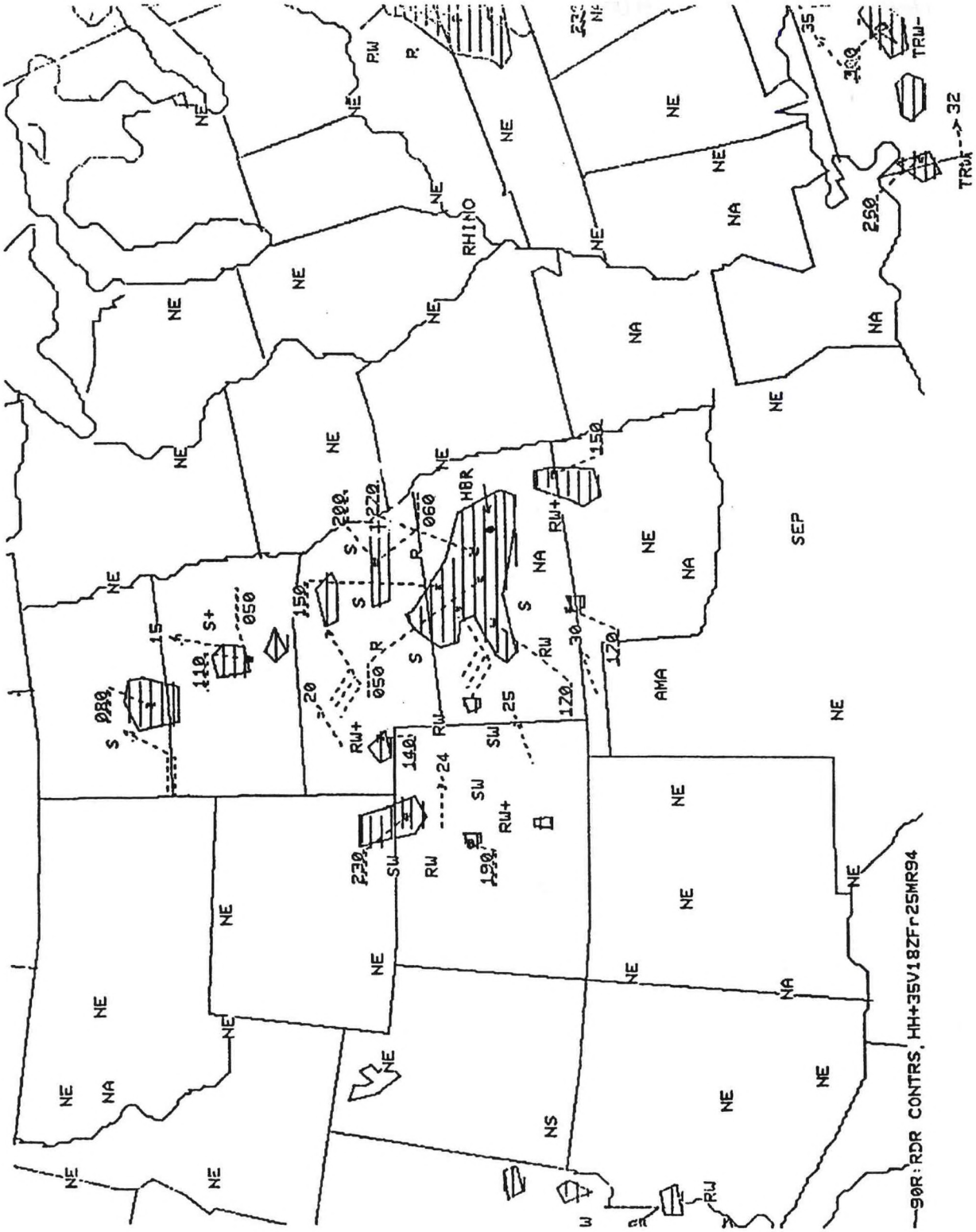

Figure 9. Radar summary chart valid 1800 UTC 25 March 1994.

Figure 10 shows that the ASOS at Concordia, Kansas, reported a ceiling of 10,000 feet around 1500 UTC. Virga was visible to the south and west with an overcast ceiling above 12,000 feet (not shown). At 1756 UTC, the temperature at the Concordia, Kansas, ASOS was 41°F with a dew point temperature of 20°F.

By 2005 UTC, ASOS reported 1/2 of a mile visibility in moderate snow and fog. The temperature was 32°F with a dew point temperature of 30°F. The ceiling measured 800 feet broken and 3,500 feet overcast.

```
CNK SA 1456 AO2A M100 OVC 10+ 244/34/19/1110/022/ 56006 OVC V BKN

CNK SA 1556 AO2A 110 SCT 10+ 251/37/20/1507/025

CNK SA 1656 AO2A CLR BLO 120 10+ 242/39/20/1310/022

CNK SA 1756 AO2A 100 SCT 10+ 229/41/20/1409/018/ 58013 10042 20025

CNK SA 1856 AO2A M32 BKN 7S- 225/37/22/1612/016/ SB50 PCPN 0000
CNK SP 1903 AO2A M27 BKN 31/2S- 226/35/27/1612/016/ PCPN 0000
CNK SP 1913 AO2A M21 OVD 13/4S-F 221/34/30/1510/015/ PCPN 0000 FIBI
CNK SP 1915 AO2A M19 OVC 11/4S-F 220/34/30/1509/014/ PCPN 0000
CNK SP 1920 AO2A W13X 3/4S-F 220/33/30/1510/014/ PCPN 0000
CNK SP 1926 AO2A 4 SCT M12 OVC 1S-F 218/33/30/1309/014/ PCPN 0000
CNK SP 1942 AO2A 4 SCT M8 BKN 35 OVC 11/2S-F 215/33/30/1408/013/ PCPN 0000
CNK SP 1945 AO2A 4 SCT M10 BKN 35 OVC 2S-F 214/33/31/1310/012/ PCPN 0000

CNK RS 1956 AO2A 4 SCT M12 BKN 33 OVC 11/4S-F 209/33/30/1308/011/ PCPN 0000
CNK SP 2005 AO2A M8 BKN 35 OVC 1/2SF 207/32/30/1207/010/ PCPN 0000
CNK SP 2013 AO2A 5 SCT M9 OVC 1/2SF 205/32/32/1208/009/ PCPN 0000
CNK SP 2017 AO2A M7 BKN 21 OVC 11/4S-F 203/33/30/1207/009/ BKN V OVC PCPN 0000
FIBI
CNK SP 2019 AO2A M5 BKN 21 OVC 11/2S-F 204/33/29/1308/010/ BKN V OVC PCPN 0000
CNK SP 2023 AO2A M5 BKN 21 OVC 2S-F 204/33/32/1409/010/ OVC V BKN PCPN 0000
CNK SP 2032 AO2A M5 BKN 10 BKN 19 OVC 7 201/33/30/1310/008/ SE32 PCPN 0000

CNK RS 2056 AO2A M7 BKN 21 BKN 10+S- 192/35/32/1109/006/ 58041 6000/ BKN V SCT
SE32B51 PCPN 0000 PRESFR
CNK SP 2103 AO2A 7 SCT 21 SCT 10+ 189/35/32/1208/005/ SE2058 PCPN 0000

CNK SA 2156 AO2A 80 SCT 100 SCT 10+ 172/37/32/1010/000/ SE2058 PCPN 0000
```

Figure 10. Surface observations from 1456 to 2156 UTC 25 March 1994 from the Concordia, Kansas ASOS.

5. Conclusion

It appears that the primary mechanism for low-level cooling in this case was due to evaporation or sublimation (since the cloud base may have been at a level where temperatures were below 0°C, sublimation could have been more important initially) (Figure 8). When precipitation falls through a very dry layer between the cloud and ground, it will experience evaporation (if liquid) or sublimation (if solid). Thus, the air temperature below-cloud base will be cooled.

In the case examined here, the time series cross-section of relative humidity clearly predicted dry air to remain in place in the lower troposphere through 1800 UTC 25 March. As the air became saturated, the temperature approached the wet-bulb temperature of this drier air. Since the wet-bulb temperature was below freezing, the precipitation fell as snow (McNulty 1988).

When deciding what precipitation type to forecast in an area of interest, "low-level" temperatures, thickness values, and the magnitude of dynamical forcing for upward vertical motion are very useful. However, the forecaster should also consider lower tropospheric relative humidity in the area of interest. This is when a PCGRIDDS time series cross-section of relative humidity (from gridded model output) may be useful.

6. Acknowledgements

The author would like to thank George Phillips, Science and Operations Officer (SOO) at WSFO Topeka, Kansas, for his valuable input into this paper.

7. References

McNulty, R. P., 1988: Winter Precipitation Type. Central Region Technical Attachment 88-4, DOC, NOAA, NWS, Central Region Scientific Services Division, Kansas City, MO.

CENTRAL REGION APPLIED RESEARCH PAPER 14-06

OBSERVATION WITH THE WSR-88D OF A STORM THAT PRODUCED A WEAK TORNADO

John Kwiatkowski
National Weather Service Office
Goodland, Kansas

1. Introduction

On the evening of May 5, 1994, severe weather struck northwest Kansas. This was almost entirely a hail event, but one storm produced a small short-lived tornado about 15 miles southwest of Goodland. The WSR-88D depicted a number of features associated with this storm that distinguished it from other storms that evening. This paper briefly examines those features.

2. Discussion

The event took place in a setting of moderate CAPE (1000-1500 J/Kg taken from a sounding modified with the SHARP program). The VAD wind profile as the event began (Figure 1) showed winds veering with height in the lower atmosphere, but unimpressive speed shear. The most distinguishing radar feature of the severe storms preceding the tornadic one was high mid level reflectivities.

Figure 2 shows reflectivity patterns from the storm at 0143 UTC, shortly before it produced its tornado (touchdown was at 0200 UTC and occurred along the line between Sherman and Wallace Counties). Figure 3 displays velocity patterns at 0143 UTC. Characteristics that separated the storm from earlier ones included a considerable overhang in the inflow (southeast) direction, and a possible BWER, as indicated at 9.9 degrees elevation angle (about 20000 feet AGL at that distance from Goodland). The velocity data at 6.0 and 9.9 degrees indicated cyclonic rotation to the north of the apparent BWER; however, the radar operator reported that cyclonic signatures with this storm were very transient and usually weak. (Velocity data from the volume scan from 0155 UTC was far less impressive in suggesting severity.)

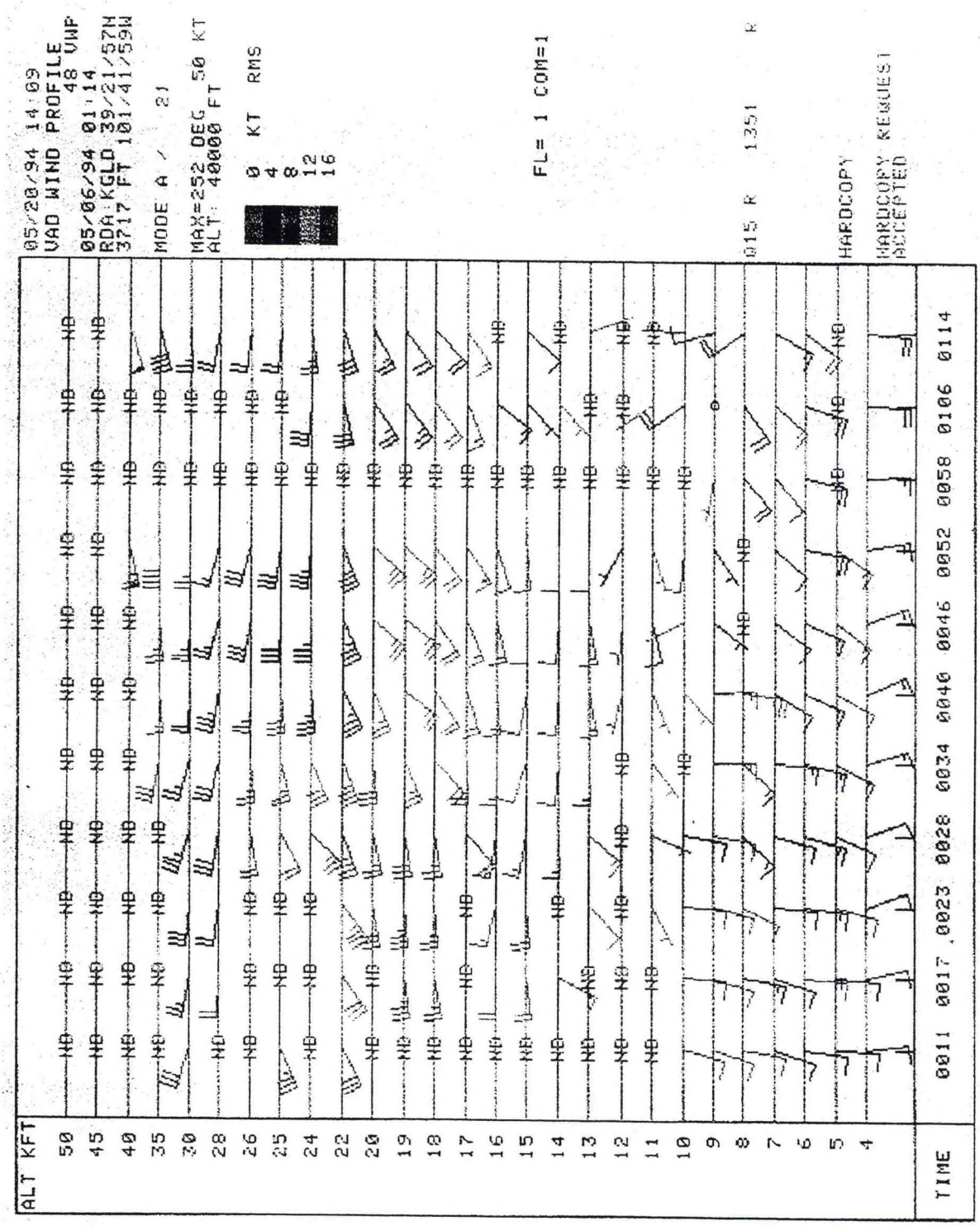

Figure 1. VAD Winds at Goodland 0114 UTC 6 May 1994.

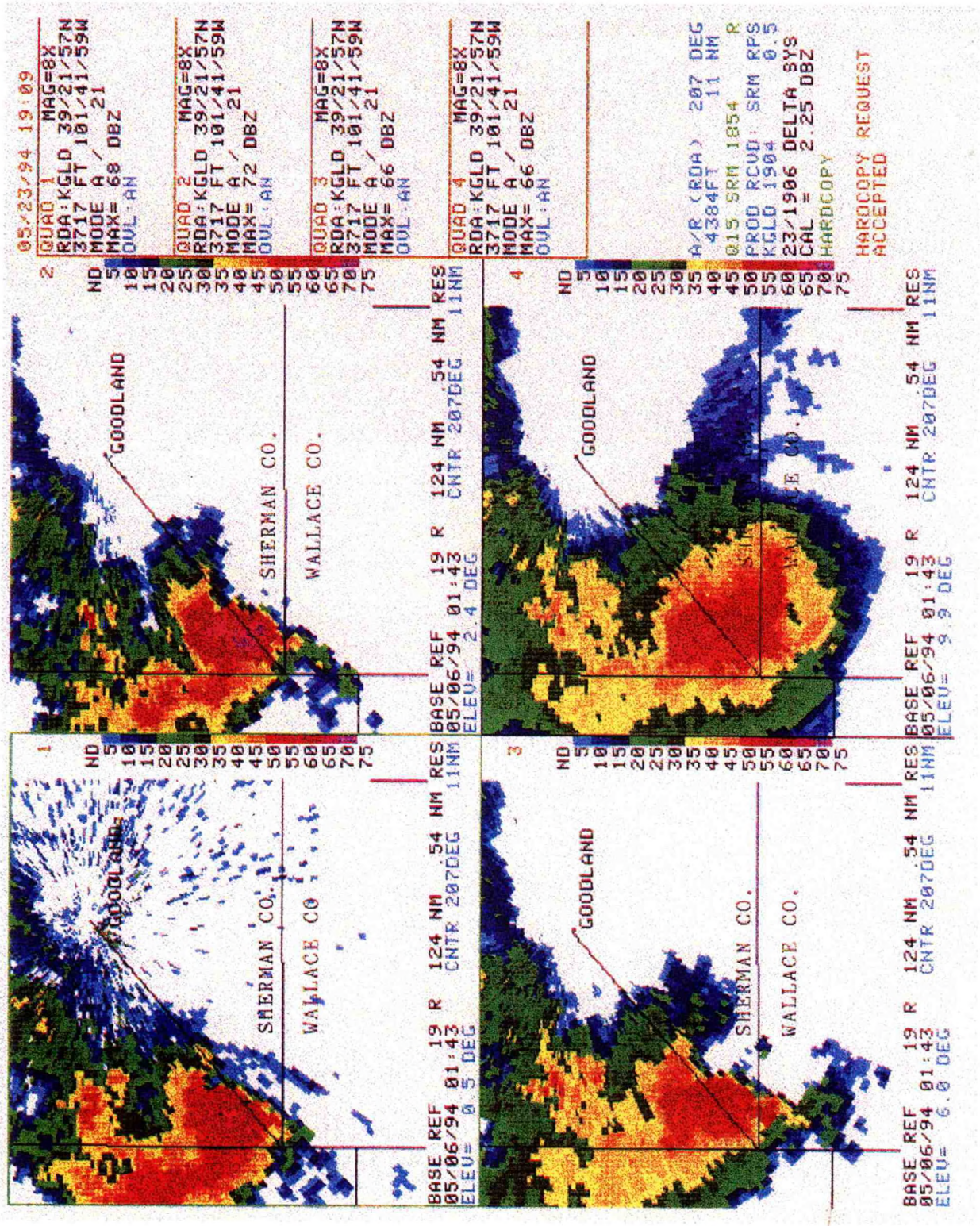

Figure 2. Four-panel Reflectivity at 0143 UTC 6 May 1994. Annotated to enhance view of overhang.

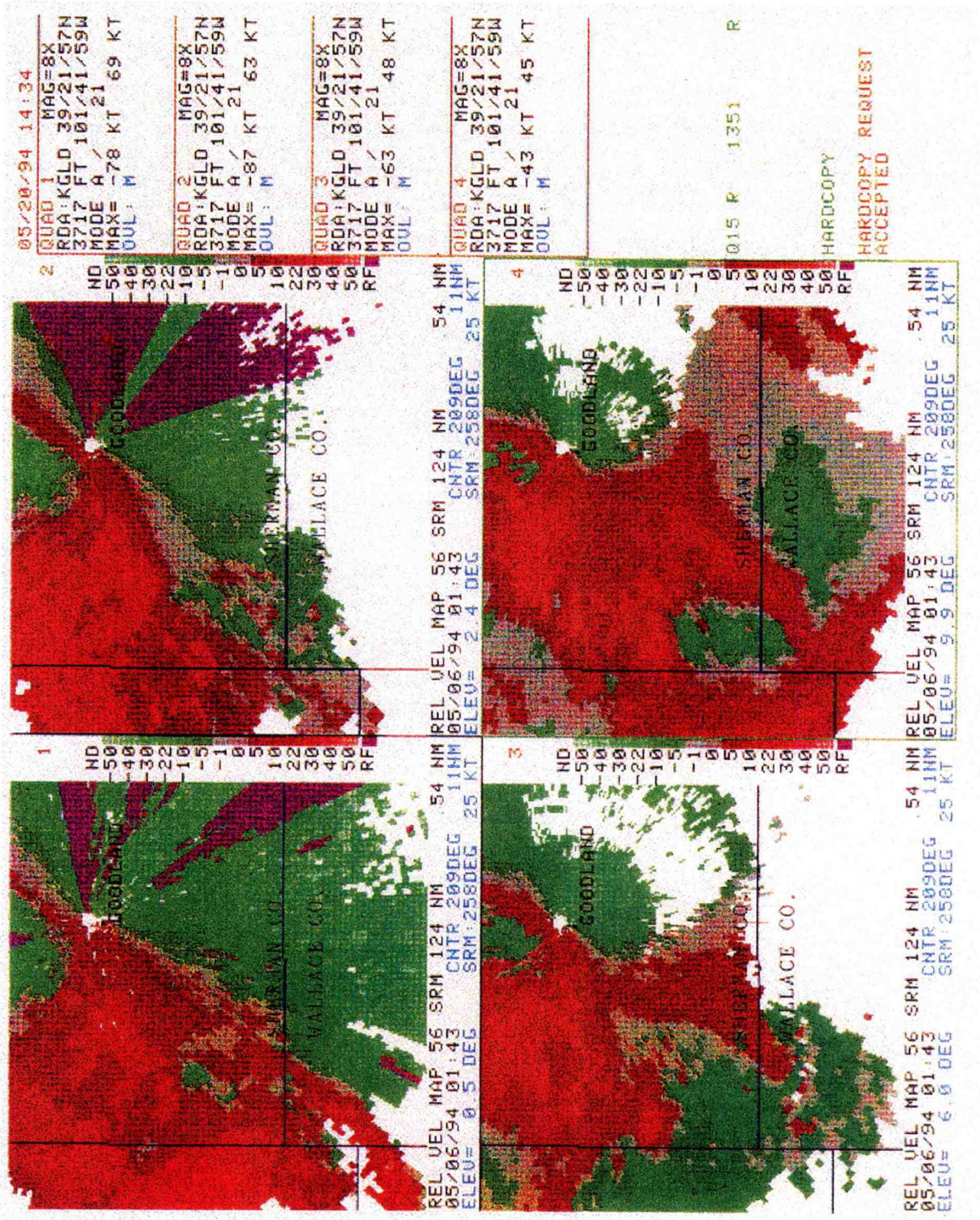

Figure 3. Four-panel Storm Relative Motion at 0143 UTC 6 May 1994.

Thus the reflectivity data, in showing a persistent, extensive mid-level overhang, was consistent in indicating the strong updraft and potential severity of the storm. However, the strength and vertical extent of rotation were far less impressive, so whether the storm was a candidate for tornado-genesis was questionable.

However, well-developed rotation through a deep level may not have been necessary for tornadogenesis. Figures 4 through 7 show significant--and unique--features of the storm's environment as it advanced towards Sherman County from northeastern Kit Carson County. Note that two boundaries came into play as the storm moved southeast. The one to the north seems to have been associated with a dryline, the one to the south was an outflow boundary from earlier thunderstorms. Interaction with the first boundary turned the storm southward. Intersection with the second occurred about 10 to 15 minutes prior to tornadogenesis. The process is much clearer on time lapse than in still graphics. The linear echo to the southwest of the storm on Figure 7 is part of the boundary that was being absorbed. The boundary farther to the southeast is part of the storm's gust front.

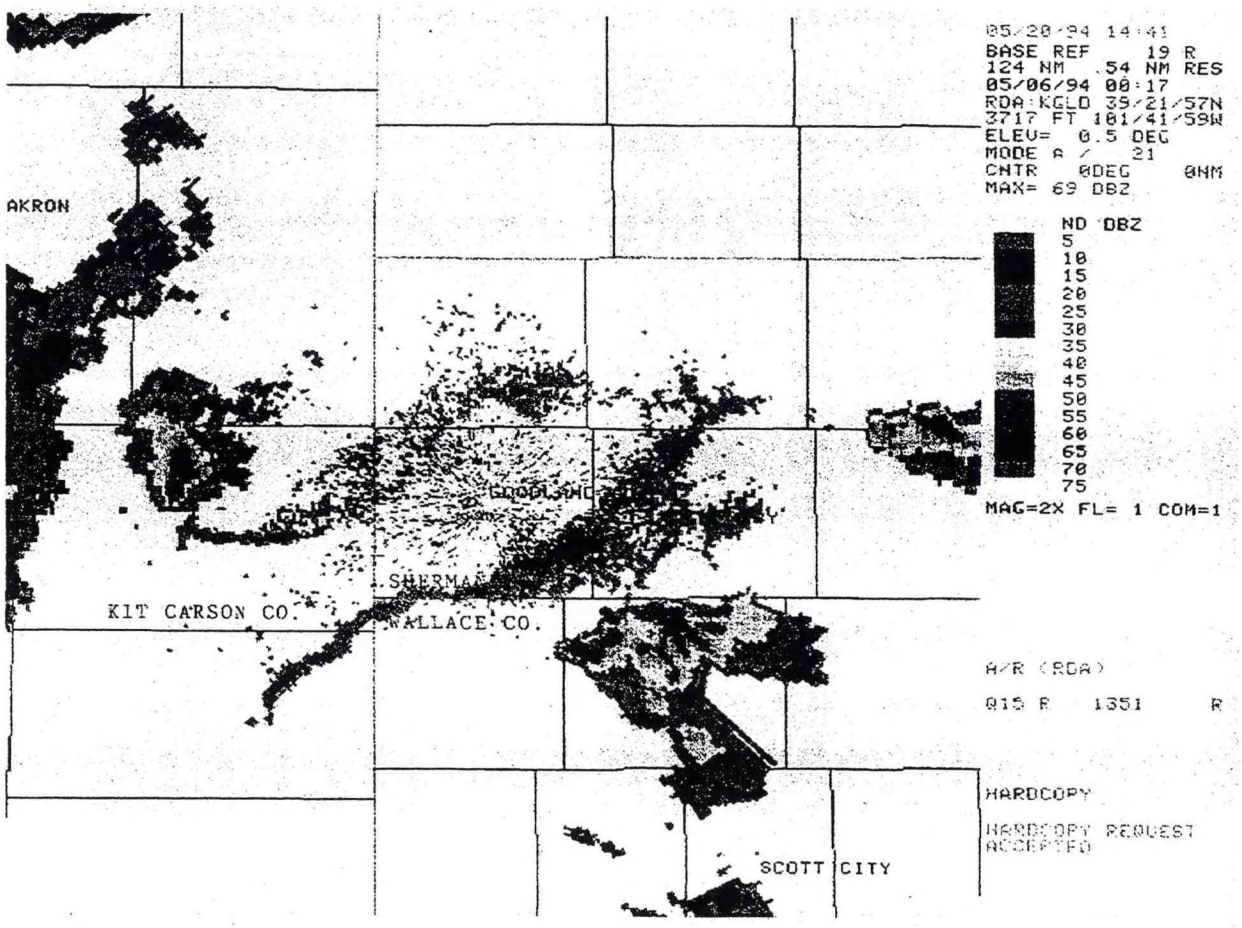

Figure 4. Half-degree Base Reflectivity at 0017 UTC 5 May 1994.

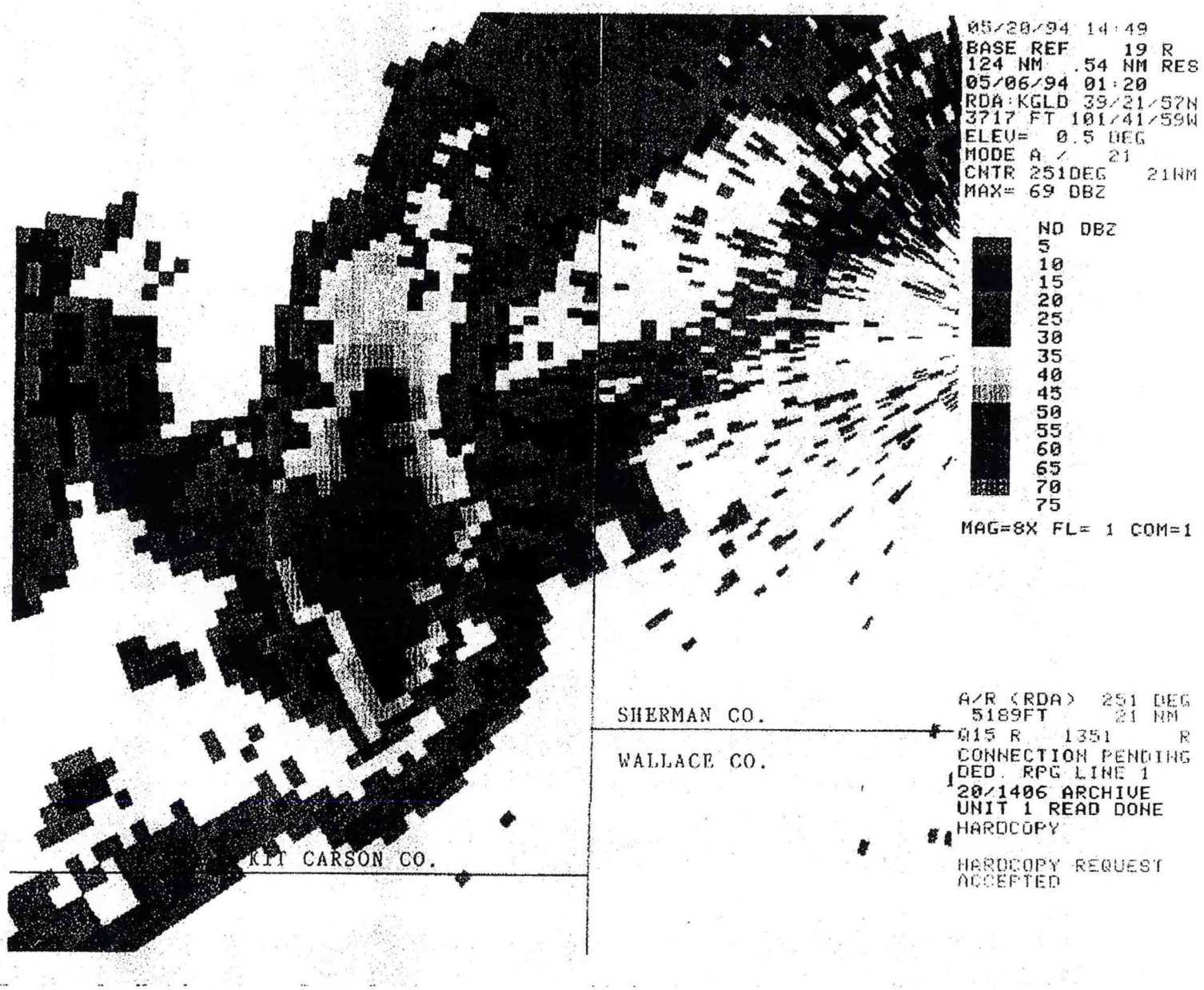

Figure 5. Half-degree Base Reflectivity at 0120 UTC 6 May 1994. Goodland near 25 dBZ indicator.

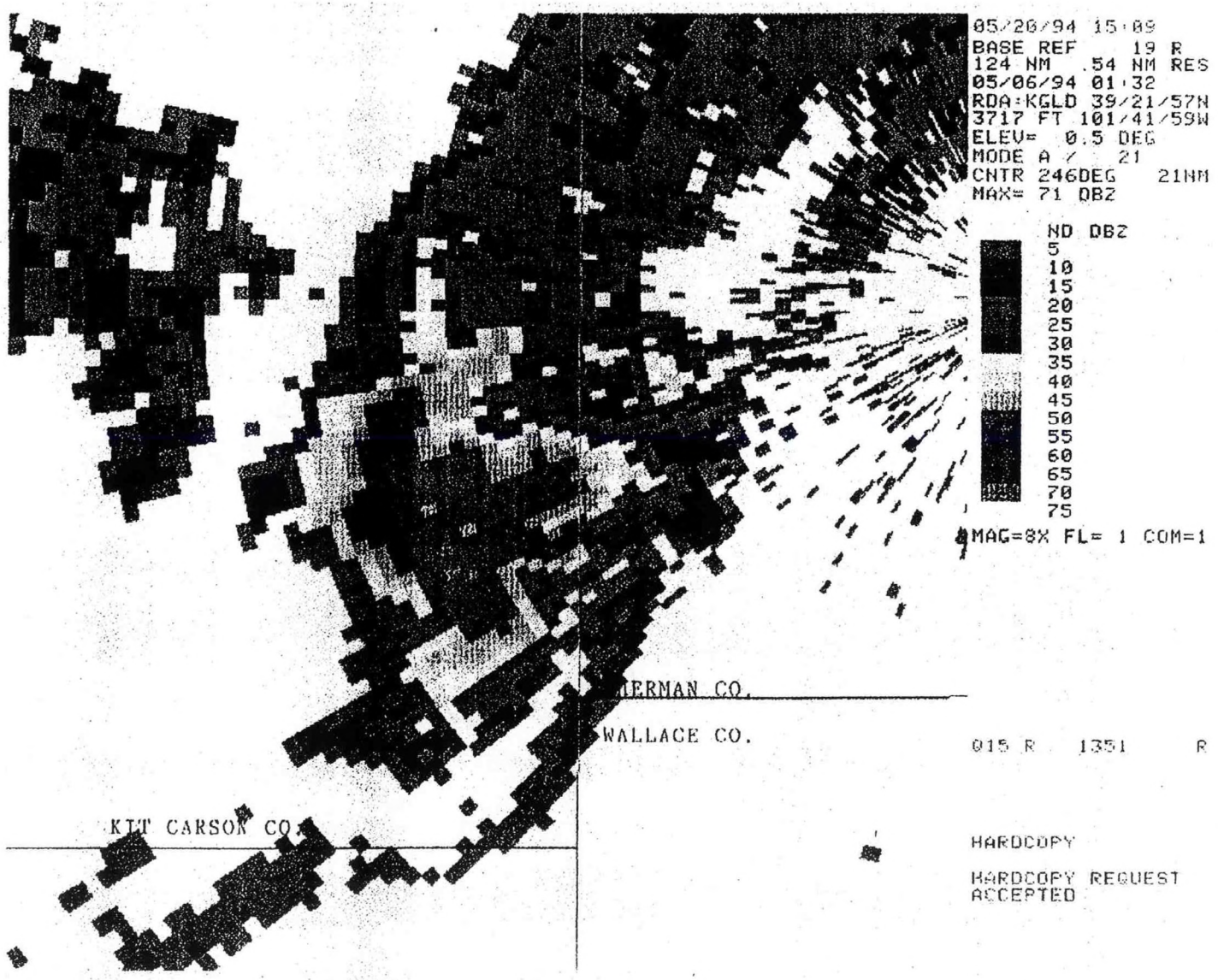

Figure 6. Half-degree Base Reflectivity at 0132 UTC 6 May 1994. Goodland near 15 dBZ indicator.

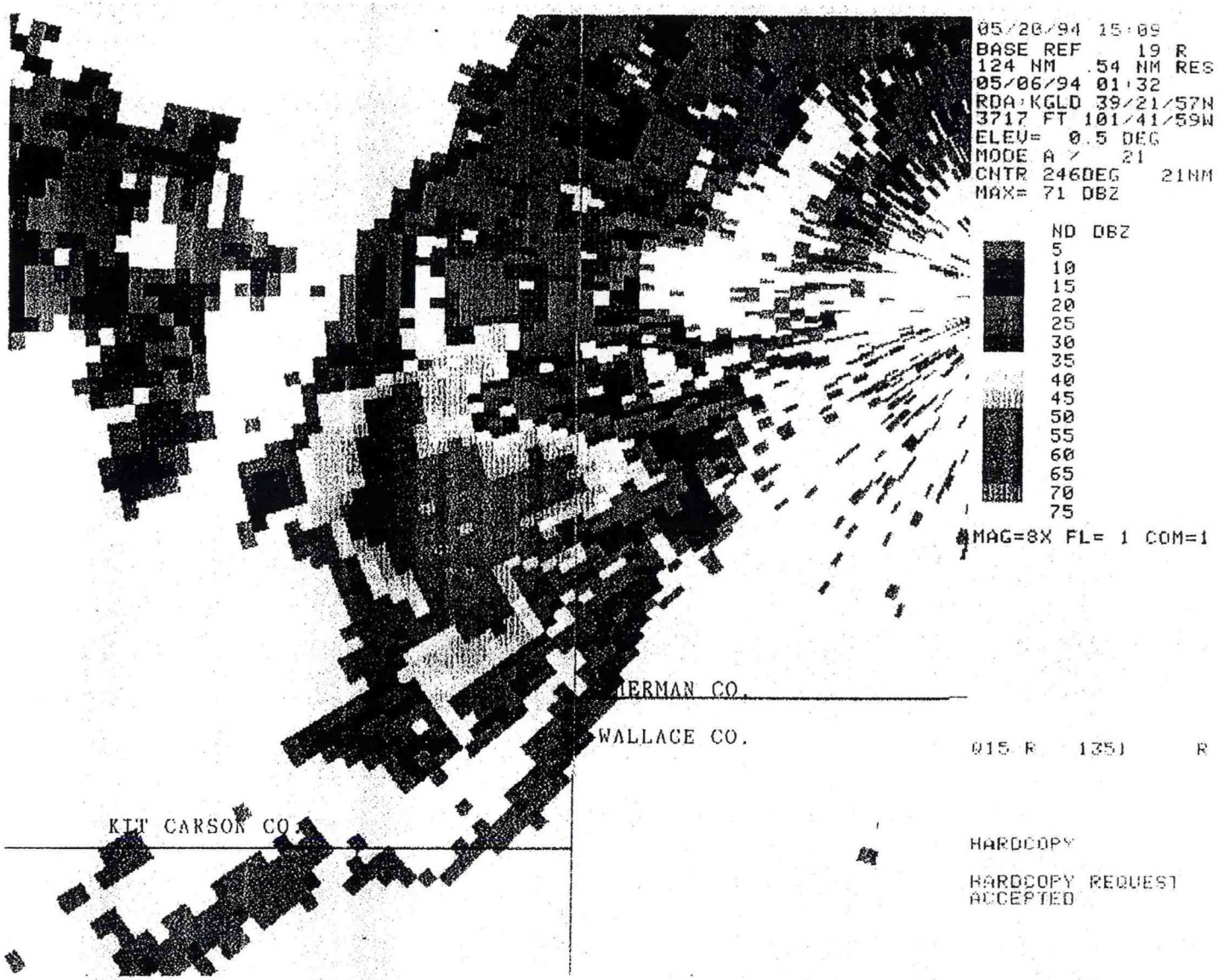

Figure 7. Half-degree Base Reflectivity at 0143 UTC. Goodland at radar center.

3. Conclusion

The upshot is that shortly after the storm turned south it experienced an environment of strong low-level convergence as it encountered the northward moving outflow boundary. The result would have been an increase in cyclonic relative vorticity. With the powerful updraft available to stretch the vorticity, it is not surprising that a small tornado was able to "spin up".

In fact, with the abundance of low level horizonal vorticity, it is quite possible that this was not a "classic" tornadic event, where a mid-level cyclone plays an indispensable role. With a strong updraft to cause stretching, there was plenty of opportunity for a small tornado regardless of whether there was deep rotation. Whether this was a spin-up or classic situation, the WSR-88D provided plenty of evidence that this storm was going to be different from others that evening. The unique aspects of the storm were recognized by WSO Goodland in a real-time basis, and a tornado warning was issued based on the 0143 UTC data.

CENTRAL REGION APPLIED RESEARCH PAPER 14-07

ASOS PERFORMANCE AT WSO CONCORDIA, KANSAS

Jeff Raberding
National Weather Service Office
Concordia, Kansas

Phil Baker
National Weather Service Office
Norfolk, Nebraska

1. Introduction

The Automated Surface Observing System (ASOS) is currently being installed around the country and will become the nation's primary surface observing network before the end of this decade. As of January 30, 1995, there was a total of 47 commissioned sites. A commissioned unit means that surface observations taken by the ASOS unit are official for that site. In the case of the Weather Service Office (WSO) at Concordia (CNK), Kansas, ASOS was commissioned on September 1, 1992.

A breakdown by region reveals Southern Region, of the National Weather Service (NWS), has the most commissioned sites; which at the time of this writing was fifteen. Following the Southern Region are the Central and Western Regions with fourteen, and the Eastern Region with four.

The purpose of this study is to inform the meteorological community of the experienced CNK staff working with ASOS in an operational setting, and some of the problems encountered. To achieve this, a quality control study, termed continuing study in this paper, of meteorological field parameters reported by ASOS versus that of manual observations has been carried out by the CNK staff. This study began on the date of commissioning, September 1, 1992 and focuses on precipitation. This will hopefully add valuable information for future improvements in ASOS.

2. Advantages of ASOS

One great advantage of ASOS is allowing the meteorologists to concentrate on other duties. It is especially important during severe weather, when all attention can be focused on monitoring the radar, coordinating with spotters, issuing warnings, and operating the NOAA Weather Radio console. In addition, being automated, it more accurately measures pressure tendencies, and beginning and ending times of intermittent precipitation. ASOS "never forgets" to take a special observation (SP) when criteria for ceiling and visibility are met, a bonus for pilots, but there could be "outages".

With ASOS preparing daily and monthly summaries, the human preparation of the Climatic Summaries is significantly reduced. ASOS stores a vast amount of easily accessible climate data, therefore, requests for climate information from the public can be handled quickly and easily. An automated phone number allows pilots, as well as the public, to call and receive current surface weather conditions at the airport, without the meteorologist being involved.

A significant advantage of ASOS over manual observations is the ability for the forecaster to connect, via computer modem, to any ASOS in the country, and download observations or even climate data. Up-to-the-minute data is available, even at most uncommissioned sites. This has been especially helpful at CNK, where the ASOS Plot Program graphically presents trends of temperature, dew point, visibility, ceilings, and wind. The ability to more effectively analyzes data has proved helpful for short-term forecasts, terminal forecasts, and even as an aid in severe weather events. The Hill City, Kansas, ASOS has been very valuable to CNK in reporting the strength of outflow winds from thunderstorms to the west of CNKs county warning area. The latest 5-minute observations are downloaded in a matter of seconds into CNKs PC. This data is then rapidly processed and analyzed to determine if significant weather is headed for Osborne, Kansas.

Staff members at CNK have estimated that ASOS saves roughly 10 minutes per hour by not requiring us to take manual observations. That adds to some 80 minutes per shift that can now be used for other duties, including only taking hourly SA observations, with no additional special observations.

3. Disadvantages of ASOS

Like any new system on the cutting edge of technology, a few problems naturally arise. However, the unit at CNK has worked extremely well and is quite dependable. There has only been a handful of times that a sensor has failed and manual backup procedures had to be implemented. Most of the sensor problems are well documented and being corrected, such as the freeze up of the wind bottles on the anemometer during icing situations and erroneous

visibility readings after a fresh snowfall. Another problem not as well documented are the false indications of a scattered deck during precipitation events, especially rain. The heated tipping bucket rain gauge performs as the old tipping buckets, but underreports precipitation, especially during times of heavy precipitation. None of these problems have been insurmountable or have burdened regular office duties. The support of the ASOS Operations and Monitoring Center (AOMC) to assist when problems arise has been very good.

Underreporting of precipitation remains a significant problem. Table I, of the following ASOS precipitation study, documents these differences since commissioning date. With a distance of 990 feet between the ASOS heated tipping bucket and the backup weighing rain gauge, one would expect differences for the reported precipitation, but these differences should average out over time. They do not. When the ASOS observation was deemed to be unrepresentative by the observer, either the report processing was turned off or ASOS was edited.

Table I
ASOS DAILY SUMMARY vs. UNOFFICIAL MF1-10B
WSO CONCORDIA, KANSAS

YEARLY PRECIPITATION SUMMARY (ASOS VS. UNOFFICIAL)

	UNOF	ASOS	DIFF (ASOS-UNOF)
1992 (9-1 > 12-31):	10.74	11.11	+0.37
1993 (1-1 > 12-31):	47.31	44.49	-2.82
1994 (1-1 > 6-30):	10.16	9.52	-0.64

Note: ASOS precipitation values obtained from "Daily Summary" pages on ASOS. Unofficial precipitation values obtained from unofficial Form MF1-10B 6-hourly precipitation totals.

Unofficial rain gauge consists of a weighing bucket gauge backed up with a tipping bucket gauge. The ASOS rain gauge is 990 feet northeast of the unofficial rain gauges.

Some ASOS daily summaries were edited to show precipitation values obtained from an unofficial rain gauge, if the observer deemed the reported precipitation value on ASOS to be unrepresentative. As a result, the above indicated difference in unofficial and ASOS precipitation values is **Conservative.**

ASOS stores a wealth of internal climate data. Yearly, monthly and daily summaries are kept. All surface observations (SAOs) are stored in the system's database, along with being transmitted longline. Other observations include one-minute observations, and five-minute Standard Hydrometeorological

Exchange Format (SHEF) observations. These data are downloaded to the National Climatic Data Center (NCDC) in Asheville, North Carolina. In determining daily precipitation, any of the above reporting methods can be used. It is no longer a simple Form F-6 put in the mail. Due to several reasons, discrepancies may exist between, for example, the Daily Summary and the sum of the 6-hourly SAO precipitation remarks. This has an adverse effect on Local Climatological Data (LCD) accuracy. The accuracy of the data contained in the LCD is the responsibility of the local office.

4. The ASOS Precipitation Study

Among the first group of NWS offices in the country to possess a fully commissioned ASOS was CNK. Since commissioning a continuity study by the NWS has been ongoing. This study consisted of manual observations of precipitation (from the Universal Weighing Rain Gauge), maximum and minimum temperatures, sky conditions (including types and amounts), and visibility, every six hours. This data was entered as unofficial on the Form MF1-10B. At the end of each month, these forms were sent to NCDC and to the Colorado Climate Center (Boulder, Colorado). From this, a persistent problem with precipitation reporting has been observed at CNK, and precipitation data from this study was used as comparison to the official heated tipping bucket of ASOS. The precipitation data examined for this paper was from commissioning on September 1, 1992 to June 30, 1994.

The reporting of precipitation amounts, by ASOS, which is less than apparently observed, is a problem. This is primarily caused by design limitations inherent to tipping bucket rain gauges. The pivoted, or tipping reservoir, is positioned directly under the funnel. The mercurial switch, connected to the tipping reservoir, registers 0.01 inch each time alternate sides of the tipping reservoir are filled and emptied. A small amount of precipitation invariably falls onto the full side of the reservoir during the tipping motion. So in effect, 0.01 inches is reported, when slightly more than 0.01 inches had fallen into the tipping reservoir. The magnitude of this error increases as the precipitation rate increases. The ASOS heated tipping bucket is subject to these errors, and attempts to compensate by using formulas written into the precipitation reporting software. As of yet, the formulas have not completely compensated for the errors inherent in the tipping bucket design.

Tables I and II summarize the results of this study. Table I documents the differences between precipitation reported by ASOS and the decommissioned weighing rain gauge at CNK. Table II documents, in greater detail, the differences between precipitation reported by ASOS and the Daily Water Equivalent listed in the monthly LCD publication.

Table II
ASOS DAILY SUMMARY vs. LCD
WSO CONCORDIA, KANSAS

DATE	ASOS DAILY SUMMARY	ASOS 6-HRLY SUMS	MONTHLY LCD	MF1-10B
09/20/92	1.08	1.05	1.07	1.06
10/18/92	TR	TR	0	0
10/20/92	0.01	0	0	0
11/03/92	0	TR	TR	TR
11/17/92	0	TR	TR	TR
12/01/92	0	TR	TR	TR
12/02/92	0	0.32	0.32	0
12/12/92	0	TR	TR	TR
12/16/92	0	TR	TR	TR
12/30/92	0	TR	TR	TR
01/03/93	0.04	0.04	0.07	0.07
01/19/93	0.14	0.14	0.18	0.18
01/20/93	0.44	0.43	0.50	0.50
01/21/93	0	TR	TR	0
05/31/93	0	0	TR	0
09/20/93	0	TR	TR	0
12/13/93	1.07	1.08	1.08	1.26

Note: After examining all the data from September 1,1992 to June 30, 1994, the 17 days listed in this table were the only ones where discrepancies were found between the ASOS daily summary and the LCD.

ASOS reports precipitation in several ways: One minute data, 5-minute hydrological observations, SAO remarks [that include hourly precipitation groups (PCPN xxxx), 3- and 6-hourly precipitation groups (6xxx/), 24-hour precipitation groups (7xxxx)], and the Daily Summary.

Before June 1993, NCDC used any or all of the various ASOS precipitation reporting methods in determining the Daily Water Equivalent. Even unofficial 6-hourly totals obtained from the continuity study were considered in determining Daily Water Equivalent. Beyond June 1993, NCDC chose, for simplicity's sake, to use the Daily Summary as the primary source of daily precipitation data for ASOS commissioned stations.

5. Concluding Remarks

Despite minor problems, ASOS, overall, has performed quite well. It has freed the staff to concentrate on other duties, such as issuing warnings and updating forecasts. The reliability of the system has been very good, with most

sensor problems occurring in the colder months of the year. Sensor outages usually last for less than two days. The accuracy of cloud base heights reported by the ASOS ceilometer has been excellent, except for the previously mentioned scattered deck that is most likely precipitation. The pressure sensor is always within tolerance with the mercurial barometer.

The heated tipping bucket performance is generally lacking year-round, and has been augmented when observer judgement dictated. As of this writing, NWS policy requires the augmentation of the heated tipping bucket with the data from the standard weighing rain gauge. Test modifications are being done at a few Central Region ASOS sites to improve heated tipping bucket accuracy. Hardware modifications to the tipping bucket forthcoming should improve its accuracy, but winter performance will remain a difficult task to conquer. As of this writing, the ASOS program office and the contractor are replacing the mercury switch used to sense the tipping of the bucket with a more reliable reed switch. They are also extending the funnel to bring the tip of its orifice closer to the top of the tipping bucket assembly. The stops are also being redesigned to improve reporting accuracy.

Table II summarizes the differences between the ASOS daily summary and the LCD at CNK. After investigation, apparently the ASOS Daily Summary is more often the place of erroneous daily precipitation information than any other source, and is a poor judge of LCD accuracy. It is unknown why the ASOS Daily Summary appeared in error, particularly on those days when a trace of precipitation fell in the latter part of 1992.

In only one of the seventeen days of the study does the ASOS Daily Summary appear to have been edited to agree with the Form MF1-10B. In the period of the study, it was left to the discretion of the observer on duty at the end of the day to edit the ASOS Daily Summary if he or she deemed ASOS reported precipitation values to be unrepresentative, due to poor performance of the ASOS heated tipping bucket gauge.

Clearly, NCDC often, particularly in 1993, relied on the continuity study precipitation values listed on the Form MF1-10B. Four of the seventeen days in the study contained discrepancies likely caused by using unofficial data for the LCD. This does not imply that the LCD Water Equivalent is unrepresentative, just that the LCD Water Equivalent does not agree with the ASOS Daily Summary.

Even more often, the discrepancies between the ASOS Daily Summary and the monthly LCD were caused by a failure, on the part of the observer, to correct erroneous precipitation remarks in the transmitted surface observation, or to make a post event paper correction on Form B-14. For unexplained rea-

sons, several days of the study had Daily Summaries in error, particularly on days a trace of precipitation fell. Usually, the Daily Summaries were not corrected at the end of the day to match the SAO precipitation remarks for the day.

The ASOS is not completely "automated" in the purest sense of the word. It is the observer's responsibility to augment the system and correct any erroneous data. This can be, at times, tedious when attempting to reconcile the Daily Summary to the SAO precipitation remarks, but it is necessary to reduce the number of discrepancies in the monthly LCD.

It is unfortunate ASOS heated tipping bucket consistently underreports precipitation. At the time of this writing, the ASOS unit at CNK has had minor modifications to the heated tipping bucket. So far, the results look promising.

The results of this study suggest the system has great potential, some of which has been realized. The problems that have arisen can be solved, and the ASOS system will only continue to improve.

5. Acknowledgement

The authors would like to give special thanks to Phil Clark, the ASOS Meteorologist for the Surface Observation Modernization Office, for his input and time in reviewing this paper.

6. References

Systems Program Office, 1994: ASOS Progress Report. Silver Spring, MD, IX, 2, 12pp.

CENTRAL REGION APPLIED RESEARCH PAPER 14-08

THE PROCESSES THAT LED TO THE DEVELOPMENT OF A WAKE DEPRESSION IN EASTERN SOUTH DAKOTA ON JULY 21, 1993

Daniel P. Mohr[1]
National Weather Service Forecast Office
Bismarck, North Dakota

1. Introduction

In the morning hours of July 21, 1993, a Mesoscale Convective System (MCS) moved from central into eastern South Dakota, where it dissipated between 1625 UTC and 1725 UTC. As the MCS dissipated east of Huron, southeast winds at the Weather Service Office (WSO) Huron (HON) gusted to 62 mph, exceeding the National Weather Service (NWS) Severe Thunderstorm Warning criteria of 58 mph. These high winds downed tree limbs in the town of Huron. As the MCS moved east of Aberdeen, southeast winds gusted to 51 mph at WSO Aberdeen (ABR). Also, according to the gust recorder at HON, winds were sustained between 35 and 45 mph for more than one hour, meeting the NWS criteria for a High Wind Warning. A Special Weather Statement was issued from HON to cover the local nature of the high winds. This paper examines the synoptic and mesoscale processes that led to the development of a wake depression that was likely a contributing factor for the high winds.

2. The Development of the MCS

The formation and maintenance of the MCS was believed to be the result of isentropic lift, and weak cyclonic vorticity advection increasing with height from an up stream short wave trough, the latter feature evident on the initial hour 1200 UTC NGM 700 hPa and 500 hPa charts (Figure 1). The analysis of the 1200 UTC 310 degree Kelvin isentropic surface (Figure 2) showed good lift over western and central South Dakota with little or no isentropic lift over eastern South Dakota. At 1200 UTC, the short-wave trough was located over the western Dakotas. The NGM forecasted the trough to move northeast into eastern North Dakota and southern Canada by 1800 UTC, where the best lift was located (Figure 1). The position of the short-wave trough on satellite (Figure 3) agrees well with the NGM's location. The 300 hPa chart (Figure 1) shows both diffluence and apparent divergence, that also would have provided support for the MCS.

[1]Current affiliation, NWS Office Aberdeen, South Dakota.

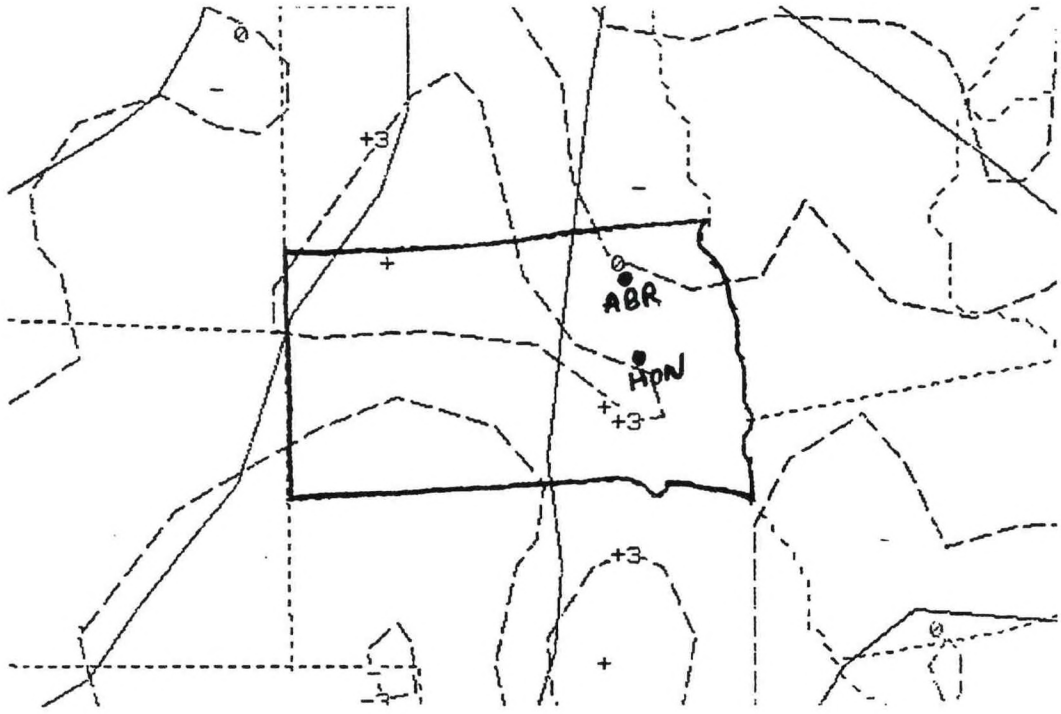

Figure 1a. Short-wave trough, progressing northeastwards across South Dakota (understood for the following figures), at 700 hPa 1200 UTC 21 July 1993.

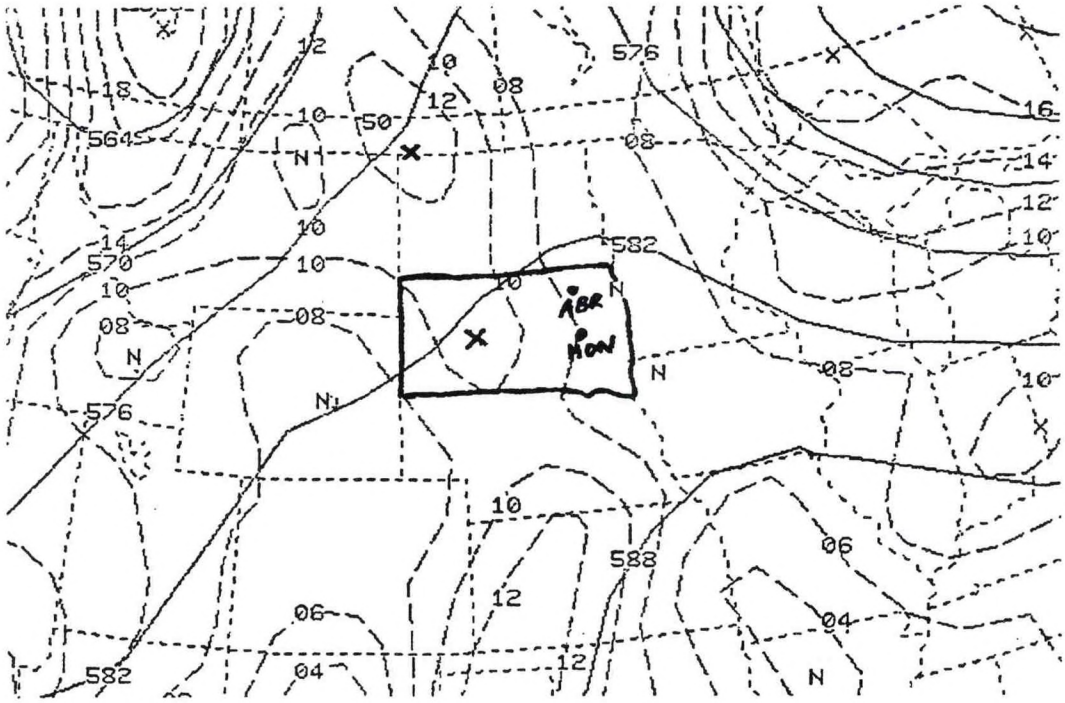

Figure 1b. Short-wave trough at 500 hPa 1200 UTC 21 July 1993.

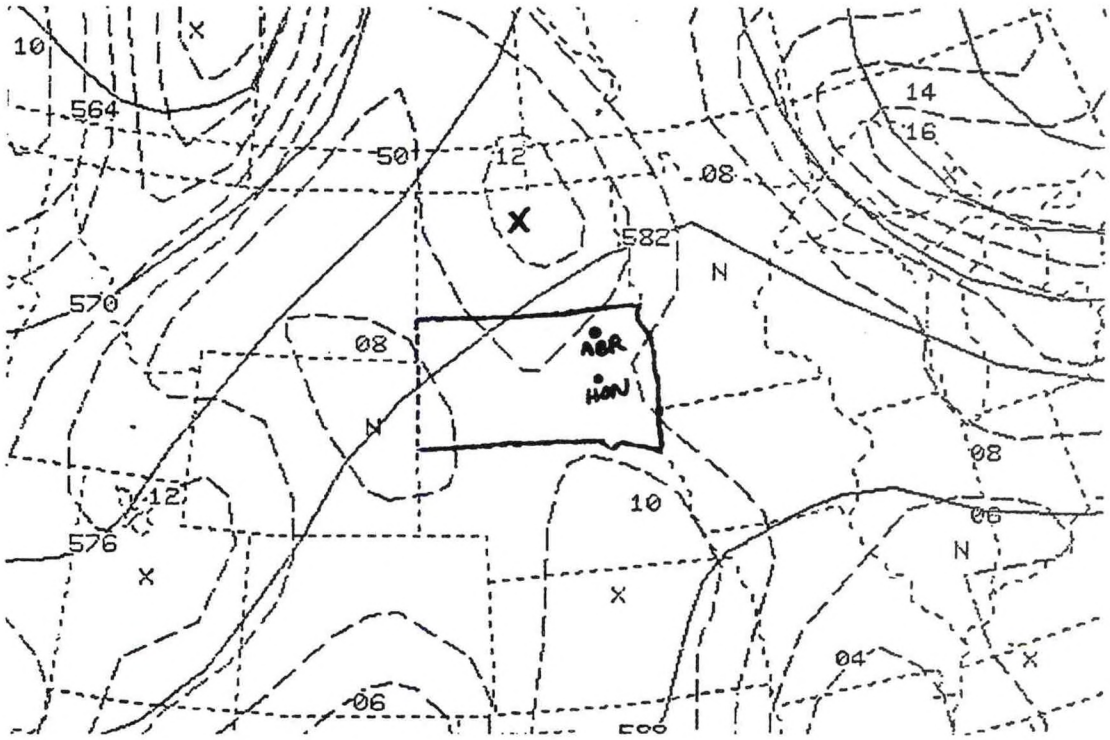

Figure 1c. Short-wave trough at 500 hPa 1800 UTC 21 July 1993.

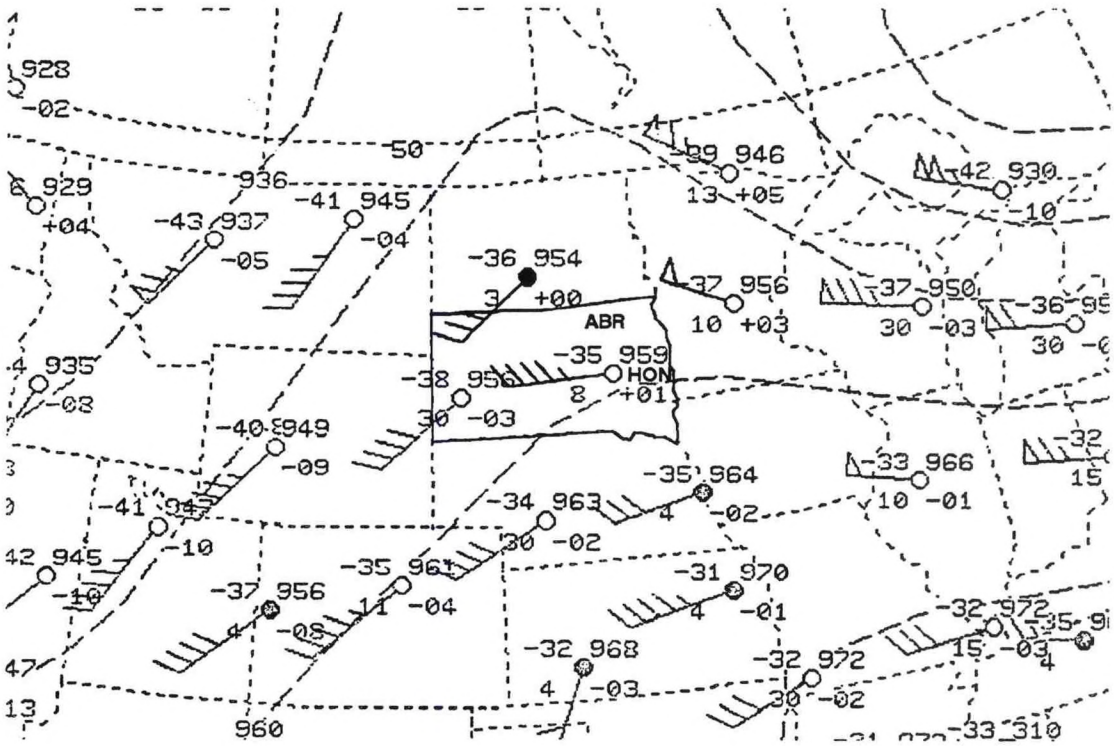

Figure 1d. 300 hPa divergence and difluence over Huron and Aberdeen (inferred from the winds -- not computed) at 1200 UTC 21 July 1993.

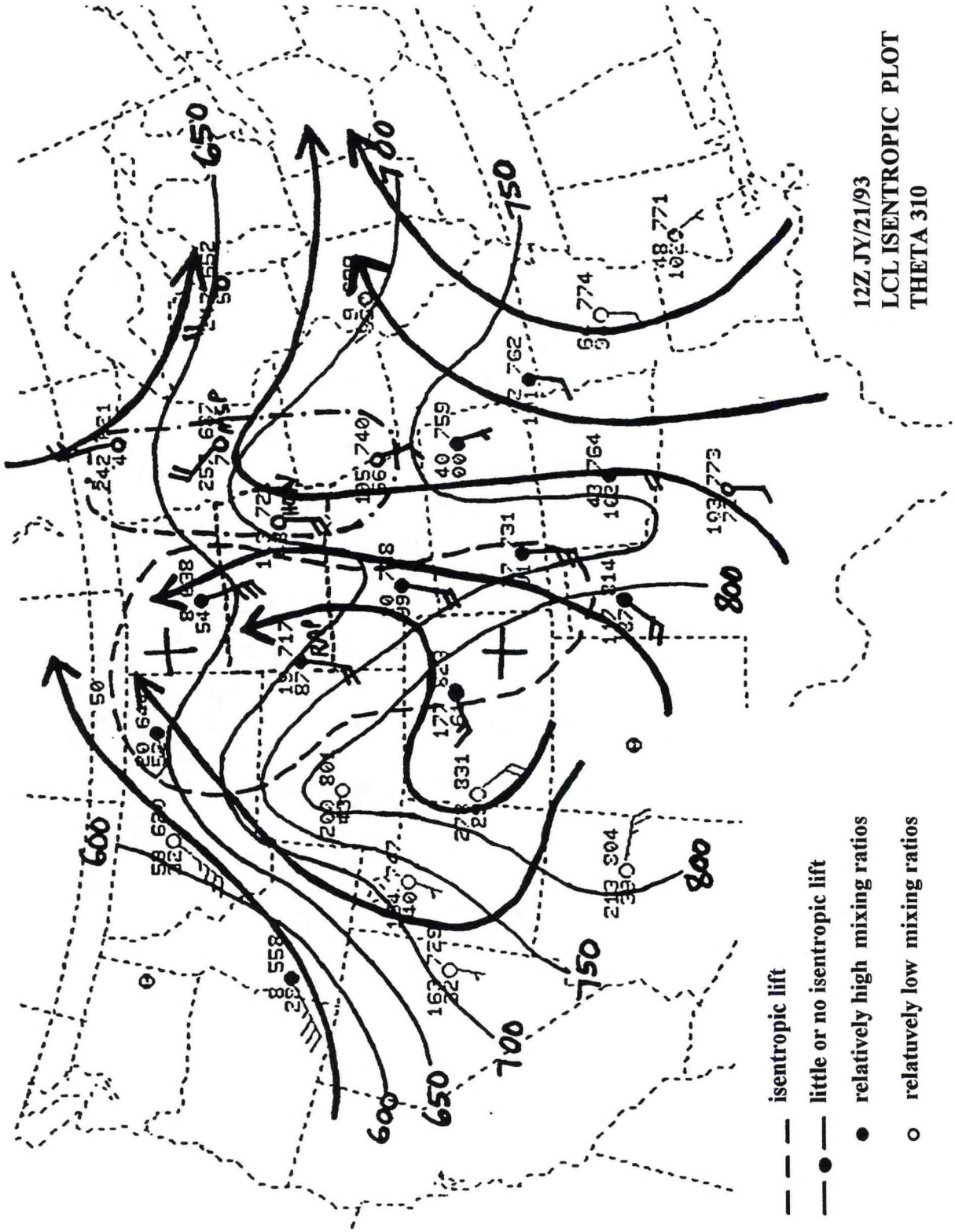

Figure 2. Local 310 Degrees Kelvin isentropic analysis for 1200 UTC 21 July 1993.

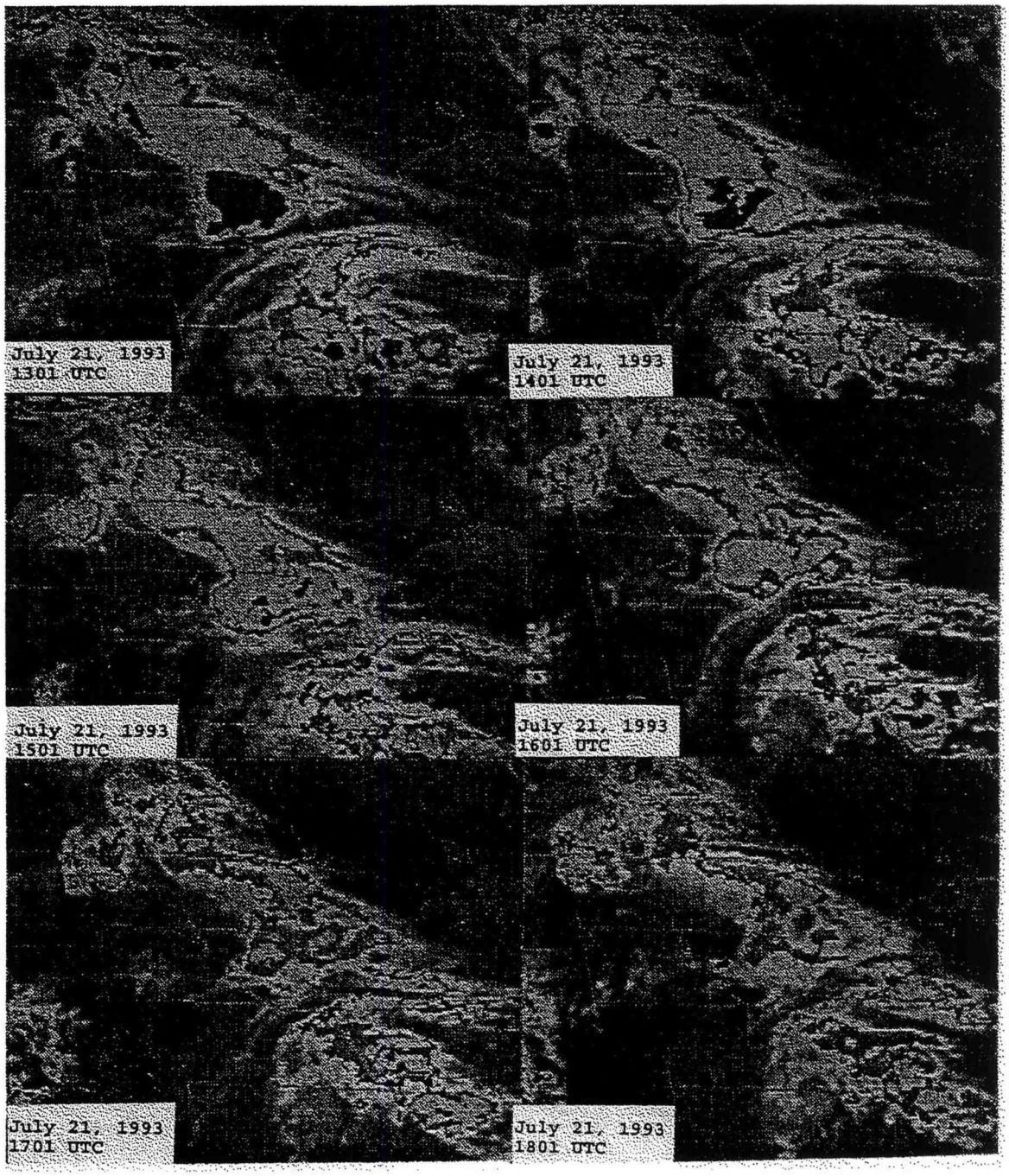

Figure 3. Infrared 1301 UTC - 1801 UTC 21 July 1993.

The 1500 UTC 21 July 1993 surface analysis (synoptic scale; mean sea-level isobars) (Figure 4a) showed high pressure located to the east of the Dakotas with low pressure and associated fronts across the western part of the region. From Figure 4a, it can bee seen that the pressure gradient across South Dakota was fairly strong. The winds forecasted for the day were to be from the southeast at 15 to 25 mph. The 1200 UTC 21 July 1993 HON sounding (Figure 4b) shows that the winds right above the surface were 30 kts from the southeast providing low-level moisture into the MCS.

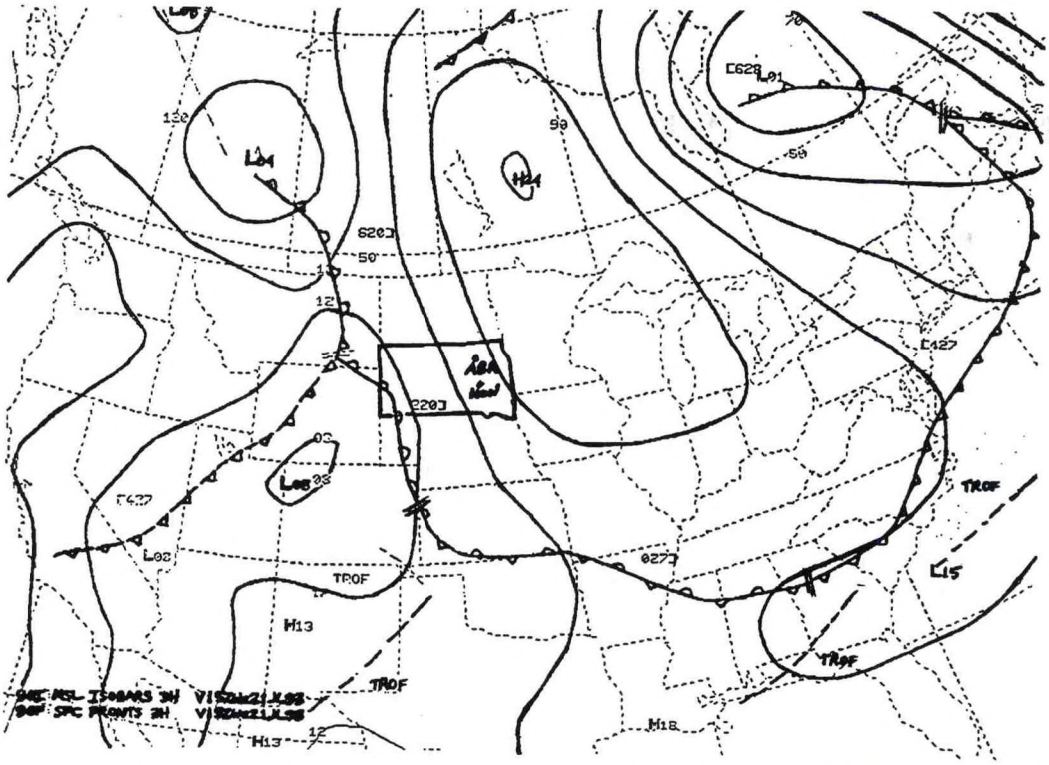

Figure 4a. Surface analysis (mean sea-level pressure) for 1500 UTC 21 July 1993.

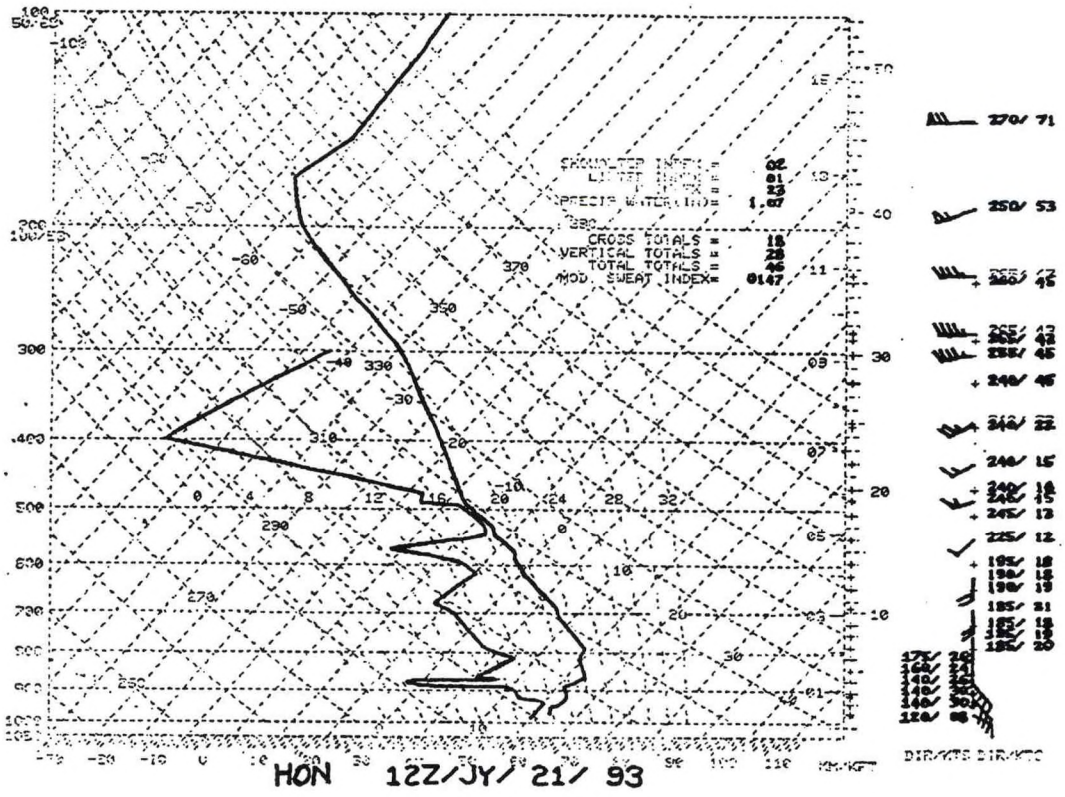

Figure 4b. HON Skew-T 1200 UTC 21 July 1993.

The overlays from the HON radar (Figure 6) and the infrared satellite pictures (Figure 3), from the morning of July 21, 1993, show part of the life cycle of the MCS and its dissipation. The radar overlays from 1325 to 1830 UTC give a good picture of the MCSs movement, strength, and dissipation. The MCS had an eastward movement of about 25 miles an hour. Echoes continued west and southwest of Huron after the MCS dissipated. The satellite pictures (Figure 3) indicated a strong MCS in central South Dakota at 1301 UTC, with its dissipation in eastern South Dakota at 1801 UTC. (Note the cloud tops warming with time.)

3. The Development of the Wake Depression

The decrease in lift from the exiting short-wave trough, increased stability, and the normal diurnal decrease in thunderstorm activity were all believed to be factors for the dissipation of the MCS in eastern South Dakota. The increased stability was evident on the HON sounding where the Showalter Index was +2 and the Lifted Index was +1 (Figure 4b).

In the pre-MCS environment, the air was dry and warm above the surface, as shown from the HON sounding (Figure 4b). The dry air was also evident across the Eastern Plains, on the 310 degree Kelvin isentropic surface. From examining Figure 2 a decrease in moisture at approximately 700 hPa can be seen. The mixing ratio on the 310 degree Kelvin isentropic surface decreased from 8.7 g/kg at Rapid City (RAP) to 4.8 g/kg at HON and to .7 g/kg at Minneapolis (MSP). Both figures depict the stable environment the MCS encountered as it moved into eastern South Dakota.

It is believed, the inversion, shown on the HON sounding (Figure 4b), restricted strong mixing of the MCSs outflow winds (mesohigh) down to the surface as the mesohigh moved through Huron and Aberdeen. This is shown in Figures 5a and 5b, where the winds became light northwest at Huron beginning at 1250 UTC as the mesohigh moved into the area. The winds then became southeast at 15 knots as the mesohigh moved east of Huron. The winds at Aberdeen decreased from the southeast at 1150 UTC, as the mesohigh entered the area, and then increased from the southeast as the mesohigh moved east of Aberdeen. However, as the MCS/mesohigh continued to dissipate in the stable environment near and east of Huron and Aberdeen, saturated parcels in the rain cooled air could now descend along the moist-adiabat permitting mixing (Figure 4b).

According to Fujita (1963), fast-moving mesohighs created by MCS can induce a wake depression in its mature to remnant stage (Figure 7). Also, according to Fujita (1963) the excess-deficit pressure (Figure 7) is highly dependent upon the traveling speeds of the mesohighs. If the mesohighs are stationary, practically no wake depression forms. However, a fast-moving mesohigh is characterized by a significant high- and low-pressure couplet.

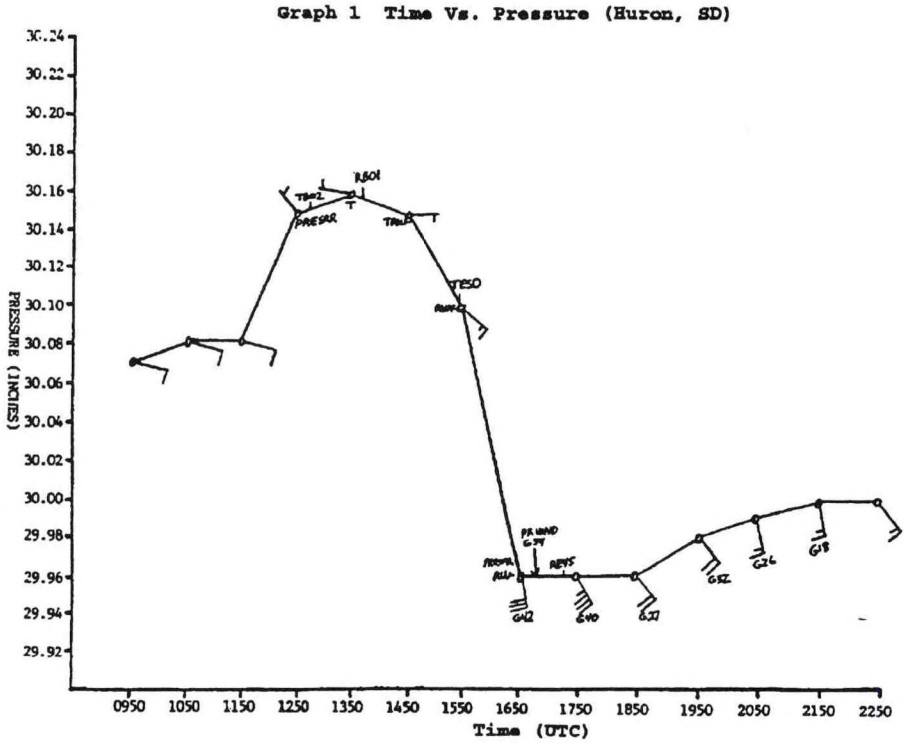

Figure 5a. Time vs. pressure graph for HON from 0950 UTC to 2250 UTC 21 July 1993.

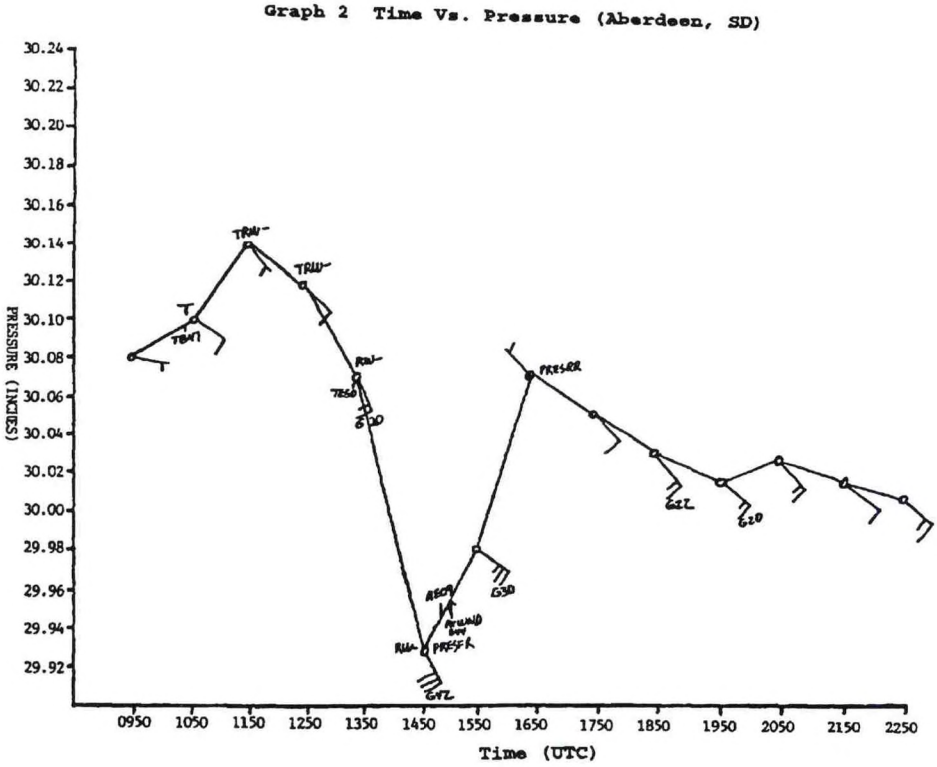

Figure 5b. Time vs. pressure graph for Aberdeen from 0950 UTC to 2250 UTC 21 July 1993.

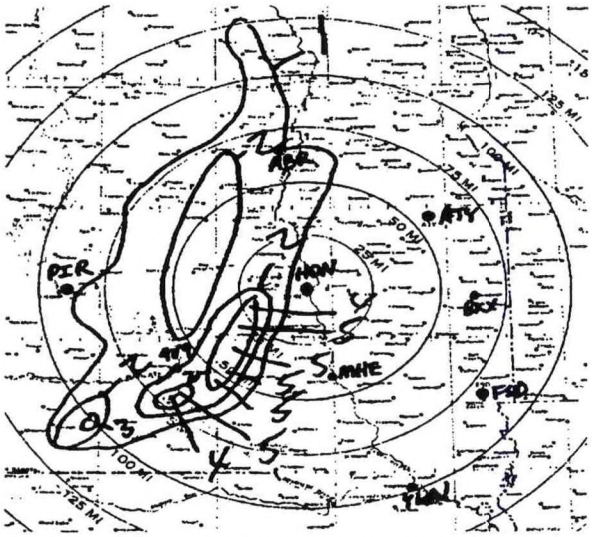

Figure 6a. 1325 UTC 21 July 1993.

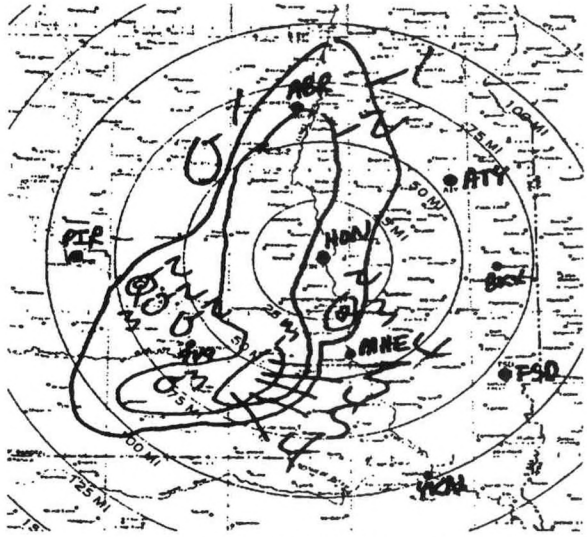

Figure 6b. 1430 UTC 21, 1993.

Figure 6c. 1525 UTC 21 July 1993.

Figure 6d. 1625 UTC 21 July 1993.

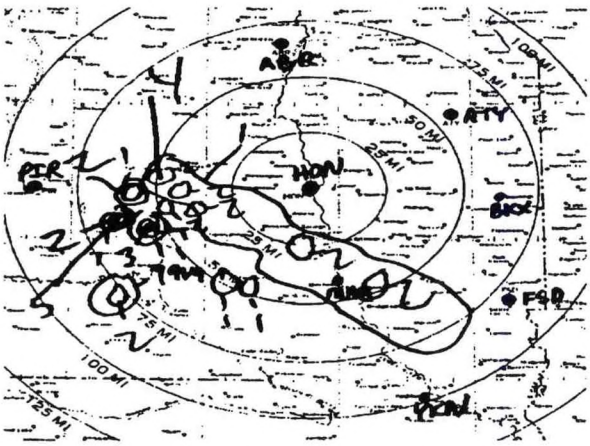

Figure 6e. 1735 UTC 21 July 1993.

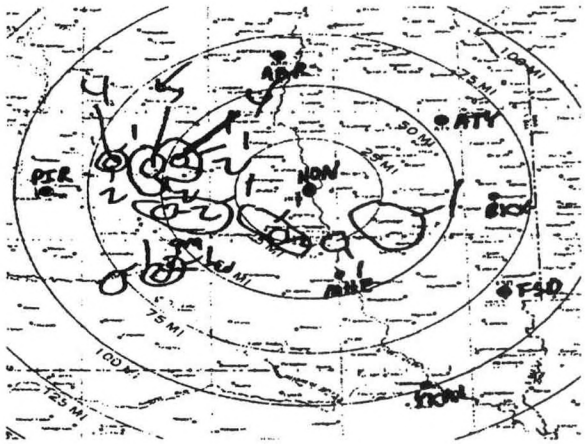

Figure 6f. 1830 UTC July 21, 1993.

Figures 6a-f. Overlays from the HON radar 1325 UTC to 1830 UTC 21 July 1993.

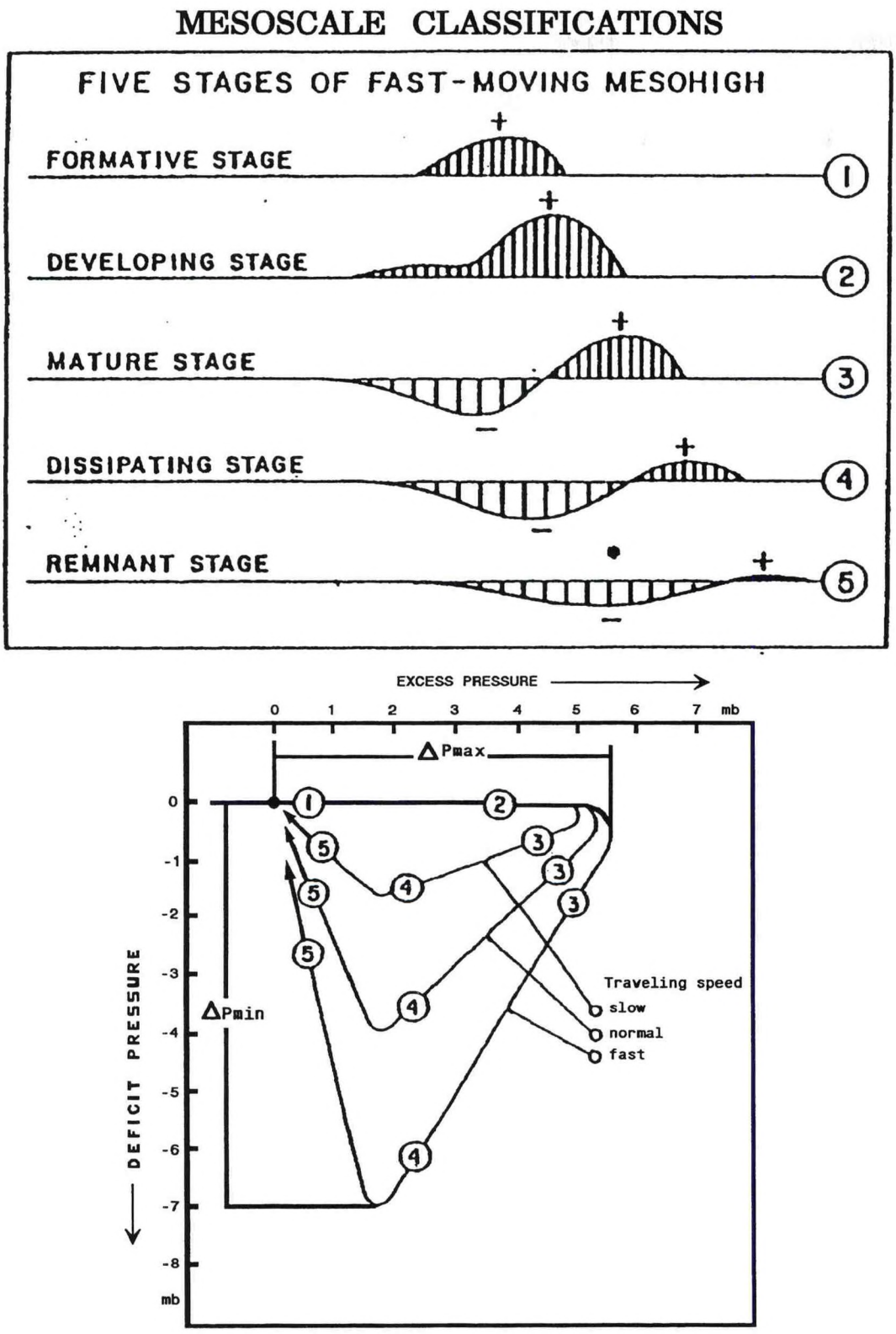

Figure 7. Five stages of a mesohigh that turns into a mesolow called a wake depression. The total lifetime is 6-12 h, so that a mesohigh formed during the night could remain as a mesolow the following morning (Fujita 1963).

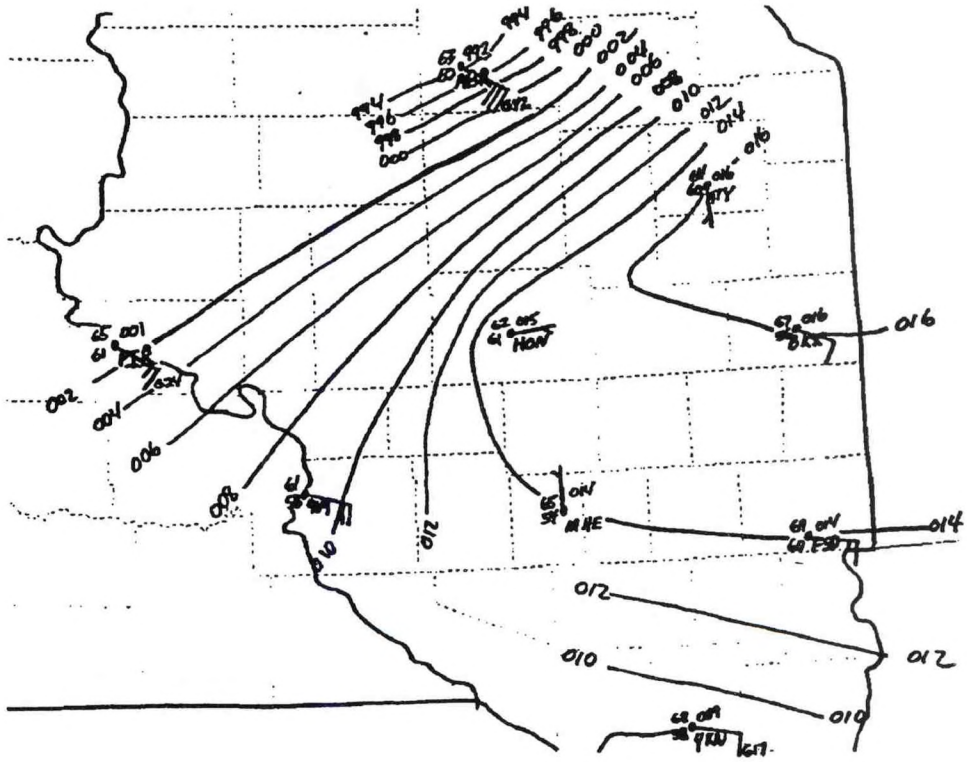

Figure 8a. Surface pressure analyses for eastern South Dakota. 1500 UTC 21 July 1993.

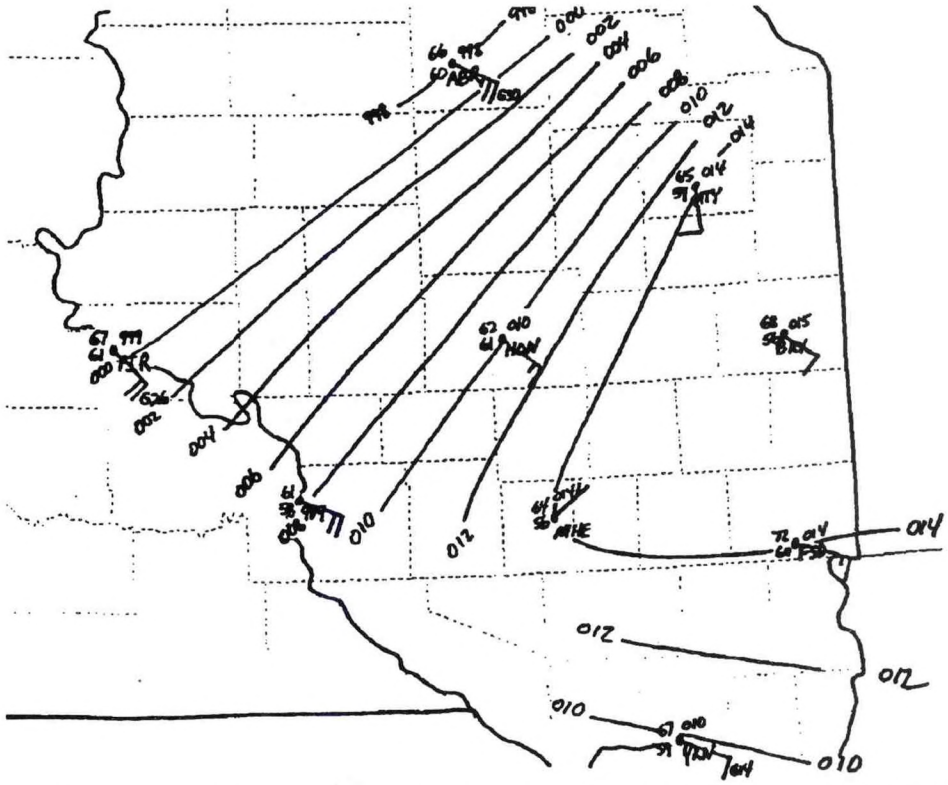

Figure 8b. Surface pressure analyses for eastern South Dakota. 1600 UTC 21 July 1993.

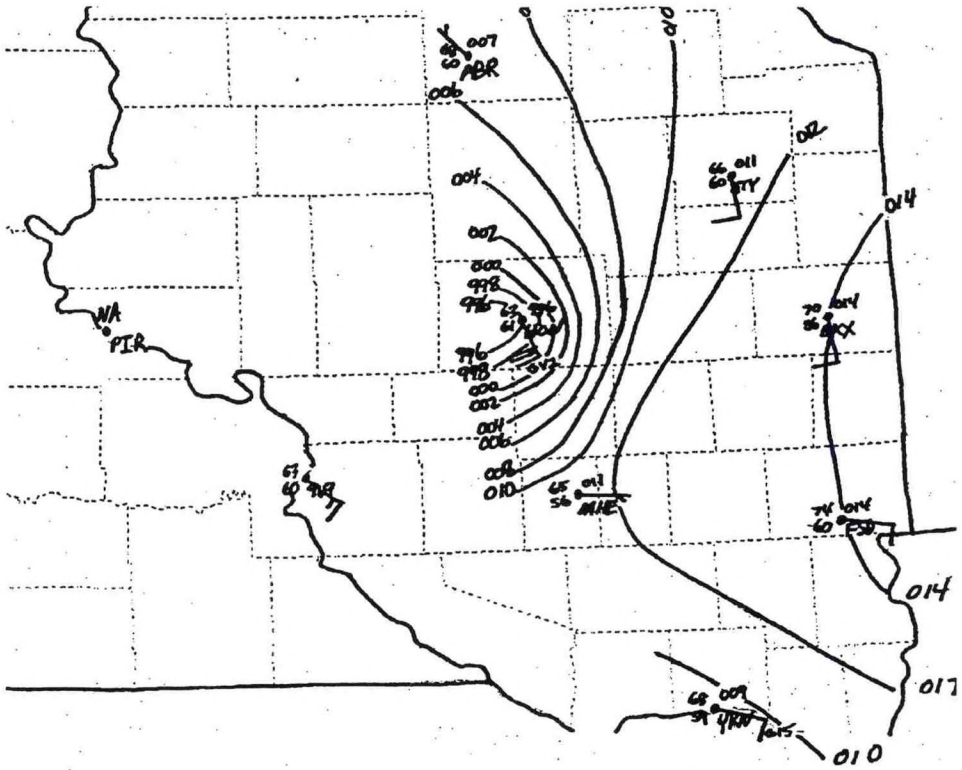

Figure 8c. Surface pressure analyses for eastern South Dakota. 1700 UTC 21 July 1993.

The following is an analogy to Fujita's mesohigh/wake depression theory. A stationary mesohigh with practically no wake depression would be analogous to a boat sitting stationary in the water. As the boat begins to move forward, water would pile up ahead of the bow. This would be analogous to the development of a mesohigh. Simultaneously, a depletion of water behind the boat would be analogous to the development of a wake depression. As the boat moves faster, the piling up of water/mass in front (mesohigh) and the depletion of water/mass behind (wake depression) would increase. As Fujita states, a fast-moving mesohigh develops a strong wake depression in its mature to remnant stage. This concept seems to be in conformity with the conservation of mass.

Due to the lack of data, the surface pressure analysis (Figure 8) does not show well the mesohigh in eastern South Dakota, but does show the trailing wake depression. Figure 9 shows what the mesohigh and wake depression (pre and post-MCS) may have resembled in central and eastern South Dakota on the morning of July 21, 1993. In the pre-MCS environment, the mesohigh was in its mature stage followed by a weak wake depression. In the post-MCS environment, the mesohigh was in its dissipating to remnant stage followed by a strengthening wake depression. Aberdeen and Huron were both between the mesohigh and wake depression (post-MCS). Therefore, strong southeast winds would have been favorable at both locations.

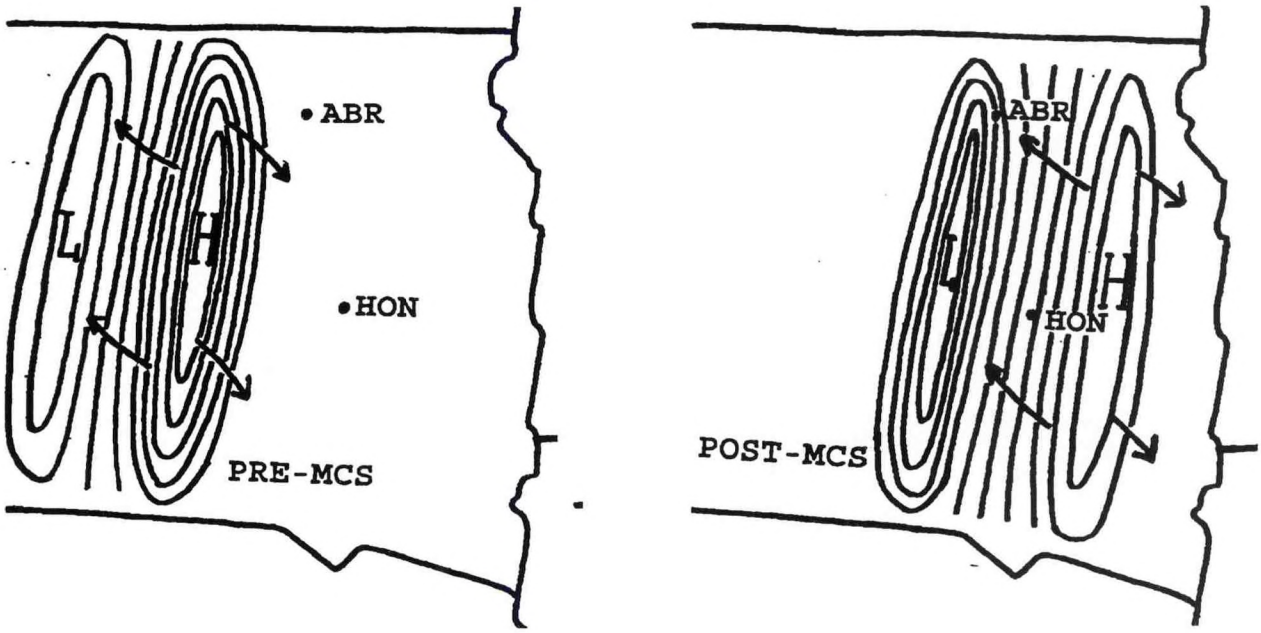

Figure 9. Conceptual model of the pre- and post-MCS mesohigh/mesolow couplet. The mesohigh weakens as it moves east through Huron and Aberdeen and the trailing wake low strengthens. The mesoscale pressure gradient was believed to have affected the winds at HON and ABR, as shown.

4. The High Wind Event

Here is a detailed examination of the surface observations from HON and ABR depicting the mesohigh/wake depression couplet. In this case, the MCS/ mesohigh was moving east at 25 mph and was entering into its remnant stage satisfying Fujita's wake depression theory. As the mesohigh moved through Huron, the altimeter reading rose from 30.08 inches at 1150 UTC to 30.16 inches at 1350 UTC and the winds became light northwest (Figure 5a). This shows the initial pressure rise associated with the mesohigh. The low level inversion was believed to have prevented mixing resulting in the light winds along the leading edge. After passage of the mesohigh, mixing was permitted as was discussed earlier. The ensuing wake depression caused the altimeter reading to drop to 29.96 inches at 1650 UTC. Between 1650 UTC and 1750 UTC southeast winds increased to 35 to 45 mph with the peak gust of 62 mph at 1659 UTC in Huron. (Note, in Figure 5a, the wind speeds are in knots.)

Similarly, as the mesohigh moved through Aberdeen, the altimeter reading rose from 30.08 inches at 0950 UTC to 30.14 inches at 1150 UTC with light southeast winds (Figure 5b). As the wake depression followed, the altimeter reading dropped to 29.93 inches at 1450 UTC. Between 1450 UTC and 1550 UTC, southeast winds increased to 30 to 45 mph with a peak gust of 51 mph at 1517 UTC. (Note, in Figure 5b, the wind speeds are in knots.)

5. Conclusion

On the morning of July 21, 1993, a strong wake depression induced by a mesohigh, mixing, and a fairly strong surface pressure gradient was all believed to be responsible for the high winds at both Huron and Aberdeen, South Dakota. In the future, based on what was learned from this event, forecasters can anticipate the possibility of local high winds created by a wake depression and the synoptic pressure gradient using the following checklist.

A. Is an MCS present on radar or satellite?

B. Is the MCS stationary or moving(Slow or Fast)?

C. Is the MCS/mesohigh in its developing, mature, dissipating or remnant stage?

D. Assess the strength of the synoptic pressure gradient (surface and "aloft") using ASOS, wind profilers, 88D VAD profiles, and surface analysis.

E. Look for high/low pressure couplets with mesoanalysis or ADAP's SAC, SC1 or SC2.

6. Is Mixing Likely Utilizing Local Plotted Soundings on Skew-T's?

Note, if mixing occurs ahead and behind a MCS/mesohigh, a location may receive high winds from the mesohigh followed by high winds from the wake depression.

7. Look for any Indication of High Winds on Doppler and/or Solicit Wind Reports from Spotters, CD's, etc.

This type of event can develop rapidly and not be observed by present day observing stations. With reliable wind reports or with the WSR-88D, depending on the proximity of the high winds from the radar and the depth of the winds, a forecaster could write a Short-Range Forecast, Special Weather Statement, or issue a High Wind Warning to cover the event.

8. Acknowledgements

I would like to thank several people for their involvement in this paper: Scott Mentzer (MIC, WFO Goodland), Hector Guerrero (WCM, WFO Aberdeen), and Steve Eddy (Meteorologist, WFO Indianapolis). I would also like to thank John Springer (MIC, WSO Huron) for the isentropic analysis.

9. References

Fujita, T.T., 1963: Analytical Mesometeorology: A Review. Severe Local Storms, *Meteo. Monogr.*, **5**, 77-125.

_____, 1986: Mesoscale Classifications: Their History and Their Application to Forecasting. *Mesoscale Meteorology and Forecasting*, P.S. Ray, ed., AMS, 24-28.

CENTRAL REGION APPLIED RESEARCH PAPER 14-09

CHANGES IN STORM RELATIVE ENVIRONMENTAL HELICITY AND LOW LEVEL INFLOW PRIOR TO TORNADO OCCURRENCE

Brian P. Walawender
and
Michael D. Gorczany[1]
NEXRAD Weather Service Forecast Office
Topeka, Kansas

1. Introduction

The development of the Wind Profiler Demonstration Network (WPDN) (Chadwick 1988) has given the forecaster access to hourly vertical wind profiles on a real-time basis. Hodographs from the profiler data allow the forecaster to make hourly diagnoses of the troposphere's ability to support organized storms with persistant rotating updrafts (supercells) and tornadoes. Davies-Jones et al. (1990) and Davies-Jones (1993) have shown storm relative environmental helicity (SREH) can sometimes be a useful parameter in distinguishing tornadic from non-tornadic severe thunderstorm cases. In addition, Johns et al. (1993) has shown SREH, when combined with CAPE, to be an indicator of whether or not the tropospheric environment can support strong or violent tornadoes. Finally, Beckman and Polston (1993) and Davies-Jones (1993) have noted increases in hourly helicity values prior to tornado and severe thunderstorm development.

In this study, wind profiler derived hodographs from three tornado events were investigated to note the changes in SREH and low-level inflow (LLI) prior to tornado occurrence. This was performed in order to demonstrate the utility of wind profiler derived hodographs in forecasting supercells and tornadoes. Data for cases were collected based on the occurrence of tornadoes within the profiler network across Kansas, eastern Colorado, southern Nebraska, northern Oklahoma and western Missouri. Doppler radar imagery from the events indicated the tornadoes were associated with mesocyclones. The SREH and LLI calculations in these cases were based on the default storm motion of 30R75 (30° to the right and 75% of the magnitude of the 0-6 km mean wind) from the AFOS wind profiler hodograph program.

[1]Current affiliation, NWS Office Green Bay, Wisconsin.

2. The Case Studies

A. May 22, 1993

Six "weak" (F scale 0 and 1) tornadoes, were reported over southeast Colorado and southwest Kansas (Figure 1) on May 22, 1993. The first tornado occurred around 2300 UTC 22 May with the final tornado occurring at 0200 UTC 23 May. Data from three profiler sites, Granada (GDA), Colorado; Haviland (HVL), Kansas; and Vici (VCI), Oklahoma, were studied for this event. The tornadoes occurred between the GDA and HVL sites.

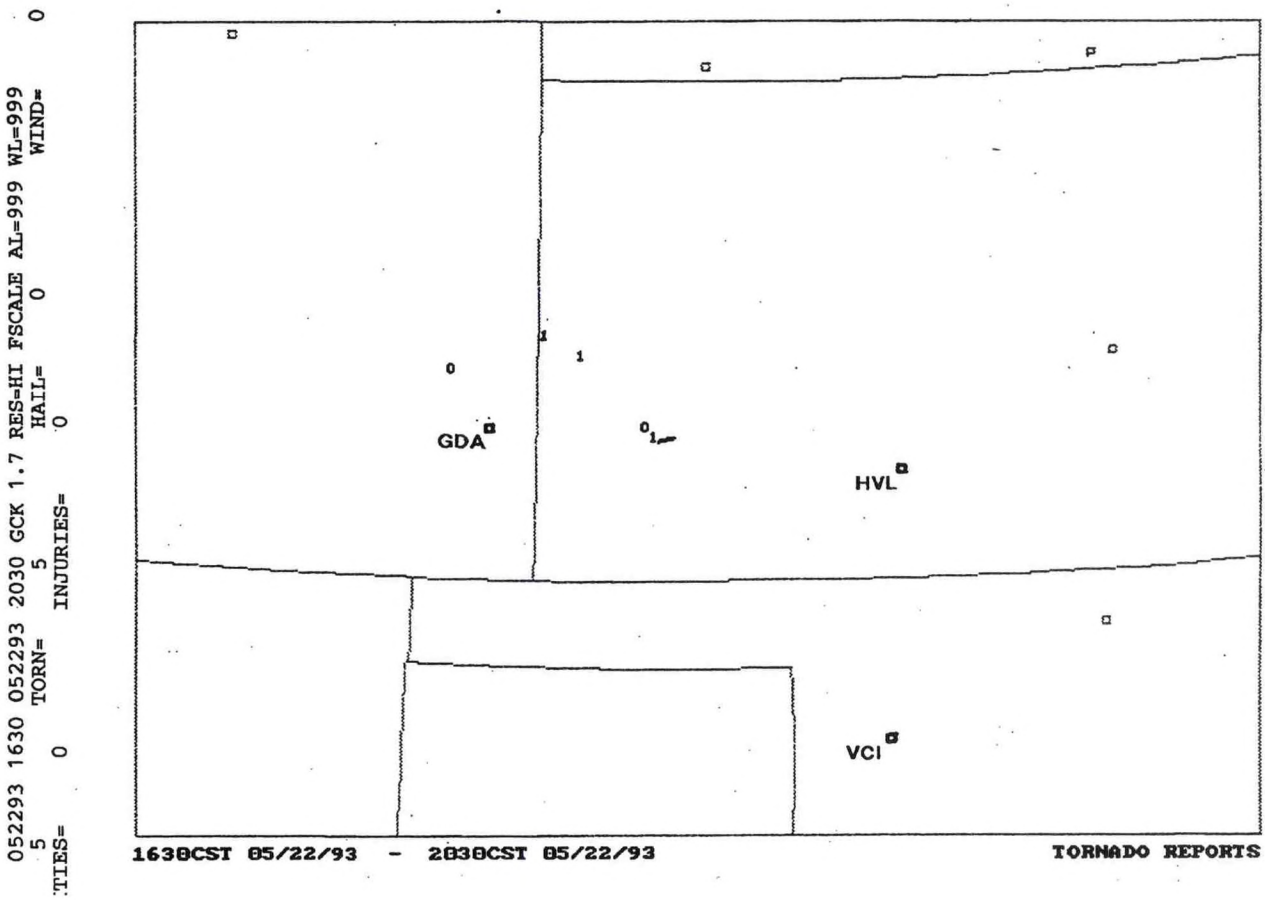

Figure 1. Profiler locations and tornado reports with F scale ratings from 1630 CST to 2030 CST 22 May 1993.

At 2000 UTC, the GDA profiler hodograph indicated negative SREH for 0-3 km (all SREH values hereafter will be for the 0-3 km layer) with weak (<15 kts) LLI. VCI and HVL had higher SREH values (the complete data set can be found in Table 1) of 89 m^2s^{-2} and 137 m^2s^{-2}, respectively. This was below the threshold value of 150 m^2s^{-2} suggested by Davies-Jones et al. (1990) for mesocyclone formation. The LLI, at these two sites, was also higher, averaging 20-25 kts.

Table 1
SREH AND INFLOW DATA FOR CASE A - 22 MAY 1993.3

Site	Time	Storm Relative Environmental Helicity m^2s^{-2}		Inflow kts	
		0-2 km	0-3 km	1000 m	1500 m
GDA	20 UTC	-9	-9	12	03
	21 UTC	-12	1	14	03
	22 UTC	-6	35	21	11
	01 UTC	169	197	20	32
	02 UTC	250	283	20	23
VCI	20 UTC	136	137	26	26
	21 UTC	86	67	26	29
	22 UTC	70	81	24	25
	23 UTC	98	118	25	27
	02 UTC	110	110	30	21
	03 UTC	200	204	29	21
HVL	20 UTC	93	89	20	12
	21 UTC	182	186	31	18
	22 UTC	118	139	29	21
	23 UTC	42	52	27	20
	02 UTC	128	125	31	18
	03 UTC	124	116	32	19

Between 2100 UTC and 2300 UTC the SREH decreased slightly at VCI and HVL and increased slightly at GDA. The SREH remained below the suggested 150 m^2s^{-2} threshold during this period. LLI remained constant at VCI and HVL, with slight increases at GDA.

A dramatic increase in SREH was noted at GDA between 2200 UTC and 0200 UTC. SREH increased to 197 m^2s^{-2} at 0100 UTC and to 283 m^2s^{-2} by 0200 UTC (Figure 2). The 1.5 km inflow also increased dramatically from 11 kts at 2200 UTC to 32 kts at 0100 UTC.

The hodographs from VCI and HVL (not shown) displayed similar trends with the SREH almost doubling between 2300 UTC and 0300 UTC. LLI at VCI and HVL remained nearly constant, averaging 20-30 kts.

In this case, the tornadoes occurred roughly from 0100 UTC to 0200 UTC. This corresponds well with the increase in SREH at the three profiler sites. LLI increased slightly before tornado occurrence averaging 25-30 kts just prior to and during the occurrence of the tornadoes.

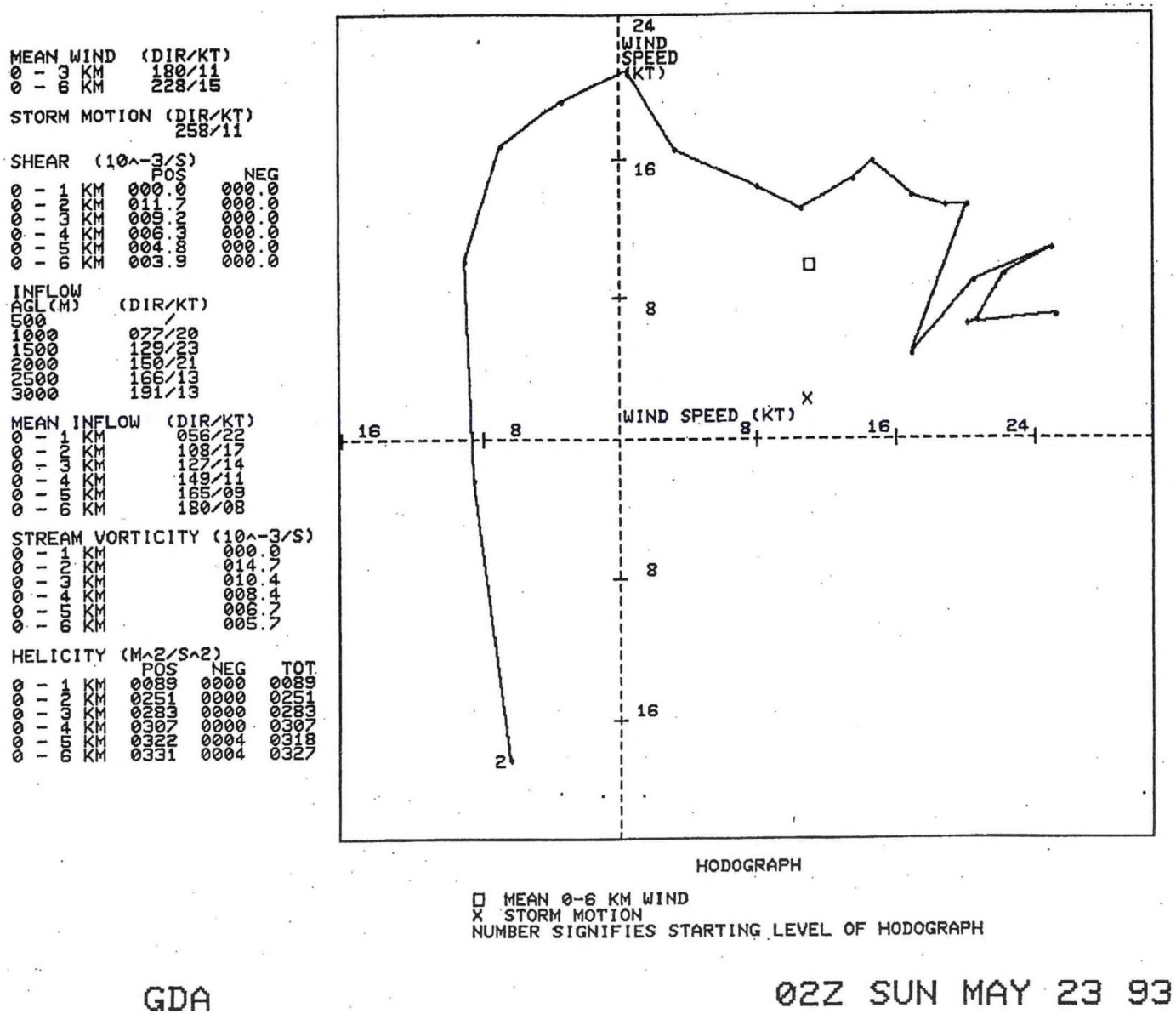

Figure 2. GDA profiler hodograph from 0200 UTC 23 May (2000 CST 22 May) 1993.

B. May 6, 1993

Eighteen tornadoes, ranging in intensity from F0 to F2, were reported across northeast Kansas and northwest Missouri (Figure 3) on May 6, 1993. The first tornado developed around 2200 UTC 6 May with the final tornado occurring around 0100 UTC 7 May. Data from three sites, Hillsboro (HBR), Kansas, Fairbury (FBY), Nebraska, and Lathrop (LTH), Missouri, were studied for this event. The tornadoes occurred between these sites. Problems with the flow of data from the Profiler Hub in Boulder, Colorado prevented a more thorough data set for this case.

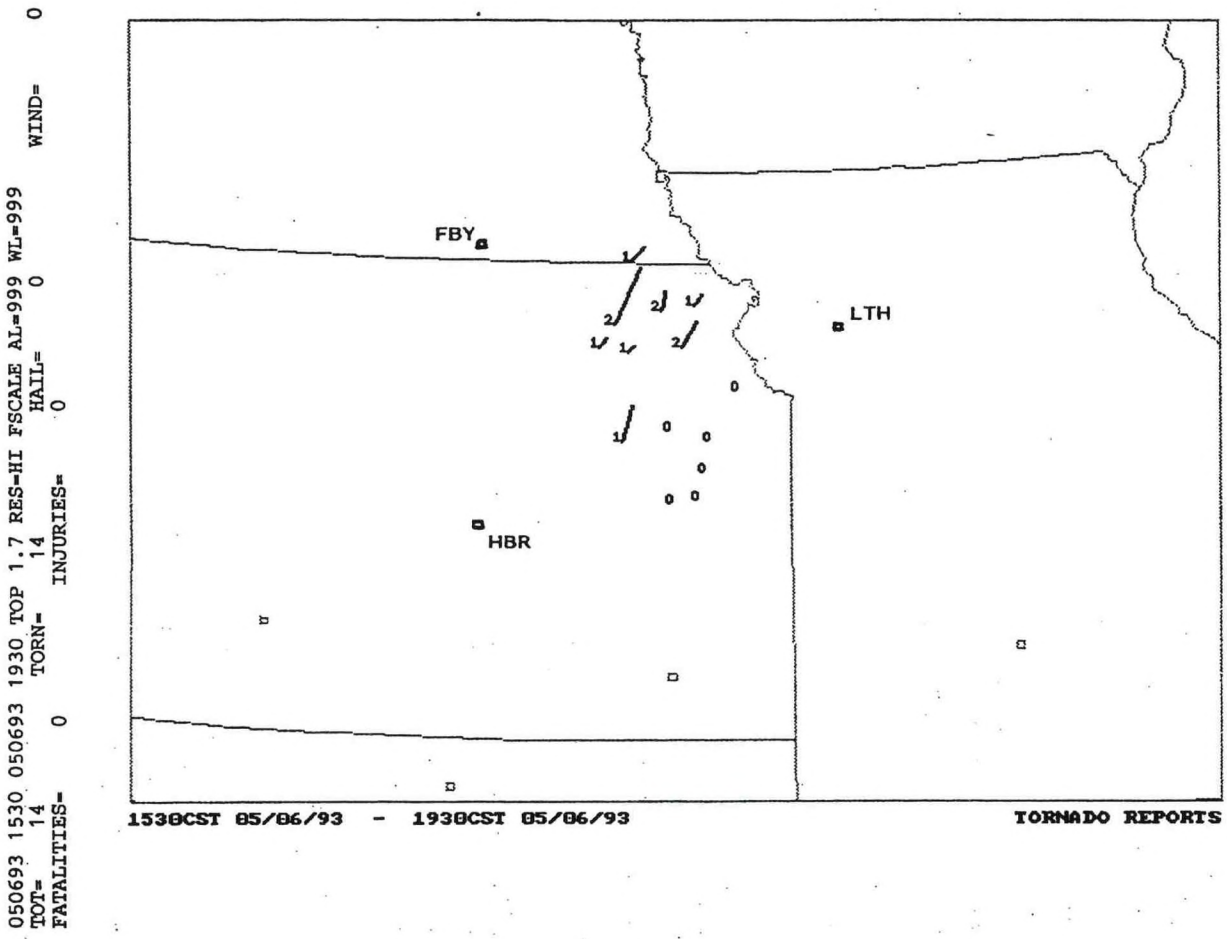

Figure 3. As in Figure 1 except from 1530 CST to 1930 CST 6 May 1993.

At 2000 UTC, HBR and FBY had high SREH values (Table 2). The SREH at HBR was 471 m^2s^{-2} (Figure 4) with 295 m^2s^{-2} at FBY. These values were well above the suggested mesocyclone threshold of 150 m^2s^{-2}. The LLI values averaged around 30 kts.

Table 2
SREH AND INFLOW DATA FOR CASE B - 6 MAY 1993.

Site	Time	Storm Relative Environmental Helicity m^2s^{-2}		Inflow kts	
		0-2 km	0-3 km	1000 m	1500 m
HBR	20 UTC	394	471	26	34
	01 UTC	276	329	44	43
FBY	20 UTC	216	295	28	30
LTH	01 UTC	296	278	33	27

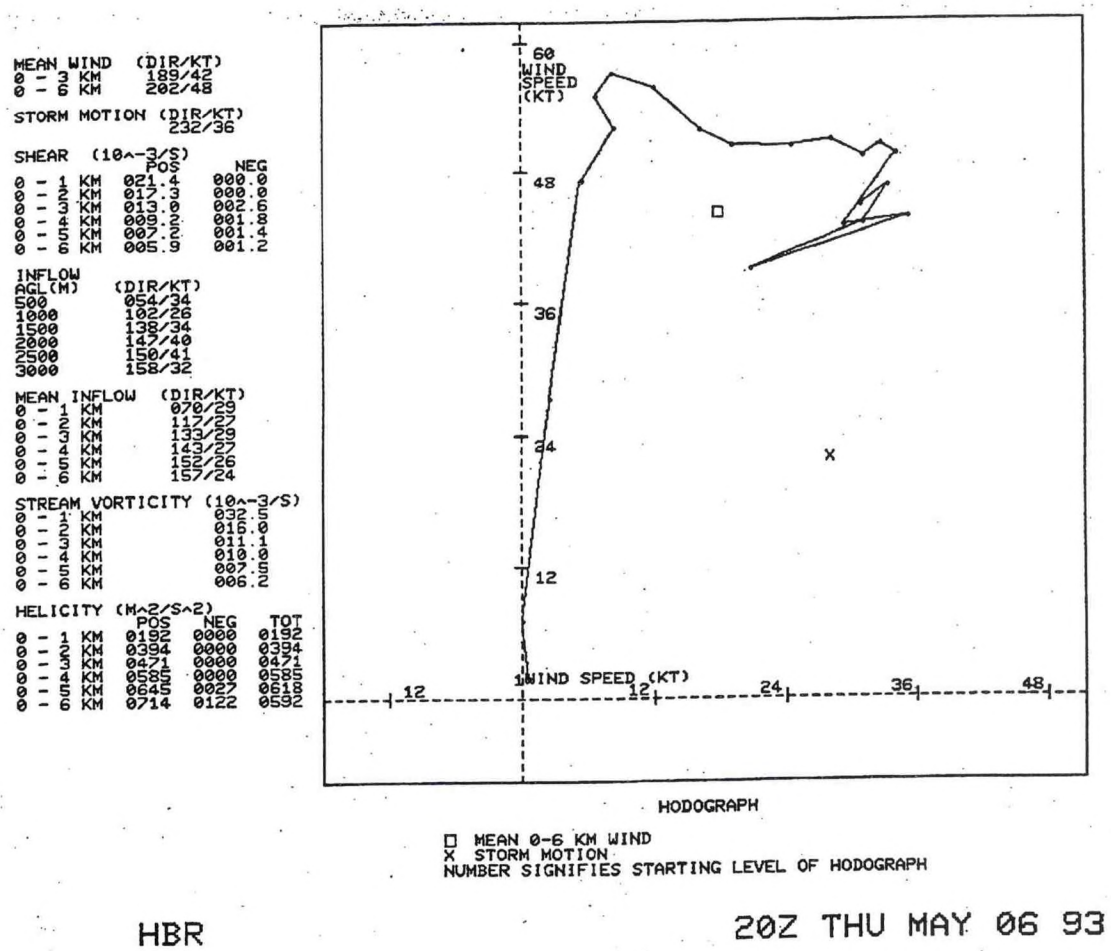

Figure 4. HBR profiler hodograph from 2000 UTC (1400 CST) 6 May 1993.

By 0100 UTC, SREH values had begun to decrease at HBR but remained high. At LTH, SREH was 278 m^2s^{-2}, again well above the suggested mesocyclone threshold. The LLI remained high at LTH and HBR, averaging 30-35 kts.

In this case, the tornadoes occurred between 2200 UTC and 0100 UTC. This corresponds well with the maximum SREH values noted on the profiler hodographs. The LLI also tended to be maximized during this time period.

C. May 5, 1993

Eleven tornadoes, ranging from F0 to F4 in intensity, were reported over the Oklahoma panhandle and southwest Kansas (Figure 5) on May 5, 1993. The first tornado occurred around 2300 UTC 5 May with the final tornado occurring around 0200 UTC 6 May. Data from three profiler sites, HVL, VCI, and McCook (RWD), Nebraska, were studied for this event. The tornadoes occurred west of the HVL and VCI sites. RWD was chosen for this case due to its close proximity to the dryline which was likely a contributing factor to the mesoscale lift that initiated the tornadic storms.

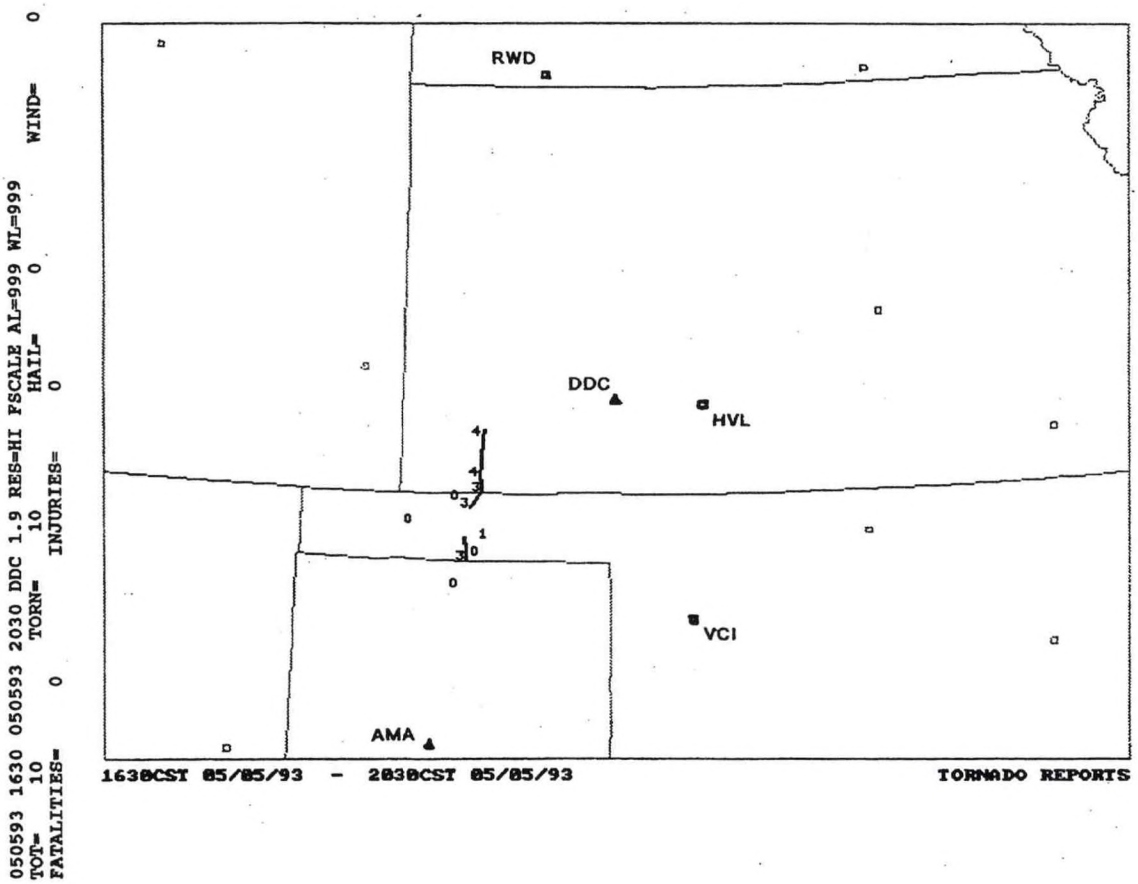

Figure 5. As in Figure 1 except from 1630 CST to 2030 CST 5 May 1993.

At 2100 UTC, all three sites had SREH values (Table 3) which were well below the suggested mesocyclone threshold of 150 m^2s^{-2}. LLI averaged 15 to 20 kts for the three sites. Between 2300 and 0100 UTC a trend toward decreasing SREH was noted on the hodographs from HVL and VCI while the LLI increased slightly.

Table 3
SREH AND INFLOW DATA FOR CASE C - 5 MAY 1993.

Site	Time	Storm Relative Environmental Helicity m^2s^{-2}		Inflow kts	
		0-2 km	0-3 km	1000 m	1500 m
RWD	21 UTC	69	118	19	13
	23 UTC	142	165	29	20
	01 UTC	79	88	28	21
HVL	21 UTC	31	19	19	17
	23 UTC	24	37	21	19
	01 UTC	40	19	22	27
VCI	21 UTC	45	32	20	19
	23 UTC	1	-22	20	25
	01 UTC	2	-20	31	18

At RWD, SREH increased markedly between 2100 UTC and 2300 UTC. The SREH increased to 165 m^2s^{-2} at 2300 UTC (Figure 6), exceeding 150 m^2s^{-2}. By 0100 UTC, the SREH had fallen well below 150 m^2s^{-2}. The LLI also increased dramatically between 2100 UTC and 2300 UTC and then remained nearly constant between 2300 UTC and 0100 UTC, averaging 25 kts.

In this case, the two closest available profilers (GDA was not available for this event) to the tornadoes, HVL and VCI, never indicated an increase in SREH prior to the tornado development. The RWD profiler did exhibit an increase in SREH prior to the development of the tornadoes at 2300 UTC. LLI increased slightly prior to tornado development, averaging 20-25 kts.

Looking at surface and sounding data from this case yields some possible explanations for why the closest profilers, HVL and VCI, never displayed a trend of increasing helicity. First, a check of the 0000 UTC 6 May Dodge City, Kansas (DDC), sounding indicates the wind profile at HVL was accurate with a SREH of less than 50 m^2s^{-2} calculated for that sounding. Second, the 1800 UTC surface map (not shown) revealed a north-south oriented dryline across western Kansas and the Oklahoma and Texas panhandles. The 0000 UTC 6 May Amarillo, Texas (AMA), sounding (Figure 7) was indicative of an environment more favorable to mesocyclonic storms with a SREH of 277 m^2s^{-2}. The AMA sounding,

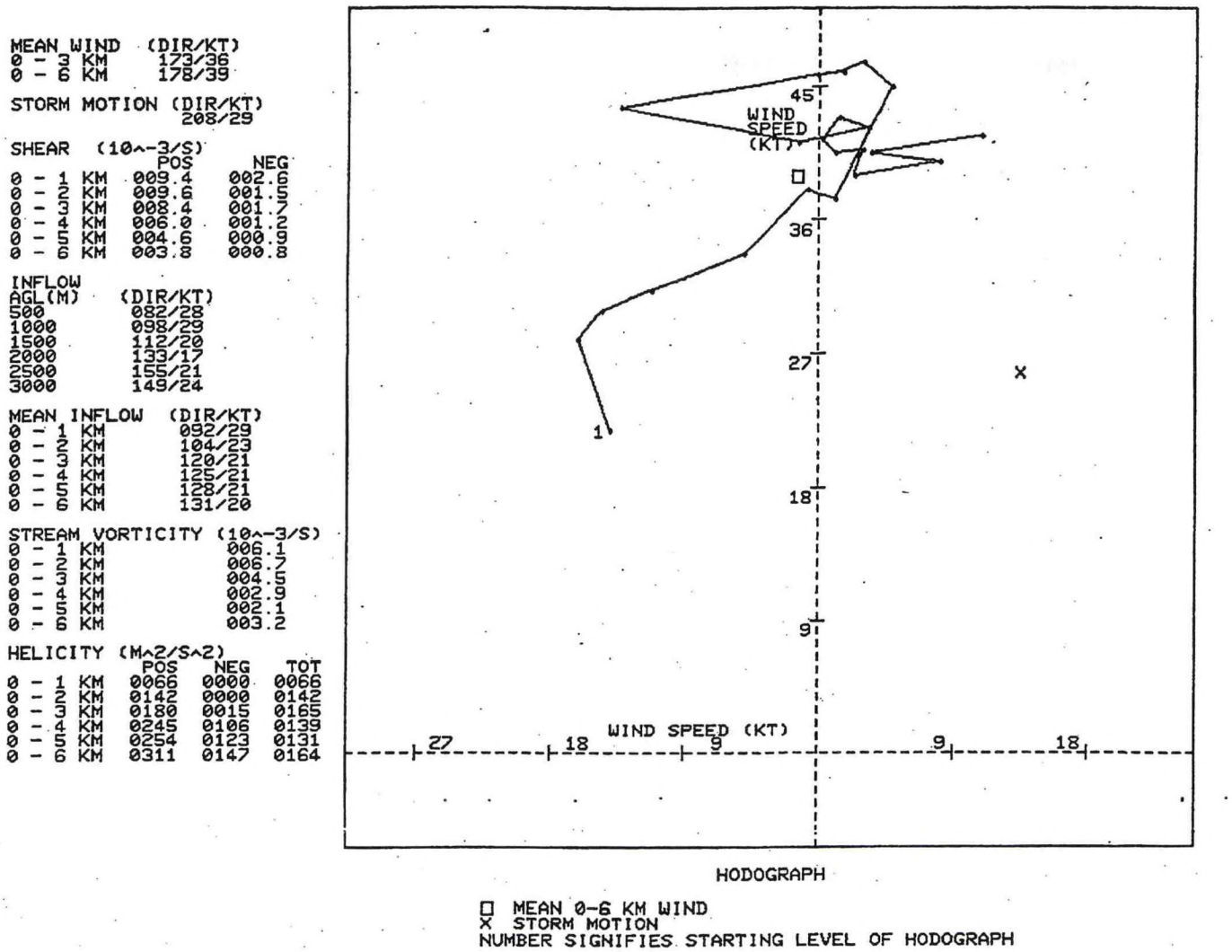

Figure 6. RWD profiler hodograph from 2300 UTC (1700 CST) 5 May 1993.

like the RWD wind profiler, was located in close proximity to the dryline. The map of tornado reports from this period showed them to be organized in a north-south linear fashion along this dryline. This suggests that localized vertical wind shear along the dry line played an important role in supercell development. This offers some possible explanations why the HVL and VCI profilers did not exhibit a trend of increasing SREH even though they were relatively close to the area where the tornadoes developed. The RWD site, which was closest to the dryline, did show an increase in SREH prior to tornado development. This case illustrates the difficulty in obtaining proximity sounding and hodograph data for tornado events.

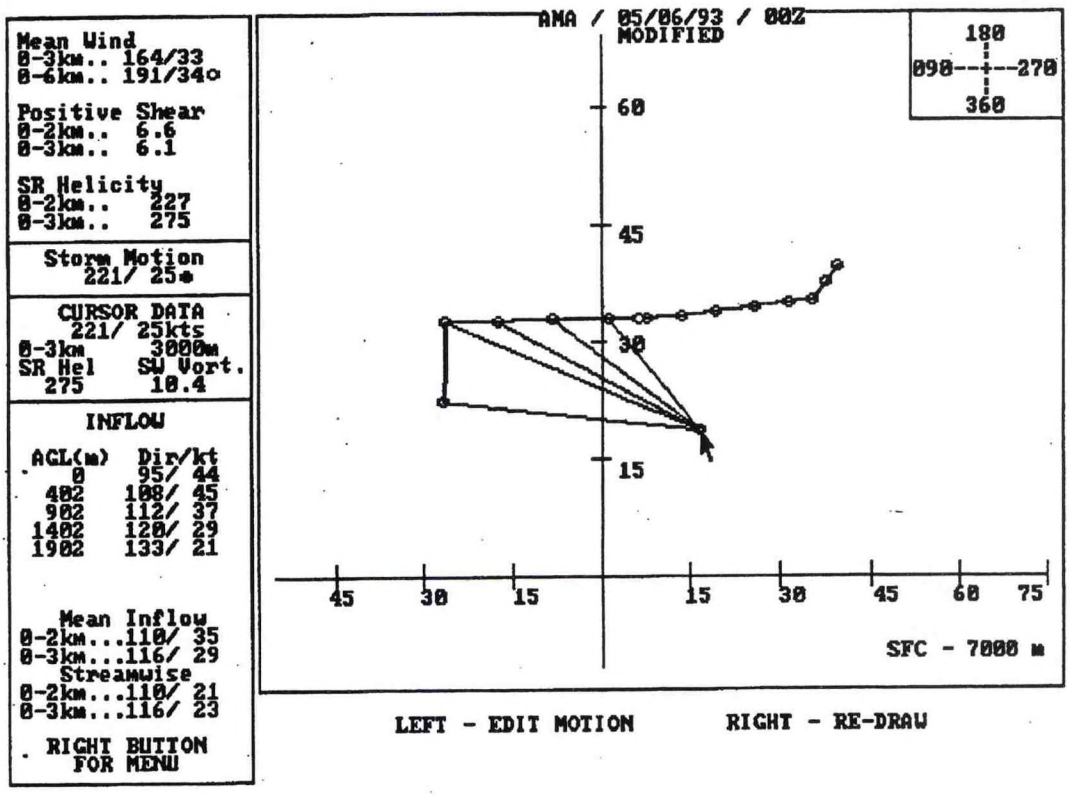

Figure 7. Amarillo (AMA), Texas, hodograph 0000 UTC 6 May (1800 CST 5 May) 1993.

3. Summary

In the three cases studied, an increase in SREH with time was noted prior to tornado development. This trend has also been observed in other tornadic cases by Beckman and Polston (1993) and Davies-Jones (1993). The authors have also observed similar increasing SREH trends in tornadic situations when using hodographs constructed from WSR-88D VAD wind profiles. LLI was also observed to increase prior to tornado development and was typically above 30 kts in the cases where an F2 or greater tornado was reported.

When wind profilers are in a favorable location such that they can sample the environment in which thunderstorms may develop, trends of increasing SREH and low-level inflow should aid forecasters in identifying situations with the potential for supercells and tornadoes. Caution should be used when interpreting hodographs and associated shear related parameters, keeping in mind what "proximity" really means (Brooks et al. 1994). The 150 m^2s^{-2} threshold suggested by Davies-Jones et al. (1990) should only be used as a guideline since CAPE also plays an important role in the development of supercells. Recent studies by Brooks et al. (1994) suggests that SREH may be a better predictor of supercells than of tornadoes. They also suggest that the balance between

mid-level storm relative winds and SREH may play a more important role in the formation of low-level mesocyclones and tornadoes which occur with some supercell storms. SREH still remains a valuable forecast tool as most strong and all violent tornadoes occur with supercells.

4. Acknowledgements

The authors would like to thank George Phillips, SOO at WSFO Topeka, and Preston Leftwich, Regional Science Officer at CRH SSD, for their review of this manuscript.

5. References

Beckman, S.K., and K.L. Polston, 1993: Preliminary Assessment in the use of the 404 Mhz wind profilers to determine severe weather potential. *Preprints, 17th Conf. Severe Local Storms,* St Louis, MO, AMS (Boston), 143-147.

Brooks, H.E., C.A. Doswell III, and J. Cooper, 1994: On the Environments of Tornadic and Nontornadic Mesocyclones. *Wea. Forecasting,* **9**, 606-617.

Chadwick, R.B., 1988: The wind profiler demonstration network. *Preprint, Lower Tropospheric Profiling: Needs and Technologies,* Boulder, CO, AMS (Boston), 109-110.

Davies-Jones, R.P., 1993: Helicity trends in tornado outbreaks. *Preprints, 17th Conf. Severe Local Storms,* St Louis, MO, AMS (Boston), 56-60.

_____, D.W. Burgess, and M. Foster, 1990: Test of helicity as a tornado forecast parameter. *Preprints, 16th Conf. Severe Local Storms,* Kananaskis Park, Alberta, Canada, AMS (Boston), 588-592.

Johns, R.H., J.M. Davies, and P.W. Leftwich, 1993: Some wind and instability parameters associated with strong and violent tornadoes, 2. Variations in the combinations of wind and instability parameters. *The Tornado: Its Structure, Dynamics, Prediction and Hazards.* (Geophys. Monogr. Series 79), C. Church, et al., Ed., Amer. Geophys. Union, 583-590.

ERRATA

CENTRAL REGION APPLIED RESEARCH PAPERS NO. 13
DECEMBER 1994

PAPER 13-02
A VERIFICATION STUDY OF THE MRF-BASED STATISTICAL TEMPERATURE GUIDANCE FOR GRAND ISLAND, NEBRASKA

Daniel D. Nietfeld
David A. Skerritt

CHANGES:
The arrangement of the figures.
The period of study.

CENTRAL REGION APPLIED RESEARCH PAPER 14-10

A VERIFICATION STUDY OF THE MRF-BASED STATISTICAL TEMPERATURE GUIDANCE FOR GRAND ISLAND, NEBRASKA

Daniel D. Nietfeld
NEXRAD Weather Service Forecast Office
Topeka, Kansas

David A. Skerritt
NEXRAD Weather Service Forecast Office
Omaha, Nebraska

1. Introduction

Since December 9, 1992, the medium range forecast (MRF) run of the NMC global spectral model has provided numerical guidance of various meteorological parameters, including temperature, for selected locations. This guidance is distributed over the National Weather Service (NWS) AFOS network under the header cccFMRxxx (Jensenius et al 1993). This study documents the accuracy of the FMR's minimum and maximum temperature forecasts for Grand Island, Nebraska during a one-year period, extending from December 9, 1992 through December 9, 1993. The authors intend to present objective results to enable the reader to answer the question, "How well did the FMR temperature guidance perform?"

2. Brief Model Description

The forecasts contained in the FMR guidance are generated by applying statistical equations to output from the spectral wave model. These equations are based on the LFM model, modified to fit the spectral wave model. A sample verification period was developed by running these equations for a 3- to 4-year period. A calibration procedure was applied to remove the systematic biases detected in the sample verification. Because of the calibrations, the product is neither a perfect prog nor a true MOS product, but is a calibrated perfect prog, which is a combination of the two. The model identifies four seasons: December 1 through February 28 defines the winter season, March 1 through May 31 defines spring, June 1 through August 31 defines summer, and September 1

through November 30 defines autumn. With each seasonal change, the equations are appropriately adjusted. In this paper, winter and autumn are periodically referred to as the cold season, and spring and summer as the warm season.

The primary predictor for the temperature forecast guidance is the 1000-500-mb thickness field. This is one of the shortfalls of the model in predicting temperatures during periods of shallow, cold air that will be shown later in the results. The 1000-500-mb thickness field can be more accurately projected in medium range periods than lower level thickness fields.

3. Data Compilation

The verification was approached through several statistical calculations (Table I) including: the mean algebraic error, the mean absolute error, and the extreme absolute error, for the maximum and minimum temperature forecasts for each forecast day. Note, a hit was considered ±3 degrees to help determine if the FMR guidance is useful for putting detail in medium range temperature forecasts.

Table I
FMR Verification Statistics for Grand Island, Nebraska
for the 12-month period extending from
December 9, 1992 - December 9, 1993

	DAY 1	DAY	2	DAY	3	DAY	4	DAY	5	DAY	6	DAY	7	DAY	8
	MAX	MIN	MAX	MIN	MAX	MIN	MAX	MIN	MAX	MIN	MAX	MIN	MAX	MIN	MAX
AVERAGE ERROR	3.21	2.5	3.84	2.07	3.26	1.07	3.28	0.84	2.68	0.44	2.48	0.43	2.48	0.62	2.81
AVG ABSOLUTE ERROR	5.97	5.25	6.58	5.29	6.76	5.38	7.2	5.56	7.57	5.67	7.61	5.91	7.76	6.23	8.1
EXTREME ABSOLUTE ERROR	31	32	34	35	38	28	34	29	35	28	29	25	30	31	29
FREQUENCY ABS ERROR=0	15	22	15	32	20	29	20	24	12	19	15	20	16	23	15
FREQ ABS ERROR 1-3	139	144	107	141	102	129	92	122	94	126	89	109	79	109	79
FREQ ABS ERROR 4-6	78	97	94	85	95	87	84	95	77	94	74	103	89	88	74
FREQ ABS ERROR 7-9	58	48	65	47	55	58	61	56	64	57	78	63	62	65	70
FREQ ABS ERROR 10-12	34	24	37	32	42	36	47	38	52	41	42	40	51	36	50
FREQ ABS ERROR 13-15	23	11	18	9	20	10	26	15	23	14	31	15	26	22	31
FREQ ABS ERROR 16-18	7	5	15	7	17	7	16	8	22	6	12	5	22	12	18
FREQ ABS ERROR 19-21	4	8	3	5	4	3	10	3	13	4	13	5	8	2	16
FREG ABS ERROR 22-24	3	2	6	3	4	2	4	1	3	2	7	3	6	3	5
FREQ ABS ERROR 25-27	1	1	2	1	3	1	3	1	2	0	1	1	2	3	3
FREQ ABS ERROR 28-30	0	1	0	1	0	2	0	1	1	1	2	0	3	0	3
FREQ ABS ERROR >30	2	1	2	1	2	0	1	0	1	0	0	0	0	1	0
FREQ OF HITS (ERROR 0-3)	154	166	122	173	122	158	112	146	106	145	104	129	95	132	94
HIT PERCENT (ERROR 0-3)	42.3	45.6	33.5	47.5	33.5	43.4	30.8	40.1	29.1	39.8	28.6	35.4	26.1	36.3	25.8

One of the best ways to visualize the accuracy of each forecast is a graphical display of the actual daily error, with a separate graph for each forecast period. Figures 1a through 1o show whether there are a warm or cold bias, specific error trends, and individual extremes. Most importantly the figures show the actual errors daily.

For this study, the authors used the maximum and minimum temperatures that occurred during the 24-hour period from midnight to midnight. This introduced a small margin of error in the verification, because the FMR is forecasting the minimum temperature to occur during the nighttime or morning hours, and the maximum temperature to occur during the daytime hours (Jensenius, et. al 1993). Throughout the course of this study, the specific time frames that the FMR considers "nighttime and daytime" were not known to the authors, as the Technical Procedures Bulletin No. 411 describing this was not published until after the last day of the study. The majority of the minimum and maximum temperatures occurred within the appropriate windows, therefore this technique had negligible effect on the patterns and trends shown.

4. Results

The FMR guidance performed better at forecasting minimum temperatures throughout the forecast period than forecasting maximum temperatures. Through days 2-8, the FMR had 1049 minimum forecast hits (or 36% of the total minimum forecasts) vs. 755 maximum forecast hits (or 26% of the total maximum forecasts). Figure 2 clearly shows that the minimum forecasts were a hit more often than the maximum forecasts for each forecast period. The difference between the percentage of minimum and maximum forecast hits for all the forecast periods are an average of 10.0%, in favor of the minimums.

During much of the period from late December to the first part of March, with few exceptions, the data showed an overwhelming warm bias. The greatest periods of warm bias occurred when arctic outbreaks were observed in the Central Plains resulting in shallow cold pools of air near the earth's surface. This is not surprising knowing that the model uses the 1000-500-mb thickness field as its main temperature predictor, which has a poor surface temperature correlation with this type of air mass. The graphs of the forecast error showed this trend well in all 15 forecast periods. With the exception of the day 6 minimum forecast period and the day 8 maximum forecast period, the extreme forecast errors for the remaining 13 periods occurred in either the last week of December or during the middle of February. Both time periods were characterized by observed temperatures that were much below normal. The extreme errors were drastically significant, ranging from +25 on the day 7 minimum temperature forecast, to +38 on the day 3 maximum temperature forecast.

At least a trace of snow was on the ground from the period 28 December 1992 through 8 March 1993, or during the period of greatest warm bias. During the verification study period, the spectral model implicitly considered snow cover on a daily basis, however it did not use an explicit method for inputting snow cover (Jensenius 1993).

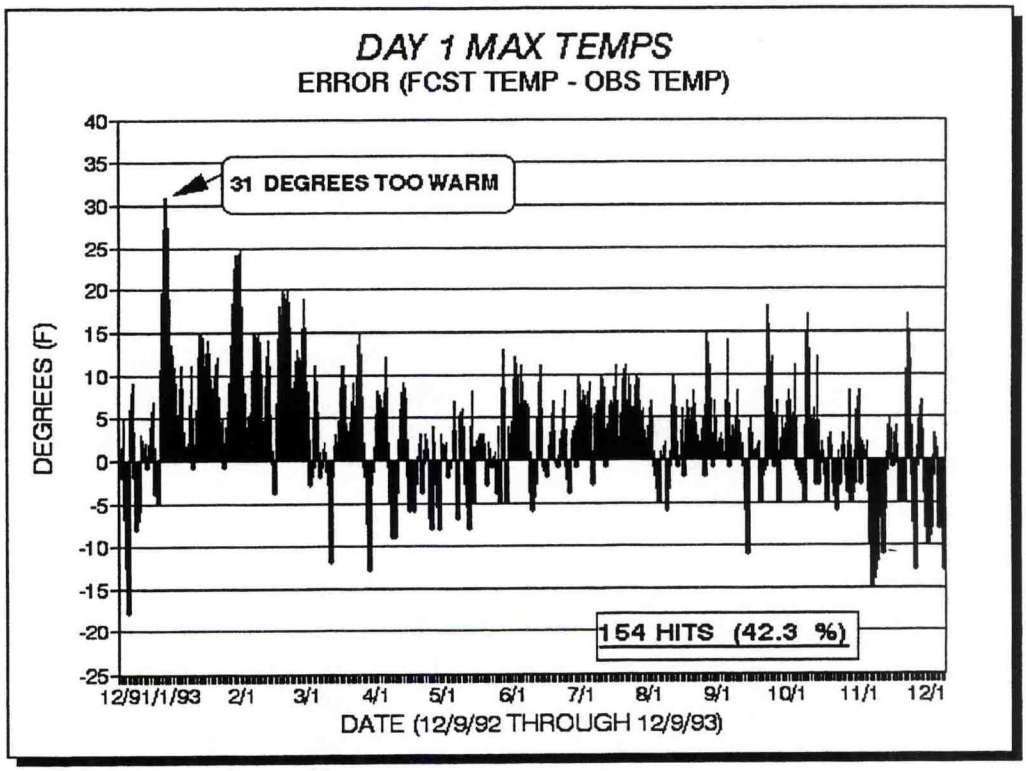

Figure 1a.

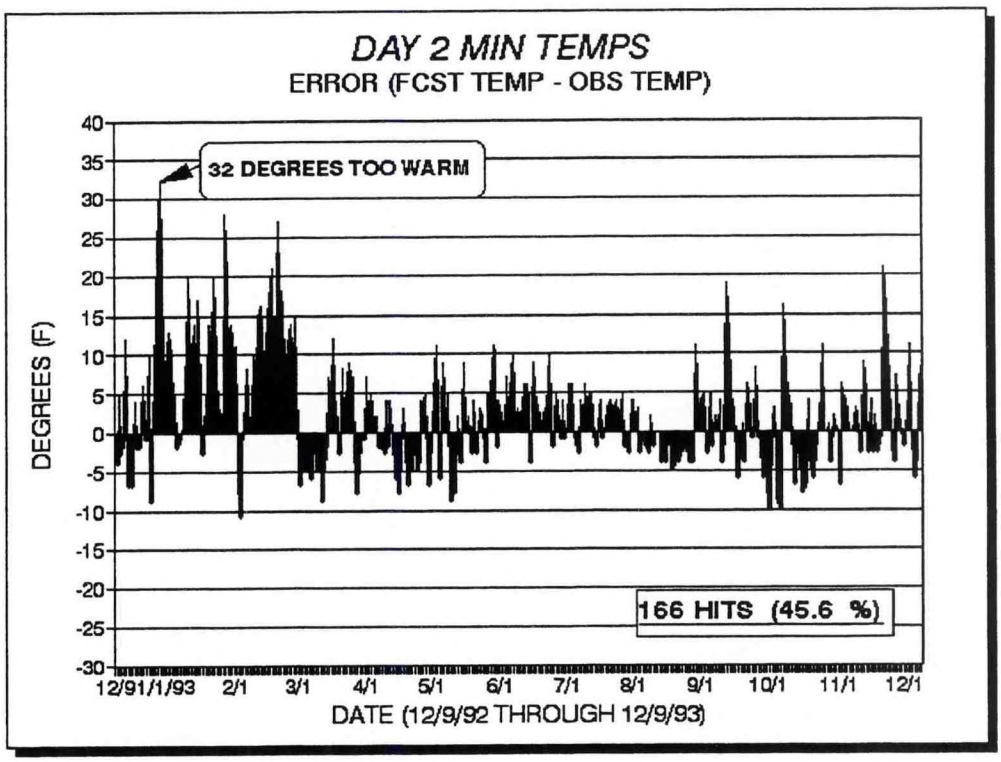

Figure 1b.

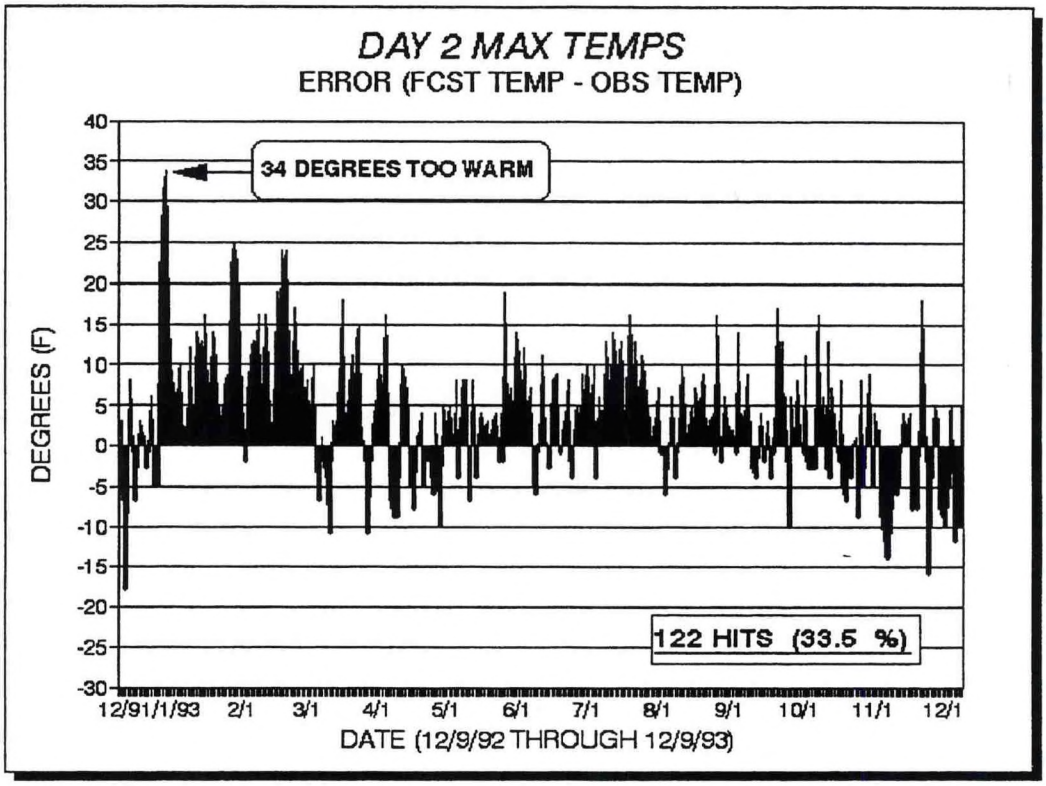

Figure 1c.

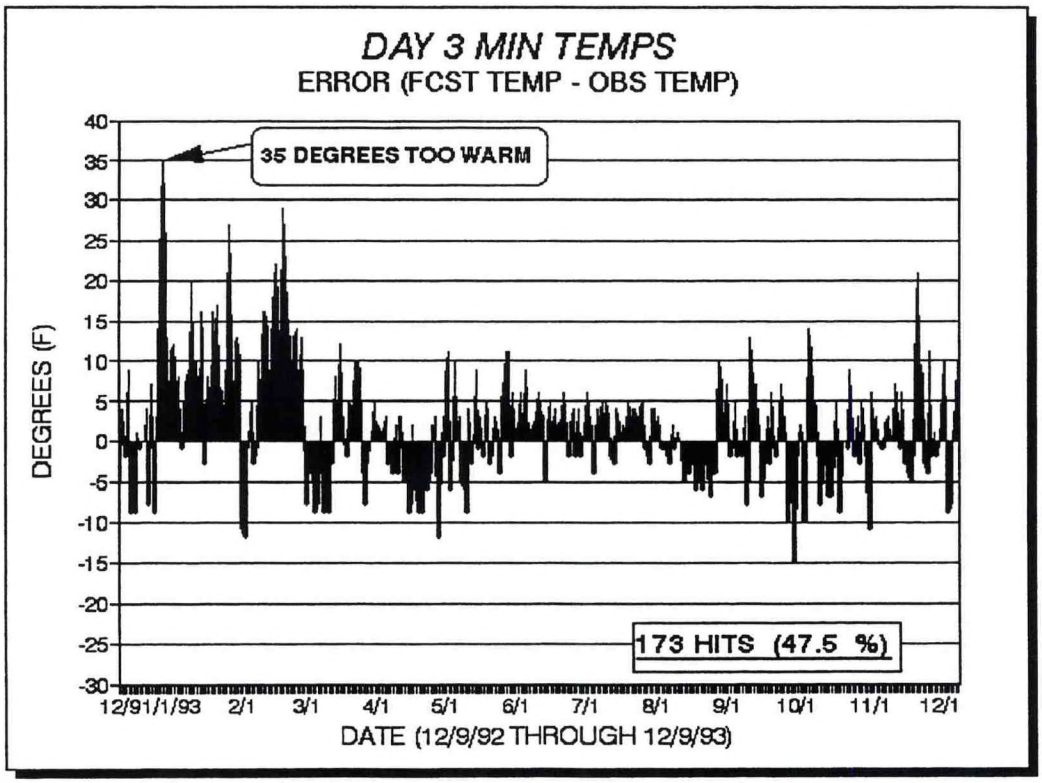

Figure 1d.

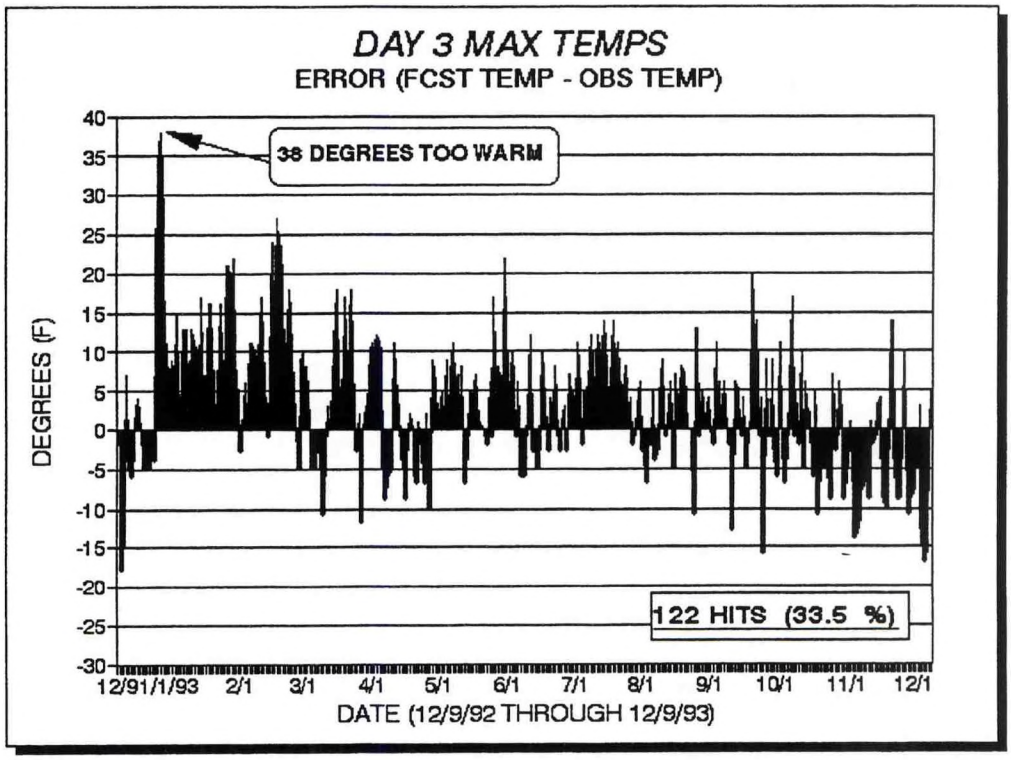

Figure 1e.

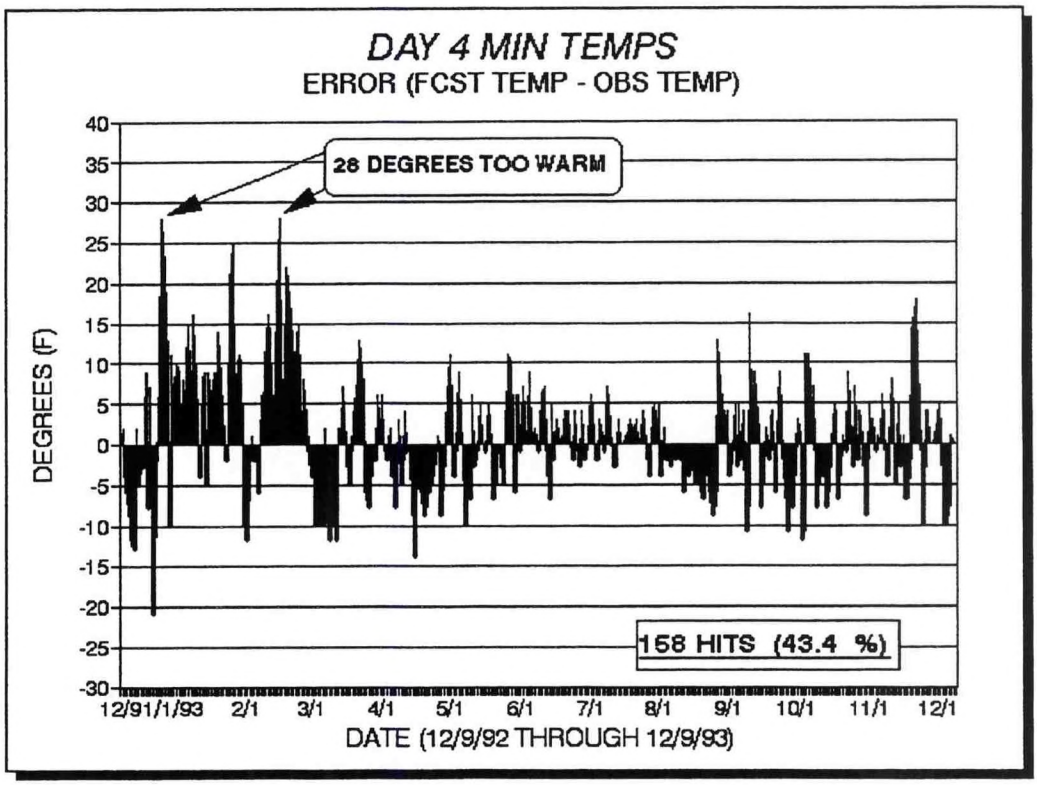

Figure 1f.

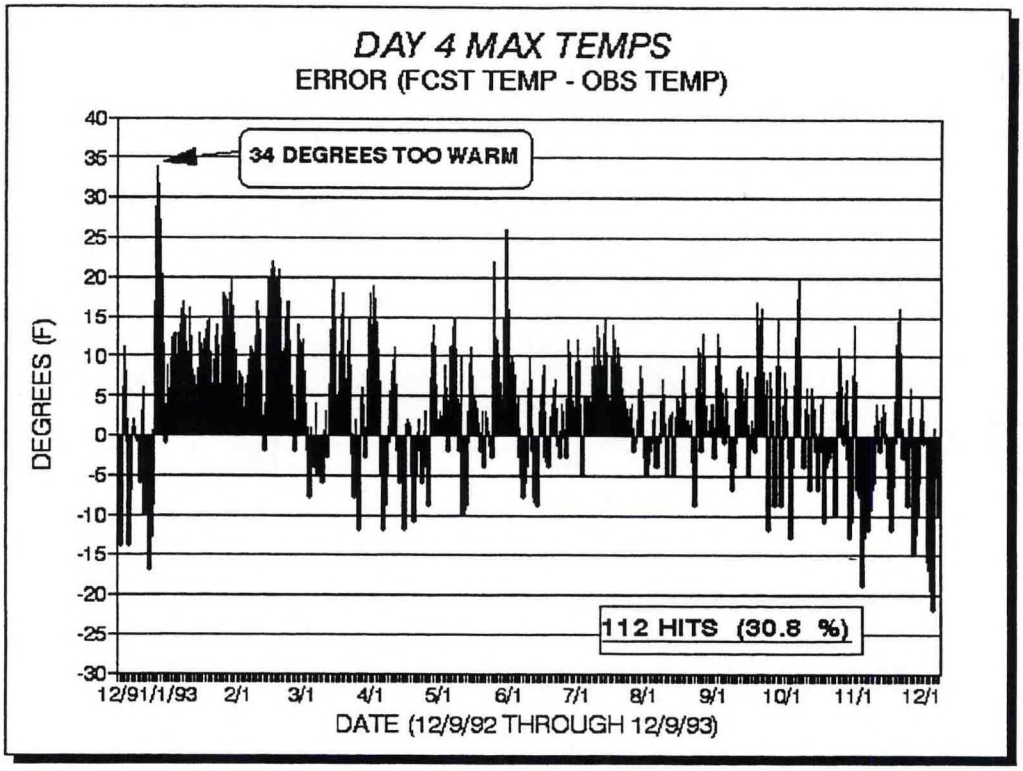

Figure 1g.

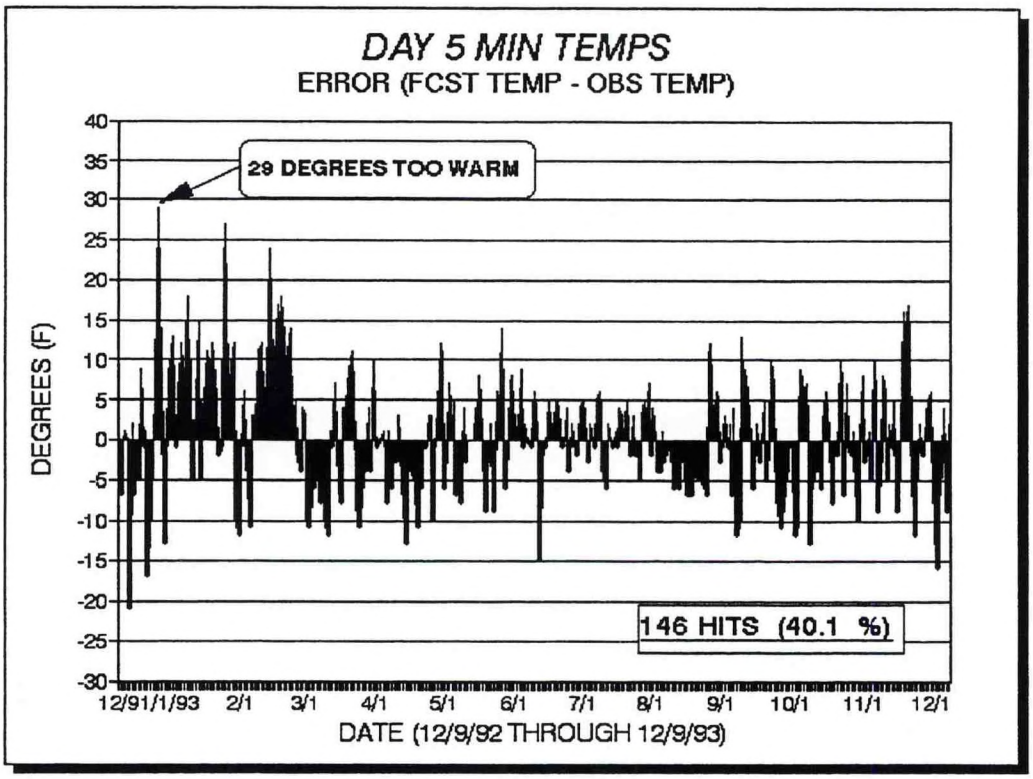

Figure 1h.

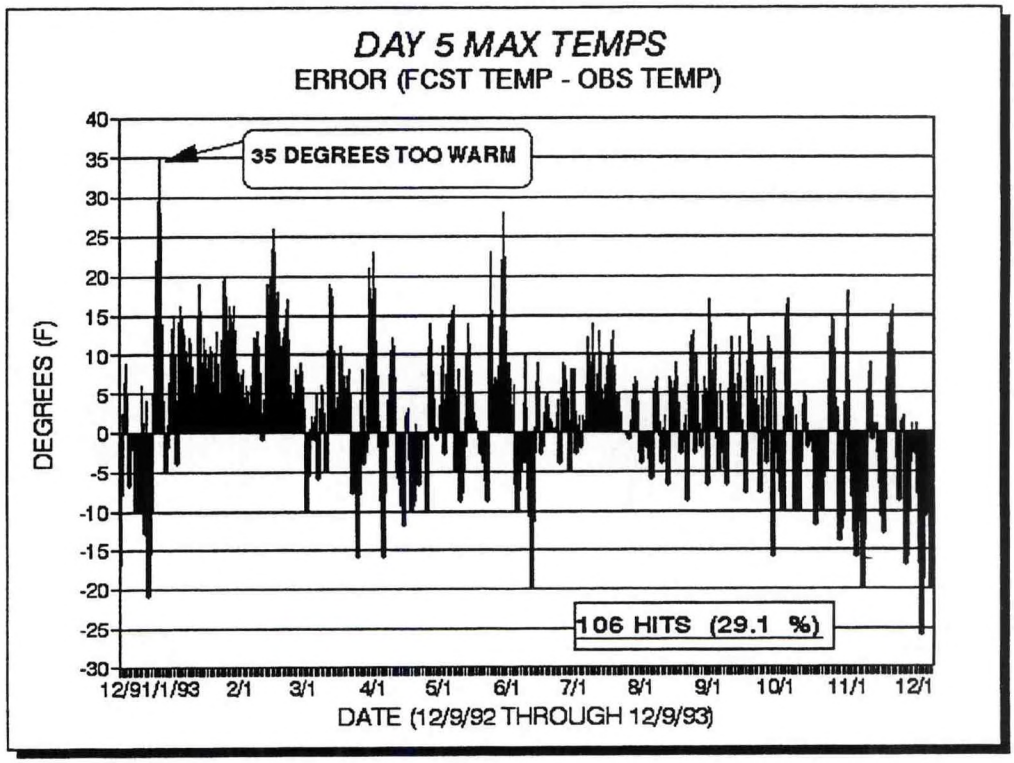

Figure 1i.

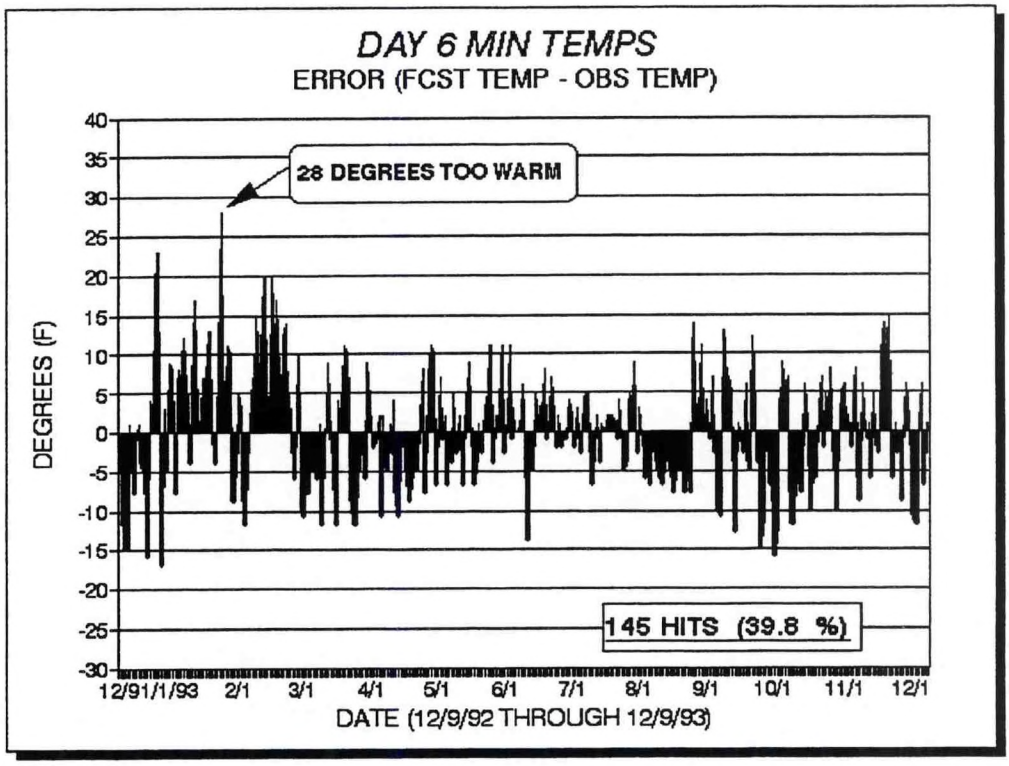

Figure 1j.

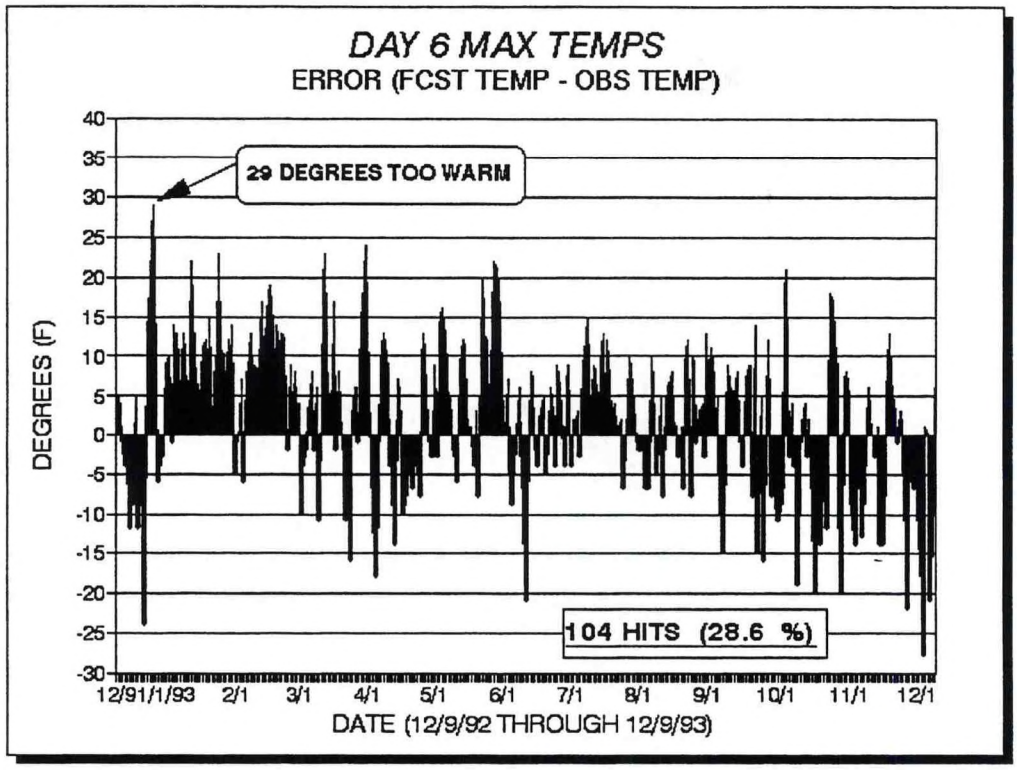

Figure 1k.

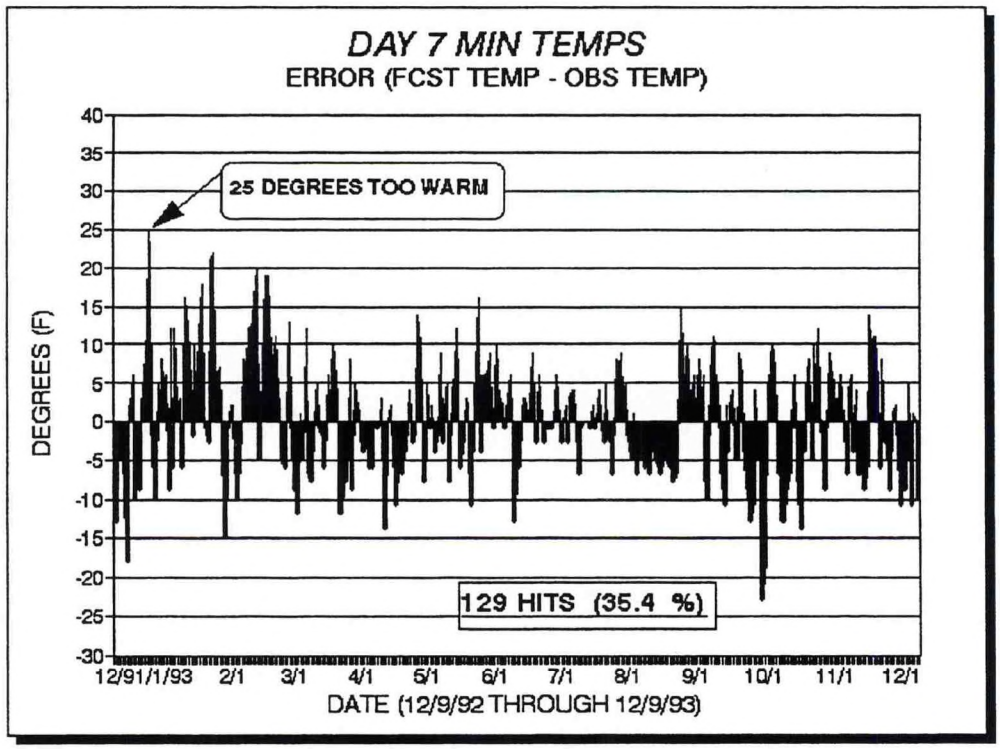

Figure 1l.

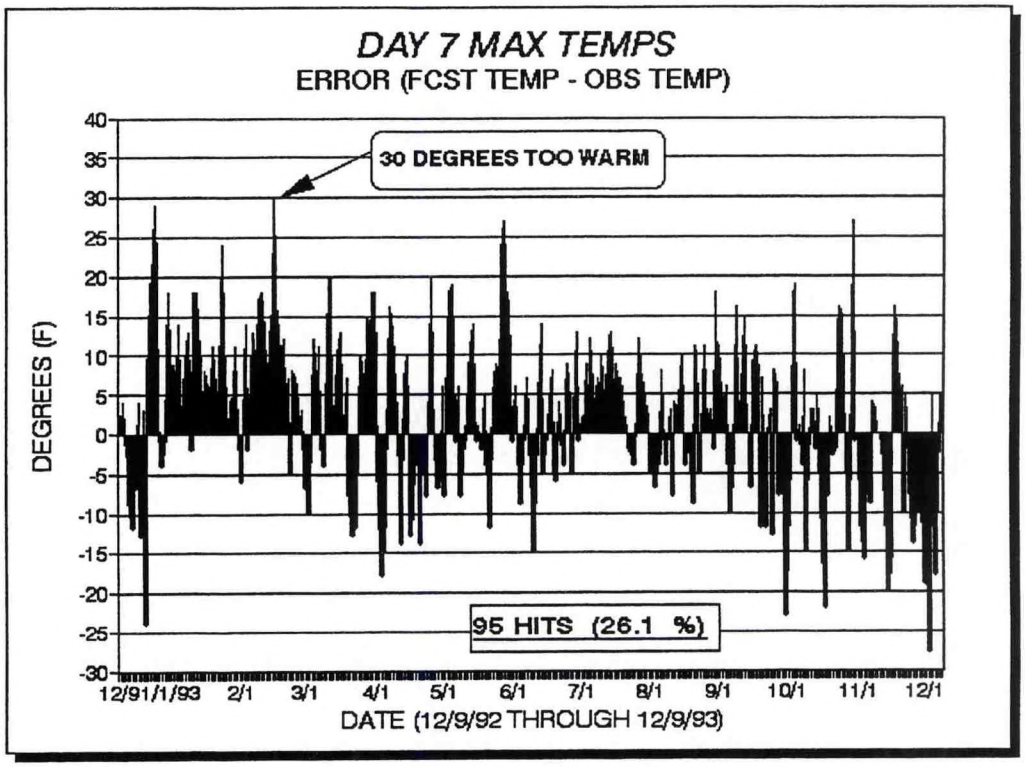

Figure 1m.

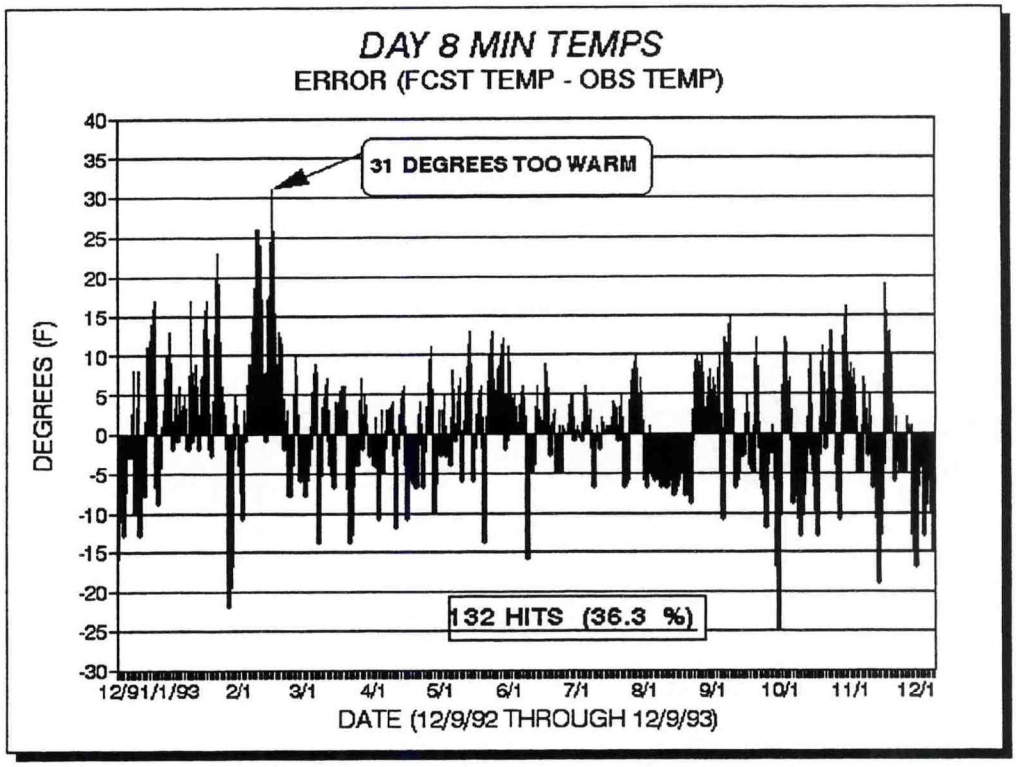

Figure 1n.

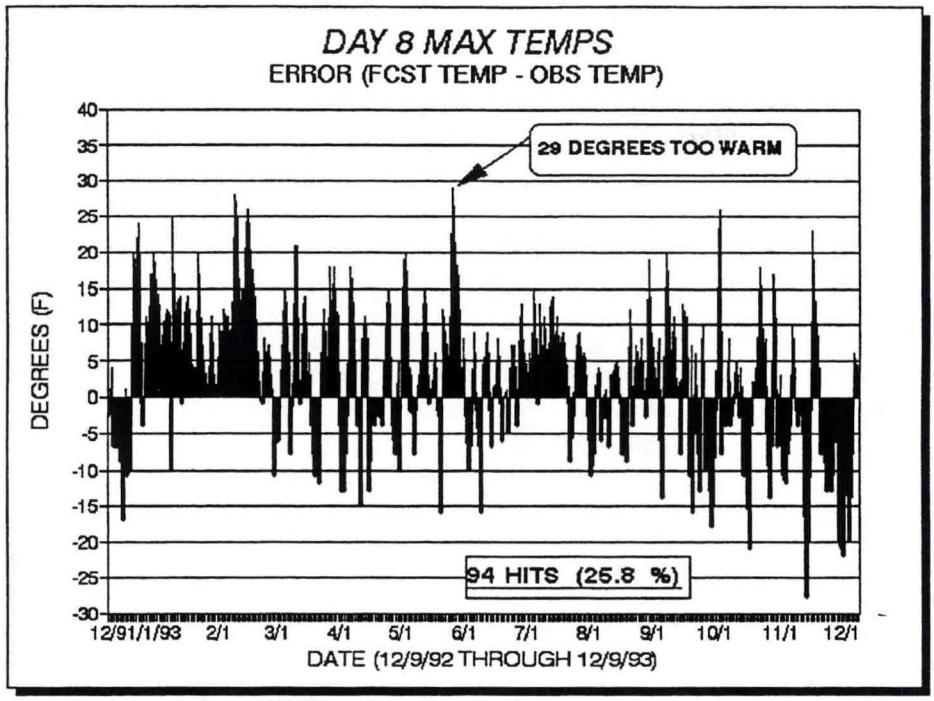

Figure 1o.

Figure 1a-1o. The error for each forecast. (a) Day 1 Maximum Temperature; (b) Day 2 Minimum Temperature; (c) Day 2 Maximum Temperature; (d) Day 3 Minimum Temperature; (e) Day 3 Maximum Temperature; (f) Day 4 Minimum Temperature; (g) Day 4 Maximum Temperature; (h) Day 5 Minimum Temperature; (i) Day 5 Maximum Temperature; (j) Day 6 Minimum Temperature; (k) Day 6 Maximum Temperature; (l) Day 7 Minimum Temperature; (m) Day 7 Maximum Temperature; (n) Day 8 Minimum Temperature; (o) Day 8 Maximum Temperature.

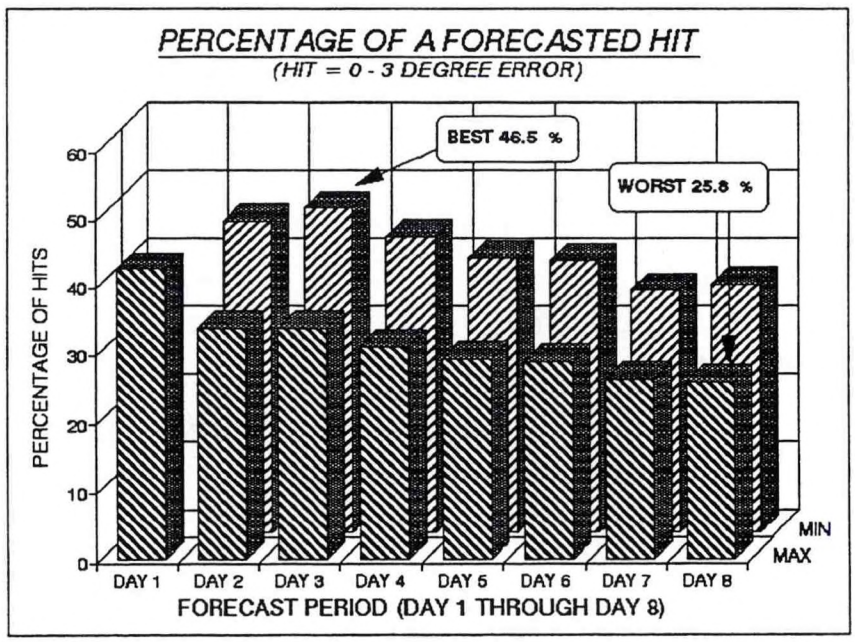

Figure 2 The percentage that the forecasts were a "hit", or were in error by ±3 degree or less.

A distinct improvement was discernible on the forecast error graphs from March 1 through September 1, when the periods of warm bias become more balanced with the periods of cold bias. This improvement correlates directly with a model seasonal change, and respective equation change. The errors are noticeably smaller in the spring and summer months than in the winter months. Often this trend is not the case for statistical guidance. Throughout the warm season, the minimum forecasts out performed the maximum forecasts to a much greater magnitude. The minimum forecast errors were seldom more than 10 degrees, while the maximum forecast errors recurrently exceeded 10 degrees. In addition to the larger magnitude of error with the forecasted maximums, the FMR guidance continued to be too warm. However, with the minimum forecasts, the warm biases were almost in balance with the cold biases during the warm season. These characteristics made the minimum temperature guidance much more reliable during the warm season than the maximum temperature guidance.

Some of the trends of the first three months showed up again during the last period of the study, namely from September 1 through December 9. With the start of the model's autumn season (with respective equation change), the magnitude of error became greater than in the summer months. The error of magnitude during the autumn months, in most forecast periods, was slightly less than what occurred during the winter. The autumn forecasts do support the fact that the guidance performed worse in the cold season than in the warm season.

There was a notable difference in the model guidance performance between the winter months and the autumn months with respect to the error bias. The autumn months did not show the warm bias characteristic of the winter months, and in fact eleven out of the fifteen forecast periods trended slightly toward a cold bias.

5. Conclusion

This study used objective methods to show how well the FMR temperature guidance verified for one location, over a 12-month period. It was shown that the FMR was most accurate in the warm season as opposed to the cold season with both the minimum and the maximum temperature forecasts. Throughout the verification period, the minimum temperature forecasts were more accurate than the maximums, and this were especially true in the warm months. The FMR persistently forecasted minimums and maximums too warm during the winter season, and continued to forecast the maximum temperatures too warm in the spring and summer seasons, although to a lesser extent. The minimum forecasts during the warm season were almost in balance between the warm and cold biases, and the magnitudes of error were less for these forecasts, making

this set of forecasts the most reliable. The warm bias of the winter season was not evident during the autumn season, however the magnitude of errors again became quite large.

The shorter period forecasts did perform better than the outer periods, as would be expected. However, the accuracy of the shorter periods was not a great deal better than the outer periods, and the accuracy dropped off at a very gradual rate with each later period. Therefore it appears that the days 4 through 8 forecasts were, in most cases, of similar reliability to the days 1 through 3 forecasts with respect to forecasting a hit.

As with any numerical guidance, the usefulness of this product depends largely upon the forecaster's knowledge of its limitations and biases. This study shows that the FMR had great difficulty forecasting temperatures during the winter months when shallow, arctic air was in place, or was moving into the area. The spectral model is not a frozen model, so its equations and predictors can be adjusted any time. The NMC's Techniques Development Lab has developed new MRF-based calibrated MOS equations to replace the calibrated perfect prog equations used for this verification study. These calibrated MOS equations incorporate low-level thickness predictors, (as opposed to 1000-500-mb thickness fields) to improve accuracy in the earlier projections. Implementation of the new equations is scheduled for the 0000Z model run on 14 April 1994 (NWS CR 1994). With further refinement in the future, the FMR has potential for being a trusted guidance product for making improved temperature forecasts out to eight days.

6. Acknowledgments

The authors thank Rick Ewald (Science and Operations Officer) of NEXRAD Weather Service Office Hastings, Nebraska; Steve Byrd (Meteorologist) of Weather Service Forecast Office Omaha, Nebraska; and Preston Leftwich (Regional Science Officer) of NWS Central Region Headquarters, Scientific Services Division, for comments and reviewing the manuscript. The authors also wish to acknowledge John Jensenius of National Meteorological Center, Office of Systems Development, for technical information and advise.

7. References

Gerrity, J.P., 1985: New Medium-Range Forecast Model. NWS Technical Procedures Bulletin No. 349, DOC/NOAA, 5pp.

Jensenius, J.S. Jr., J.P. Dallavalle, and S.A. Gilbert, 1993: The MRF-Based Statistical Guidance Message. NWS Technical Procedures Bulletin No. 411, DOC/NOAA, 5pp.

_____, 1993: Personal Communication.

NWS Central Region, 1994: National Weather Service Central Region Highlights, P, Slattery, ed., March, 47pp.

Panofsky, H.A., and G.W. Brier, 1958: Some Applications of Statistics to Meteorology. The Pennsylvania State University, 224pp.

CRARP No. 12 Central Region Applied Research Papers 12-01 through 12-14, August 1994.

CRARP No. 13 Central Region Applied Research Papers 13-01 through 13-11, December 1994.